



Biologie

# The Role of Sphingolipids in *Drosophila* Neuronal Development

Inaugural-Dissertation  
zur Erlangung des Doktorgrades der  
Naturwissenschaften im Fachbereich Biologie  
der Mathematisch-Naturwissenschaftlichen Fakultät  
der Westfälischen Wilhelms-Universität Münster

vorgelegt von

**Junfeng Zheng**

aus Liaoning, P.R. China

- 2010 -

---

Dekan: Prof. Dr. Christian Klämbt  
Erster Gutachter: PD Dr. Thomas Hummel  
Zweiter Gutachter: Prof. Dr. Christian Klämbt

Tag der mündlichen Prüfung: 24.01.2011

Tag der Promotion: 04.02.2011

---

# CONTENTS

## 1 INTRODUCTION 1

- 1.1 *Drosophila* olfactory system as a model for studying neuronal development in peripheral nervous system (PNS) 1
  - 1.1.1 The organization of *Drosophila* adult olfactory system 1
  - 1.1.2 The mechanisms of olfactory neuron targeting 2
- 1.2 *Drosophila* mushroom body as a model for studying neuronal development in the central nervous system (CNS) 3
- 1.3 Sphingolipid biology 6
  - 1.3.1 Sphingolipid metabolism 6
  - 1.3.2 Sphingolipid function in neuronal development 8
  - 1.3.3 Sphingolipid in protein sorting, endocytosis and cell polarity 11
- 1.4 Aim of the work 15

## 2 MATERIALS AND METHODS 16

- 2.1 Materials 16
  - 2.1.1 Solutions 16
  - 2.1.2 Antibodies 20
  - 2.1.3 Fly Stocks 21
- 2.2 Methods 26
  - 2.2.1 Genetic methods 26
  - 2.2.2 Histological methods 27
  - 2.2.3 Biochemistry methods 29

## 3 RESULTS 32

- 3.1 Identification of genes involved in olfactory targeting in *Drosophila* 32
- 3.2 *spt* function in olfactory system 34
  - 3.2.1 *spt* is required for class-specific ORNs targeting 34
  - 3.2.2 *Spt-I* and *lace* mutations exhibited identical phenotypes in the olfactory system 35
  - 3.2.3 *spt* mutants do not affect axon sorting among maxillary palp ORNs 38
  - 3.2.4 ORNs targeting is not affected in MARCM clone, but the fine structure of individual mutant axon terminals within glomerulus is abnormal 39

3.2.5 Rescue of the <i>lace</i> phenotype	41
3.2.6 <i>lace</i> mutations have weak phenotype at lower temperature	43
3.2.7 Genetic dissection of sphingolipid function in ORNs targeting	43
3.2.8 General Detergent-resistant membrane (DRM) components are not changed in <i>lace</i> hypomorphic mutants	49
3.2.9 Genetic interaction between <i>Spt</i> and <i>Dscam</i>	50
3.3 <i>spt</i> function in mushroom body (MB) development	54
3.3.1 MB development and structure	55
3.3.2 <i>spt</i> mutations have mushroom body defects.	57
3.3.3 Genetic dissection of sphingolipid function in MB	57
3.3.4 <i>Dscam</i> Mutant has MB phenotype	60
3.3.5 <i>spt</i> mutant axons are normal in MARCM clones	60
3.3.6 Genetic interaction between <i>spt</i> and <i>dscam</i> in MB	63
3.3.6.1 Overexpress <i>Dscam</i> [TM1] and <i>Dscam</i> [TM2] isoforms in MB	63
3.3.6.2 Mislocalization of <i>Dscam</i> [TM1] in <i>lace</i> mutant	63
3.3.6.3 Overexpression of <i>Dscam</i> [TM1] in <i>lace</i> background enhance MB phenotype	65
3.3.6.4 Knockdown of <i>Dscam</i> [TM1] in <i>lace</i> background suppress MB phenotype	66
3.3.7 Dendritic proteins mistargeting in <i>lace</i> mutant	68
3.3.8 Protein sorting and transport machinery disruption gives MB phenotype	70
3.3.9 Rab4 and <i>dscam</i> 17.1GFP co-localize in MB neurons	72
<b>4 DISCUSSIONS</b>	<b>74</b>
4.1 non-cell-autonomous functions of <i>spt</i>	77
4.2 Genetic interaction between <i>spt</i> and <i>dscam</i>	78
4.3 Genetic dissection of sphingolipid function by RNA interference	79
4.4 Neuronal polarity and protein polarity localization in neuron	81
4.4.1 The mechanisms of protein polarity localization	81
4.4.2 <i>Dscam</i> [TM1] and other dendritic proteins mislocalization	83
4.4.3 Axon initial segment (AIS), could MB as an in vivo model?	86
4.4 Outlook	90
<b>5 SUMMARY</b>	<b>92</b>

---

**6 BIBLIOGRAPHY** 94

**7 APPENDIX** 104

7.1 List of Figures and tables 104

7.2 Abbreviations 106

## **1 INTRODUCTION**

The nervous system is often described as the most complex system in the universe (Koch and Laurent 1999). The enormous complexity corresponds to the highly sophisticated function of the brain. Understanding how neurons form connections is the key of understanding brain function. *Drosophila melanogaster* has around 100,000 neurons (Williams and Herrup 1988). The relative 'simple' brain together with other advantages, such as elegant genetics tools, makes the small fly a popular model organism for neurobiology. Sophisticated manipulations make it possible to hunt a gene in a genetic screen and to answer questions of signal transduction, neuronal development or adult behavior (Bellen, Tong et al. 2010).

### **1.1 *Drosophila* olfactory system as a model for studying neuronal development in peripheral nervous system (PNS)**

#### **1.1.1 The organization of *Drosophila* adult olfactory system**

The convergence of olfactory neurons expressing particular odorant receptor (Or) genes onto their targets in the brain is one of the most dramatic examples of axon projection in developmental neurobiology (Figure 1.1). There are around 1300 olfactory receptor neurons (ORNs) located in two types of peripheral sensory appendages, the antenna and maxillary palpus. Each ORN in the antenna expresses one or two kinds of receptor molecule among 80 ORs. OSNs in the antenna and maxillary palp each extend a single axon, which fasciculates in the antennal or maxillary nerve and project to the periphery of the antennal lobe then individual axons sort out to target glomeruli in the antennal lobe. A glomerulus is a spherical structure which receives incoming ORN axons. Within glomeruli, OSNs synapse with

projection neurons (PNs), the functional equivalent of mitral and tufted cells in the vertebrate olfactory bulb. Each PN extends a dendrite that branches within a single glomerulus and an axon that targets higher brain regions, the mushroom body and lateral horn of the protocerebrum (Hallem and Carlson 2004). Local inhibitory neurons interact with both OSNs and PNs to modulate olfactory signals (Wilson and Mainen 2006). The olfactory map formation is highly regulated.

### **1.1.2 The mechanisms of ORN targeting**

Unlike the ORs of mammals, which act as receptors or adhesion molecules sensing guidance cues and targeting via G-protein signaling (Mombaerts 2006; Chesler, Zou et al. 2007), *Drosophila* ORNs express ORs after axon converge into distinct glomeruli, indicating an OR-independent mechanism in ORN targeting in the fly. There is a distinct and sequentially acting mechanisms in *Drosophila* ORNs targeting (Jefferis, Vyas et al. 2004). Generally, axons fasciculate and find the way to the antennal lobe, then, axon sort out and converge onto target glomeruli to form synapse with the projection neurons. Several axon guidance molecules have been implicated in ORN axon targeting in *Drosophila*. For example, *Down syndrome cell adhesion molecule* (*Dscam*) mutant axons are mistargeting to ectopic glomeruli (Hummel, Vasconcelos et al. 2003). *Dscam* has more than 39,000 isoforms due to alternative splicing (Schmucker, Clemens et al. 2000). This high degree of diversity appears to be important, since over-expression of *Dscam* in whole ORN class prevents early stopping phenotype, but lead to a failure of axon convergence in the target area (Zierau et al. in preparation).

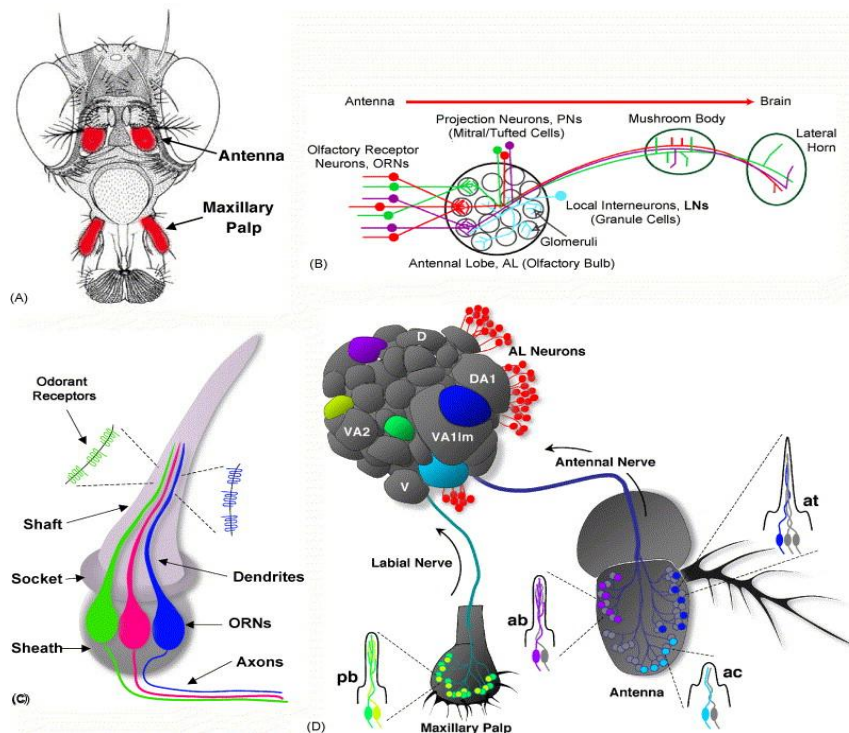


**Figure 1.1: Organization of the *Drosophila* olfactory system**

(A) Olfactory organs, the third antennal segment (upper) and the maxillary palp (bottom). (B) Cartoon schematic of the olfactory pathway from the peripheral sense organs to higher olfactory centers. (C) Organization of an olfactory sensillum housing 3 ORNs. (D) General organization of the peripheral olfactory system and ORN axon projections into the AL (Adapted from Jefferis & Hummel 2006).

Comparing with the *Dscam* mutation, the mutants of transmembrane molecule *Semaphorin-1a* and the Ca-dependent cell adhesion molecule *N-Cadherin* (*N-cad*), lead to more local axon targeting defects. *N-cad* mutant ORN can reach the target region in AL, but cannot converge into distinguish glomeruli (Hummel and Zipursky 2004). *Sema-1a* mutant ORN axons are able to induce local convergence, but axons of the same class split into multiple adjacent glomeruli (Lattemann, Zierau et al. 2007).

## 1.2 *Drosophila* mushroom body as a model for studying neuronal development in central nervous system (CNS)

Mushroom body (MB) are the center of olfactory learning and memory and are



functionally equivalent to the hippocampus in mammals (Heisenberg 2003).

*Drosophila* adult MB neurons derive from four neuroblasts per brain hemisphere. Each neuroblast generates three types of Kenyon cells, the  $\gamma$ ,  $\alpha'/\beta'$  and  $\alpha/\beta$ . (Ito, Awano et al. 1997). The Kenyon cell bodies are clustered on the dorsal posterior surface of the protocerebrum (Ito, Awano et al. 1997; Lee, Lee et al. 1999). The cell bodies send out fibres inwards to form the calyx neuropile (dendrites). From the calyx, the fibres extend anteriorly via the pedunculus to reach the anterior protocerebrum, where they form the  $\alpha$ ,  $\alpha'$ ,  $\beta$  and  $\gamma$  lobes (Figure 1.2). The calyces of MBs receive olfactory information from the antennal lobes via the prominent antennal glomerular tracts. The peduncles and lobes send neural commands through their connections to the major brain regions including the lateral protocerebrum (Kurusu, Nagao et al. 2000).

MB neurons are born in a sequential fashion (Figure. 1.2). The earliest born  $\gamma$  neurons initially extend axons both medially and dorsally during late embryonic and early larval stages (Lee, Lee et al. 1999). These larval-specific axons are then pruned back to the peduncle by 18 hours after pupal formation (APF) and re-extend medially during pupal remodeling. The late larval-born  $\alpha'/\beta'$  and pupal born  $\alpha/\beta$  neurons have bifurcated axons with one dorsal ( $\alpha'$  or  $\alpha$ ) and one medial ( $\beta'$  or  $\beta$ ) projections. Moreover, these axonal lobes can be distinguished by fasciclin II (FasII) antibody staining, where strong signals were detected on  $\alpha/\beta$  axons, weak signal on  $\gamma$  axons, however, no signals on  $\alpha'/\beta'$  axons, cell bodies or dendrites of MB neurons (Ito and Hotta 1992; Lee, Lee et al. 1999).

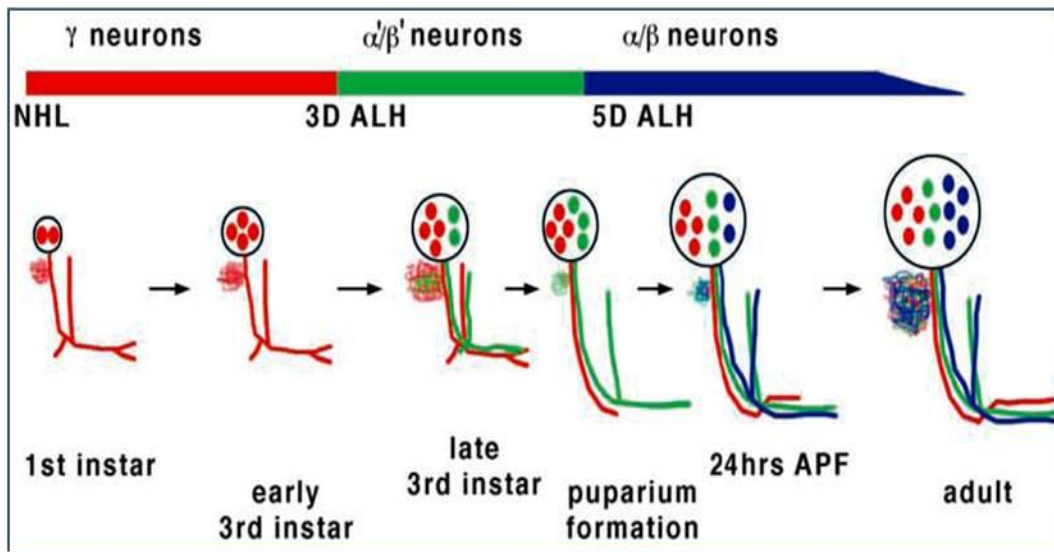


**Figure 1.2: MB neurons development**

(A) A summary of the mushroom body development. Three distinct types of neurons,  $\gamma$  neurons (red),  $\alpha'/\beta'$  neurons (green), and  $\alpha/\beta$  neurons (blue) are sequentially derived from common precursors. At the adult stage,  $\gamma$  axons project medially without dorsal branching, while  $\alpha'/\beta'$  and  $\alpha/\beta$  axons form separate sets of dorsal and medial bundles. (Adapted from Lee et al. 1999).

MB are highly polarized structures, which make it a useful model system for various aspects of neuronal function and developmental studies, such as axonal growth and targeting, axon bifurcation, neuronal remodeling, dendrite arborization and protein distribution (Jefferis, Marin et al. 2002).

Genes that affect MB development have been identified through forward genetic screens. These genes include various types of molecules, such as transcription factors, GTPase, motor proteins and cell adhesion proteins, which affect cell number, membrane protein distribution, cell size, and axon morphogenesis (Heisenberg 1980; Melzig, Rein et al. 1998; Reuter, Nardine et al. 2003; Watts, Hoopfer et al. 2003; Zhu, Lin et al. 2006). For example, *mushroom body defect* (*mud*), a p21-activated kinase and *enoki mushroom* (*enok*) encoding a histone acetyltransferase, regulate MB neuroblast number or proliferation (Kurusu, Nagao et al. 2000; Scott, Lee et al. 2001).

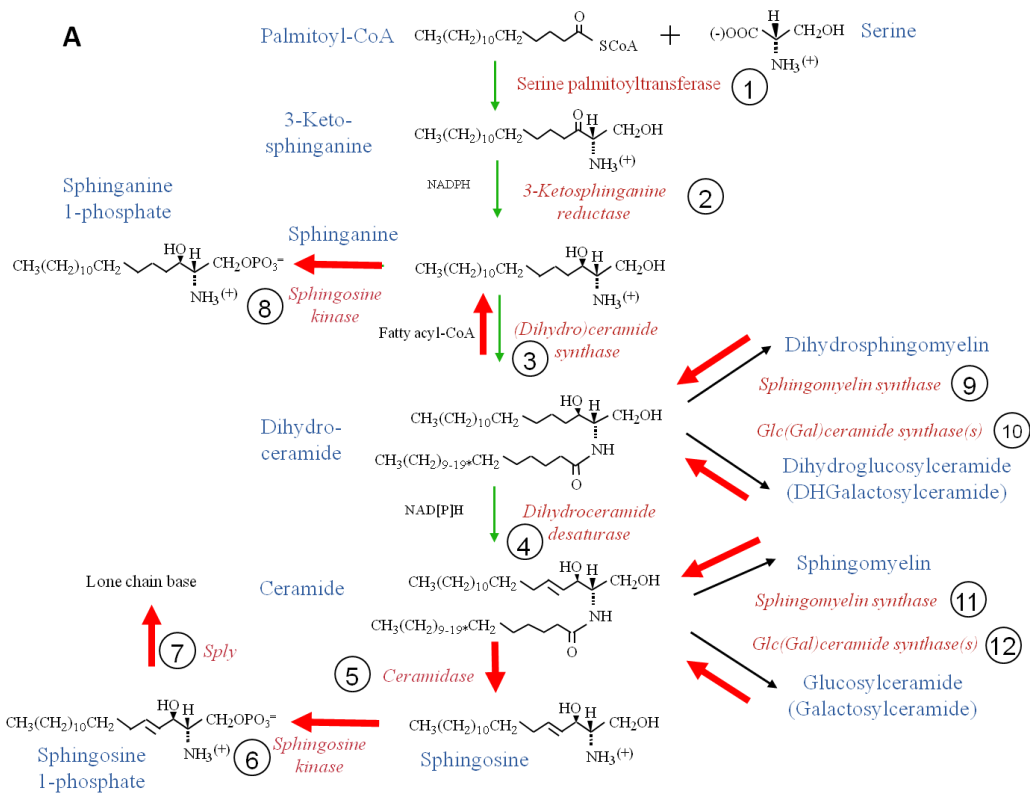
Additionally, the transcription factor *eyeless*, and another nuclear protein gene, *dachshund*, regulate MB development by controlling axon pathway selection (Kurusu, Nagao et al. 2000; Martini, Roman et al. 2000). Moreover, cell adhesion protein *Dscam* is required for MB neuron branch segregation (Schmucker, Clemens et al. 2000; Wang, Zugates et al. 2002; Wojtowicz, Flanagan et al. 2004). In the absence of *Dscam*, the branches extend randomly in either dorsal or medial directions. By contrast, *Eph* mutant axons branches in MB are often reduced or absent  $\alpha'$  and  $\alpha$  lobes, with an associated increase in the thickness of  $\beta'$  and  $\beta$  lobes, meanwhile, *Eph* mutant axon branches in MB do not tightly associate with each other and often projects both medially, which suggest that *Eph* has a more specific role in the guidance of dorsal projections and sister branches (Boyle, Nighorn et al. 2006).

### **1.3 Sphingolipid biology**

#### **1.3.1 Sphingolipid metabolism**

Sphingolipids are essential components of eukaryotic cells where they play important roles in intracellular signalling and membrane structure (Dickson 1998; Futerman and Hannun 2004). All sphingolipids are composed of a long-chain base (LCB), a fatty acid and a polar head group. The sphingoid bases (containing 1,3-dihydroxy-2-aminoalkane and its derivatives) were first isolated by Thudichum who characterized the brain alkaloid “sphingosin” over a century ago (Thudichum 1884). The chemical structure of the family of sphingolipids was subsequently characterised by Carter and colleagues five decades later (Carter, Haines et al. 1947). Serine palmitoyltransferase (SPT; EC 2.3.1.50), which is located in the endoplasmic reticulum (ER) and consists of at least two heterologous monomer subunits, long

chain base 1 and 2 (LCB1/LCB2, also known as SPT1 and SPT2, respectively) catalyses the first and rate-limiting step of the sphingolipid biosynthetic pathway in all organisms studied to date (Hanada 2003). This reaction is a pyridoxal 5'-phosphate (PLP)-dependent, decarboxylative, Claisen condensation of the amino acid L-serine and the long-chain (C16) fatty acid palmitoyl-CoA, which produces the sphingolipid precursor 3-ketodihydrosphingosine (KDS) (Fig?). The catalytic pathway is comprised of the following steps: formation of an external aldimine via displacement of the lysine-PLP internal aldimine (holo-SPT) by the incoming amino acid substrate; formation of a quinonoid intermediate by abstraction of the  $\alpha$ -proton from the PLP-amino acid external aldimine; a Claisen condensation with the fatty acid-CoA substrate followed by displacement of the CoA to form a  $\beta$ -ketoacid; decarboxylation of this species to form a product quinonoid; protonation of this quinonoid to form the product external aldimine and finally release of the  $\alpha$ -oxoamine product and regeneration of the enzyme PLP-internal aldimine. The product of this reaction is 3-ketodihydrosphingosine (KDS) is quickly converted to erythro-dihydrosphingosine (DHS, also called sphinganine) by 3-keto-sphinganine reductase. A long fatty-acid chain attached to a sphingoid base through an amide linkage forms ceramide, which is transported from ER to the lumen of the Golgi apparatus via both vesicular and non-vesicular mechanisms, where it serves as a precursor for sphingosine, sphingosine 1-phosphate (S1P), sphingomyelin (SM), and complex sphingolipids (Nagiec, Lester et al. 1996) (Figure 1.3).



**Figurer 1.3: Scheme of sphingolipid metabolism**

*De novo* synthesis of sphingolipid (green and black arrows). Sphingolipid degradative pathway (red arrows). The enzymes are in red and intermediates are in black with common name in blue. The numbers label the different enzymes. (adapted from (Merrill 2002))

### 1.3.2 Sphingolipid function and Sphingolipid disorder disease

The biological functions of sphingolipids are as complex and diverse as their structures. First, sphingolipids are important components of cell membrane.

Sphingolipids are located only in the outer (exoplasmic) leaflet of the plasma membrane bilayer, while glycerophospholipids such as phosphatidylinositol, phosphatidylserine and phosphatidylethanolamine occur only in the inner (cytoplasmic) leaflet (Marek Cebecauer 2009). Further, sphingomyelin and other sphingolipids together with cholesterol are located in an intimate association in specific sub-domains or 'rafts' of membranes. As sphingolipids containing long, largely saturated acyl chains, they pack more tightly together, thus giving

sphingolipids much higher melting temperatures than membrane glycerophospholipids. This tight acyl chain packing is essential for raft lipid organization, since the differential packing facility of sphingolipids and cholesterol in comparison with glycerophospholipids is believed to lead to phase separation in the membrane, giving rise to sphingolipid-rich regions ('liquid-ordered' phase) surrounded by glycerophospholipid-rich domains ('liquid-disordered' phase). This ordering is responsible for the resistance to attack by detergents. As these rafts are relatively small (approximately 50 nm diameter and containing roughly 3000 sphingomyelin molecules) and mobile (Brown and London 2000). It also should be recognized that lipid rafts in general are dynamic structures, which can be formed or undergo compositional changes during signaling events and are short-lived (milliseconds or less)(Simons and Ikonen 1997). Thus, rafts are not easy to study by microscopic methods

Raft has important biological functions (for review(Bartke and Hannun 2009) . For example, raft is involved in the initiation of T cell signaling by enabling efficient interaction between antigens and receptors. It is also apparent that the biological functions of neurotransmitters and their receptors, in particular acetylcholine and serotonin receptors, are highly dependent upon sphingolipids and cholesterol in raft domains. The lipids interact with receptors to alter their conformation, thus regulating neurotransmitter binding and signal transducing functions amongst other events. Moreover, lipid rafts also play an important role in axonal growth and guidance. Axonal guidance cues such as EphrinA were shown to be raft located through their glycosyl-phosphatidylinositol (GPI) anchors (Gauthier, Couturier et al. 2003), transmembrane receptor DCC is also present in rafts for netrin-1-induced

axon turning (Guirland, Suzuki et al. 2004). Similarly, molecules involved in neuritogenesis, such as NCAM, L1 or integrins, have been shown to localized in a ligand-dependent manner in lipid rafts (Kleene, Yang et al. 2001; Niethammer, Delling et al. 2002).

In addition to the structural function in the cell membrane, sphingolipids are also involved in numerous cell function pathway. For instance, complex sphingolipids participate in cell signaling by affecting the properties of receptors directly (Hannun and Obeid 2008). Moreover, the lipid backbones, such as ceramide, sphingosine and S1P also participate in signal transduction (Holthuis, Pomorski et al. 2001).

In the "classic" signaling pathways, receptor activation induces the hydrolysis of a membrane sphingolipid (e.g. sphingomyelin) to ceramide that can serve as a lipid second messenger or be converted to downstream metabolites to activate or inhibit downstream targets that control cell behavior(van Blitterswijk, van der Luit et al. 2003).

The complex sphingolipids also have important biological functions. For example, the loss of the *Drosophila* glycosyltransferases *egghead (egh)* leads to the absence of elongated glycosphingolipids and the accumulation of truncated precursor glycosphingolipids (Wandall, Pedersen et al. 2003). *egh* mutant die as pupae and show defects in epithelial morphogenesis during oogenesis and embryogenesis, such as abnormal neurogenesis, compound egg chambers, and a dorsal appendage fusion phenotype (Goode, Melnick et al. 1996; Wandall, Pedersen et al. 2003). It has been proposed that these genes are required for the morphogenesis of the follicle cells by regulating germ line-follicle cell adhesion (Goode, Melnick et al. 1996).

Abnormal sphingolipids metabolism also leads to human disease. For instance, *Spt-I*

mutation causes a clinical disorder called hereditary sensory neuropathy type I (HSN1), which is a dominantly inherited disease involving the progressive degeneration of lower limb sensory and autonomic neurons. The symptoms begin with loss of pain and temperature sensation in feet and hands, often complicated by severe infections, which can finally lead to osteomyelitis and amputations. Until now, three point mutation are reported and the missense mutations in the human *LCB1* (*SPTLC1*) gene can alter a specific amino acid residue (Cys133 or Val144) in the *LCB1* subunit (Bejaoui, Wu et al. 2001). Research has provided that the activity of SPT mutant enzyme is reduced to 50% of wild type (Hornemann, Penno et al. 2009). However, the steady-state levels of LCB1 and LCB2 subunits are normal. Not a sentence!

### **1.3.3 Cell polarity, protein sorting, endocytosis and Sphingolipids**

Neurons are highly polarity cells. They are compartmentalized into two molecularly and functionally distinct domains, axons and dendrites. The polarity transport proteins and the polarity orientation of cytoskeleton are the basement of neuronal polarity. Different extracellular and intracellular signals converge on the regulation of the cytoskeleton. Most notably, Rho GTPases, PI3K, Ena/VASP, cofilin and SAD kinases are major intracellular regulators of neuronal polarity (Tahirovic and Bradke 2009). And proper cellular morphology and function depends on the polarized distribution of organelles and proteins in distinct subcellular compartments. For example, in mammalian and fly neurons, Golgi outposts localize to dendrites is important to dendritic branching. (Zheng, Wildonger et al. 2008). In addition, dendritic localized voltage-gated channels have been proposed to play a critical role in regulating the



propagation of synaptic signals and action potentials in dendrites (Stuart, Schiller et al. 1997). Another interesting example is the polarized distribution of different *Drosophila* Down Syndrome cell adhesion molecule (Dscam) isoforms (Wang, Ma et al. 2004). The transmembrane domain of Dscam is encoded by one of two exon 17 alternatives (exon 17.1 and exon 17.2). Expression by a mushroom body driver Gal4-OK107, Dscam17.1 (termed Dscam [TM1]) isoforms is preferentially localized in the cell bodies and dendrites. In contrast, Dscam isoforms carrying exon 17.2 (termed Dscam [TM2]) are always distributed throughout cell bodies, dendrites, and axons (Wang, Ma et al. 2004). In contrast to the strong expression, produced at low level with the Dscam promoter, Dscam[TM1] is preferentially localized to dendrites, while Dscam[TM2] is largely restricted to axons (Yang, Bai et al. 2008).

It is also known that sphingolipid signaling is important for neuronal Polarity. For instance, the plasma membrane ganglioside sialidase (PMGS), which hydrolyzes gangliosides, is a very early marker of neuronal polarity. It is enriched in the neurite that will become an axon and signals to the actin cytoskeleton. The PMGS seems to be essential for axon formation since its depletion results in axon inhibition, whereas its increased activity *accelerates neuronal polarization* (Da Silva, Hasegawa et al. 2005). PMGS activity localizes TrkA, a nerve growth factor (NGF) receptor, in one neurite, thereby spatially restricting phosphatidylinositol-3-kinase (PI3K) signaling and Rho activation. This enables triggering of axon inducing signals in a single neurite.

Sphingolipids can affect endocytosis by physically altering the local environment or by initiating signaling events. For instance, *lcb1-100* is a temperature-sensitive mutation in the *LCB1* gene. AT the restricted temperature, *lcb1-100* exhibits

endocytosis defects (Zanolari, Friant et al. 2000). Other studies extended this finding by showing that at restrictive temperatures the mutant cells have an abnormal non-polarized cortical distribution of actin filaments associated with the endocytic defects. This phenotype is rescued by providing medium containing dihydrosphingosine (DHS) or phytosphingosine (PHS) (Zanolari, Friant et al. 2000), which indicate that the sphingoid base synthesis is required for endocytosis.

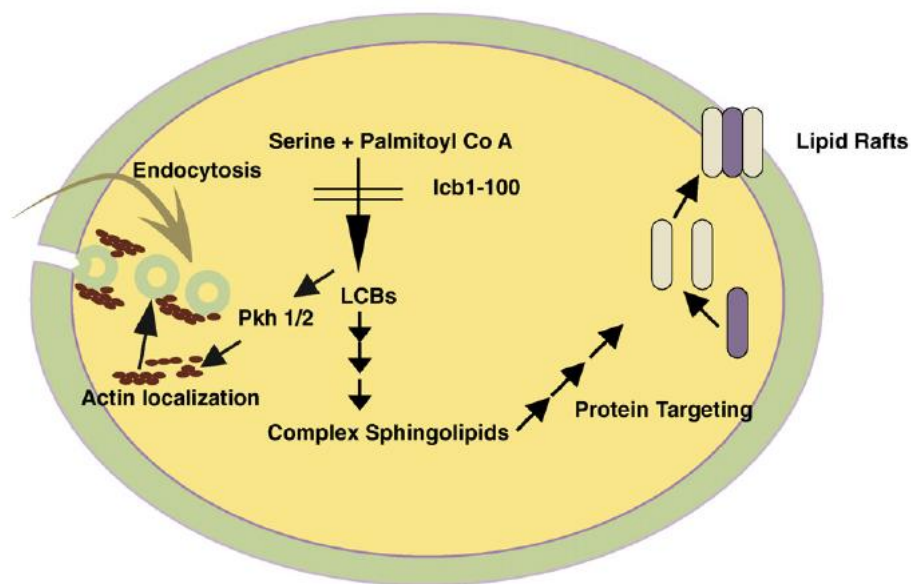


**Figure 1.4: A schematic representation of the modulation of endocytosis by sphingolipids.**

In yeast, *lcb1-100* is a temperature-sensitive mutation in the *LCB1* gene leading to abnormal non-polarized cortical distribution of actin filaments associated with the endocytic defects. *PKH1* or *PKH2* (orthologues of mammalian protein-phosphoinositide dependent protein kinase 1 or PDK1) restores the actin localization defects in the *lcb1-100* mutant (Rao and Acharya 2008).

Moreover, the deregulation of actin dynamics has been shown to affect the internalization step in endocytosis (Lamaze, Fujimoto et al. 1997) (Figure 1.4). Subsequent studies indicated that proper sphingoid base synthesis is required to control protein phosphorylation events that are crucial for endocytosis and overexpression of *protein kinase C1* (*PKC1*) and *PKH1* or *PKH2* (orthologues of

mammalian *protein-phosphoinositide-dependent protein kinase 1* or *PDK1*) restores the actin localization defects in the *lcb1-100* mutant (Friant, Lombardi et al. 2001). These studies provide a genetic link between sphingolipids and cytoskeletal organization.

Defects of sphingolipid metabolism can also disturb exocytosis. Mutations in four genes involved in ceramide biosynthesis, *elo3*, *SurP*, *YPC1*, and *Ayr1* were identified in yeast (Proszynski, Klemm et al. 2005). Mutants of *elo3*, which generates a C26:0 fatty acid, cannot synthesize long-chain fatty acids for ceramide biosynthesis and mis-sort cargo to the vacuole instead of the plasma membrane. A mutation in the *SurP* affects the hydroxylation of the sphingosine backbone, and these mutants accumulate cargo in the trans-Golgi network. Mutants of *YPC1* (encoding a ceramidase) show defects in the exit of the cargo protein from the Golgi. Mutation in *Ayr1p* also affects protein targeting to the plasma membrane. It is not clear if the mistargeting of the sphingolipid metabolites that accumulate in these mutants is caused by general deleterious effects on protein sorting or by changes in the membrane composition of vesicles owing to faulty sphingolipid biosynthesis.

In *Drosophila*, it has been demonstrated that modulation of sphingolipid biosynthesis in vivo rescues photoreceptor degeneration in an endocytosis mutant *arrestin 2<sup>3</sup>* (Kitamoto 2001; Acharya, Patel et al. 2003). *Drosophila arrestin 2* acts as a clathrin adaptor, mediating endocytosis of arrestin-rhodopsin complexes. *arr2<sup>3</sup>* mutant is defective in endocytosis, accumulate abnormal multivesicular bodies, show extensive retinal degeneration, and undergo necrotic cell death (Kiselev, Socolich et al. 2000). Expression of ceramidase, which decreased ceramide levels by 50% in *arr2<sup>3</sup>* suppressed retinal degeneration. Moreover, expression of ceramidase also

suppressed retinal degeneration in a dynamin mutant, suggesting that modulation of ceramide levels effect on *arr2*<sup>3</sup> mutant by altering the dynamics of the endocytic process.

#### **1.4 Aim of the work**

In a large scale forward genetic screen *Serine palmitoyltransferase (spt)* mutations were identified leading to specific defects in the projection pattern in the olfactory system of *Drosophila*. The scope of this work was to identify multiple phenotypes of *spt* and explore the mechanisms of *spt* function in neuronal development.

To understand the *spt* defects, one part of this thesis was to identify which downstream enzymes in sphingolipid metabolism pathway are important in neuronal development, therefore tried to find the candidate sphingolipid and to clarify its function in neuronal development. Second part was to investigate the relationship between *spt* and *dscam* and tried to figure out how sphingolipids can affect the function of cell adhesion molecule function in neuronal development.

## 2 MATERIALS AND METHODS

### 2.1 Materials

#### 2.1.1 Solutions

All reagents and chemicals were purchased from following companies at quality level pro-analysis:

Aldrich (Steinheim)	Baker (Groß-Gerau)	Biomol (Hamburg)
Biozym (Hameln)	Fluka (Neu Ulm)	Roche (Mannheim)
Invitrogen (Darmstadt)	Merck (Darmstadt)	Pharmacia/LKB (Freiburg)
Roth (Karlsruhe)	Serva (Heidelberg)	Sigma (Deisenhofen)

Avanti Polar Lipids (Hamburg)

#### ***Drosophila* standard medium (per liter):**

77g corn flour

8,5g of agar

18g dry yeast

10g soy flour

82g malt extract

41g of sugar beet syrup

4, 5 ml propionic acid

15 ml Nipagin solution

Water, Corn flour and Agar and are cooked while stirring. Soy flour and dry yeast are dissolved in water until no clots remain then added together with malt and syrup to the boiling food. When the temperature has cooled down to 60°C propionic acid and Nipagin solution are added.

**Nipagin solution:** 100g Nipagin (methyl 4-hydroxybenzoate) in 1000ml 70% EtOH

**PBS:** 130 mM NaCl 7 mM Na<sub>2</sub>HPO<sub>4</sub> 3 mM KH<sub>2</sub>PO<sub>4</sub> 2,7 mM KCl, pH 7,6

**PBT:** 0,1% Triton X-100 in PBS

**Paraformaldehyd-stock (PFA,8%):**

dilute 0,8 g Paraformaldehyd in 10 ml ddH<sub>2</sub>O, add 70µl of 1M NaOH, incubate for 30 min at 37°C. For fixation of brains and antenna dilute the stock with PBS up to 2% concentration.

**Squishing buffer (SQUIB):**

10mM Tris pH 8,2

1mM EDTA

25mM NaCl

200µg/ml Proteinkinase K (final concentration)

**TBE:**

50mM Tris/HCl,

50 M boracic acid

5 mM EDTA

**DNA Loading Buffer (10x):**

4 M urea 50 mM EDTA spatula tip of bromophenol blue spatula tip of xylene cyanol

**Ethidium Bromide:** 10mg/ml stocksolution, using 1ul/50mL agrosegel

**SDS-7B :**

Protein Molecular weight [kD]

A2-Macroglobulin 172,5

$\beta$ -Galactosidase 112,5

Fructose-6-phosphate kinase 86

Pyruvate kinas 62,5

Fumarase 53

Lactic dehydrogenase 33,5

Triosephosphate isomerase 31,5

**Prestained Protein Standards (dual color):**

250 kD – 150 kD – 100 kD – 75 kD – 50 kD –37 kD – 25 kD – 20 kD – 15 kD – 10KD

**TNE Puffer:**

10 mM Tris HCl, pH7.5

150 mM NaCl

5 mM EDTA

**Lysepuffer:**

1470  $\mu$ l TNE+1 % Triton X-100

30 $\mu$ l 50 x Protease Inhibitor Cocktail

<b>Sucrose gradient:</b>	% Sucrose	g / 100 ml TNE
	85	85
	35	35
	5	5

**Laemmli sample buffer (4x):**

Upper buffer

0.5M Tris-HCl/ 0.4% SDS

**4x sample buffer:**

Upper buffer 1.25ml

10% SDS 100 $\mu$ l

Glycerol 1ml

0.05% bromophenol blue 400 $\mu$ l

$\beta$ -mercaptoethanol 550 $\mu$ l

**Immunohistochemistry:**

Wash buffer

1xPBS/ 1% TritonX-100

Blocking and antibody solution

Wash buffer/ 10% Normal goat serum



Staining solution

0.1M Tris-HCl, pH7.5/ 0.1% Tween-20

**2.1.2 Antibodies****2.1.2.1 Primary antibodies**

Name	Origin	Dilution	Source
Anti-GFP	rabbit	1:1000	Invitrogen
Anti-Ncadherin	rat	1:20	Hybridoma Bank
Anti-Fasciclin II	mouse	1:10	Hybridoma Bank
Anti-Flotillin 2	mouse	1:50	BD Biosciences
Anti CD2	mouse	1:1000	Invitrogen
Anti CD8	rat	1:1000	Caltech
22C10	mouse	1:50	Hybridoma Bank
Anti c-Myc	mouse	1:5	Hybridoma Bank
Anti-HA	mouse	1:100	Sigma

### 2.1.2.2 Secondary antibodies / intercalating dyes

Name/ specificity	Conjugation	Dilution	source
Goat anti mouse	Alexa 488	1:500	Molecular Probes
Goat anti rabbit	Alexa 488	1:500	Molecular Probes
Goat anti mouse Highly cross absorbed	Alexa 568	1:300	Molecular Probes
Goat anti mouse	Alexa 568	1:300	Molecular Probes
Goat anti rabbit	Alexa 568	1:300	Molecular Probes
Goat anti Rat	Alexa 568	1:300	Molecular Probes
Goat anti Rat	Alexa 637	1:300	Molecular Probes
Toto3		1:5000	Molecular Probes

### 2.1.3 Fly Stocks

#### 2.1.3.1 General stocks

Stock	Source/reference
<i>W<sup>1118</sup></i>	Lindsley & Zimm, 1992
<i>eyFLP; Gla Bc hs-hid/ CyO</i>	Thomas Hummel, unpublished
<i>eyFLP UAS-CD8; Tft/CyO</i>	Georg Steffes, 2007
<i>eyFLP UAS-CD2; Tft/CyO</i>	Georg Steffes, 2007
<i>eyFLP UAS-syt; Tft/CyO</i>	Georg Steffes, 2007
<i>eyFLP UAS&gt;CD2&gt;CD8; Tft/CyO</i>	Georg Steffes, 2007
<i>eyFLP UAS&gt;CD2&gt;CD8 UAS-dsRed; Tft/CyO</i>	Georg Steffes, 2007
<i>hsFLP; Tft/CyO</i>	Golic & Lindquist, 1989

<i>hsFLP UAS-CD2; Tft/CyO</i>	Georg Steffes, 2007
<i>Tft/CyO</i>	Thomas Hummel, unpublished
<i>Gla/CyO<sup>twiG4 UAS-GFP</sup></i>	Tobias Storck
<i>Sp/CyO; MKRS/TM2</i>	Thomas Hummel, unpublished
<i>Bl/CyO; TM2/TM6</i>	Thomas Hummel, unpublished
<i>Sp/CyO<sup>twiG4 UAS-GFP</sup>; TM2/TM6<sup>GFP</sup></i>	Thomas Hummel, unpublished
<i>TM3/TM6</i>	Thomas Hummel, unpublished
<i>Sp/CyO; sb delta 2-3/TM2</i>	Georg Steffes, 2007
<i>eyFLP; FRT42 ubi-GFP nls/CyO</i>	Bloomington Stock Center
<i>Sp/CyO; UAS-CD2/TM2</i>	Thomas Hummel, unpublished
<i>FRT42 Gal80</i>	Lee & Luo, 1999
<i>FRT42 PCNA</i>	Thomas Hummel, unpublished
<i>FRT42 PCNA/CyO;</i> <i>“Multimarker 1”/TM3 Ser</i>	Ariane Zierau
<i>UAS-CD8/CyO</i>	Lee and Luo, 1999)
<i>eyFLP;FRT42 GMR-GFP Or22a:syt/CyO</i>	Georg Steffes
<i>FRT42/CyO; TM2/TM6</i>	Thomas Hummel, unpublished
<i>Sp/CyO twiGal4 UAS-GFP ; UAS-laminGFP/TM2</i>	Thomas Hummel, unpublished
<i>eyFLP gl-lacZ; FRT82 GMR-hid/TM6</i>	Thomas Hummel, unpublished
<i>UAS-Rab4-RFP</i>	Bloomington Stock Center
<i>UAS-Khc::nod::lacZ / TM3,Sb</i>	Bloomington
<i>UAS-Khc::nod::GFP/III</i>	Bloomington

### 2.1.3.2 Gal4 driver

Stock	Source/reference
<i>dllGal4 UAS-CD8/CyO</i>	Christian Heringer, 2007
<i>dllGal4/CyO; Or46a:syt, Or47a:syt/TM2</i>	Christian Heringer, 2007
<i>eyFLP elavGal4; FRT42 Gal80/CyO</i>	Thomas Hummel, unpublished
<i>FRT42 Gal80/CyO; elavGal4 UAS-CD8/TM6</i>	Thomas Hummel, unpublished
<i>FRT42 Gal80/CyO; conGal4 UAS-CD2/TM6</i>	Zierau, 2007
<i>GH146Gal4</i>	Stocker et al., 1997

<i>E132Gal4</i>	Halder et al., 1995
<i>elavGal4</i>	Lin and Goodman, 1994
<i>201Y Gal4</i>	Bloomington Stock Center
<i>OK107 Gal4</i>	Bloomington Stock Center
<i>eyGal4</i>	Bloomington Stock Center

### 2.1.3.3 OR Marker

The Or-Gal4 were recombined with UAS-sytGFP, UAS-CD8GFP and UAS-CD2GFP and established with an FRT42 either PCNA or Gal80 to perform single class analysis.

Stock	Source/reference
<i>Or23aGal4</i>	Vosshall et al., 2000
<i>Or46aGal4</i>	Vosshall et al., 2000
<i>Or47aGal4</i>	Vosshall et al., 2000
<i>Or47bGal4</i>	Vosshall et al., 2000
<i>Or59cGal4</i>	Hummel et al. 2003
<i>Or71aGal4</i>	Hummel et al. 2003
<i>Or83bGal4</i>	Larsson et al. 2004
<i>Or47a::sytGFP</i>	Vosshall et al., 2000
<i>Or47b::CD8GFP</i>	Couto et al. 2005
<i>Gr21dGal4</i>	Scott et al. 2001

### 2.1.3.4 Deficiencies & lethal P-insertions

Stock	Deleted segment
<i>Df(2R)Exel8057/ CyO,</i>	49F1-49F10
<i>Df(2L)r10, cn[1]/CyO</i>	35D1-36A7

<i>Df(2R)cos-2, cn<sup>1</sup> bw<sup>1</sup> sp<sup>1</sup>/CyO</i>	43B1--43B2
--	------------

### 2.1.3.5 EMS mutations, P-Element insertions and recombinant chromosomes

Stock	Description	Source/reference
<i>Adh<sup>n7</sup> lace<sup>2</sup> cn<sup>1</sup> vg<sup>1</sup>/CyO</i>	hypomorphic allele	Ashburner et al., 1990
<i>lace<sup>2</sup> 201Y Gal4</i>		This work
<i>lace<sup>2</sup> ;UAS- dscam [TM2]<sup>RNAi</sup></i>		This work
<i>y<sup>1</sup>; P{w[+mC]=lacW}lace<sup>K05</sup>/CyO</i>	letale P-Element-Insertion in lace	Gene Disruption Project members
<i>lace<sup>K05</sup> FRT40</i>		Georg Steffes, 2007
<i>lace<sup>K05</sup> UAS HA lace</i>		This work
<i>FRT42 Spt-I<sup>P1</sup></i>		Georg Steffes, 2007
<i>FRT42 Spt-I<sup>P1</sup> UASmGFP</i>		This work
<i>FRT42 Spt-I<sup>1626</sup></i>	hypomorphic allele	Georg Steffes, 2007
<i>Spt-I<sup>Q90</sup></i>	EMS allele	Sean Sweeney (unpublished)
<i>Spt-I<sup>C251Y</sup></i>	EMS allele	Sean Sweeney (unpublished)
<i>FRT42 Spt-I<sup>Q90</sup></i>		This work
<i>FRT42 Spt-I<sup>Q90</sup></i>		This work
<i>FRT42 Dscam<sup>21</sup></i>	Null allele	Hummel et al., 2003
<i>FRT42 Dscam<sup>21</sup> Spt-I<sup>III B2-009</sup></i>		Georg Steffes, 2007
<i>FRT42 Dscam<sup>33</sup></i>		Hummel et al., 2003
<i>FRT42 Dscam<sup>24</sup> Spt-I<sup>III B2-009</sup></i>		Georg Steffes, 2007
<i>FRT42 Dscam<sup>21</sup> Spt-I<sup>P1</sup></i>		this work
<i>FRT42 Dscam<sup>24</sup> Spt-I<sup>P1</sup></i>		this work
<i>sphingosine phosphatlyase<sup>5091</sup> (sply)</i>	P-Element-Insertion	Herr et al., 2003

### 2.1.3.6 RNAi Stocks for endocytosis analysis

Stock	Trans-formant ID	Chromosome	off targets	Source
<i>UAS Shi<sup>dsRNA</sup></i>	3799	III	1	VDRC
<i>UAS eps15<sup>dsRNA</sup></i>	8784	III	0	VDRC
<i>UAS hook<sup>dsRNA</sup></i>	12598	III	0	VDRC
<i>UAS hrs<sup>dsRNA</sup></i>	9846	II	0	VDRC
<i>UAS vps25<sup>dsRNA</sup></i>	8432	II	0	aus Fly
<i>UAS bchs<sup>dsRNA</sup></i>	6556	III	0	VDRC
<i>UAS ruby15<sup>dsRNA</sup></i>	7300	II	0	VDRC
<i>UAS Ap1γ<sup>dsRNA</sup></i>	3275	III	0	VDRC
<i>UAS Ap1σ<sup>dsRNA</sup></i>	12913	II	0	VDRC
<i>UAS PKD<sup>dsRNA</sup></i>	6491	II	0	VDRC
<i>Arf72A<sup>dsRNA</sup></i>	17826	III	0	vdrc
<i>Arf84F<sup>dsRNA</sup></i>	4433	III	0	VDRC

### 2.1.3.7 sphingolipids enzyme RNAi stocks

Stock		Chromosome	off tausets	Source
<i>UAS spt-I<sup>dsRNA</sup></i>	10021	III	1	VDRC
<i>UASlace<sup>dsRNA</sup></i>	21803	II	0	VDRC
<i>UASCDase<sup>dsRNA</sup></i>	40628	II	0	VDRC
<i>UAS Ugt86a<sup>dsRNA</sup></i>	8573	III	1	VDRC
<i>UAS GlcT-1<sup>dsRNA</sup></i>	44912	II	0	VDRC
<i>UAS sply<sup>dsRNA</sup></i>	37975	II	1	VDRC
<i>UAS SK1<sup>dsRNA</sup></i>	32930	II	0	VDRC
<i>UAS SK2<sup>dsRNA</sup></i>	41905	II	0	VDRC
<i>UAS CK<sup>dsRNA</sup></i>	43412	II	0	VDRC
<i>UAS SMase<sup>dsRNA</sup></i>	12226	III	1	VDRC
<i>UAS bbc<sup>dsRNA</sup></i>	7989	II	0	VDRC
<i>UAS PE -Cyt<sup>dsRNA</sup></i>	27460	II	0	vdrc

## 2.2 Methods

### 2.2.1 Genetic methods

#### Cultivation of flies

All stocks are kept at 25°C on *Drosophila* standard medium. For crossings virgin females were collected 0-4h after eclosion and crossed to males of various ages.

#### Clonal analysis

To circumvent the lethality of the alleles and allow the examination of ORN targeting defects in the adult olfactory system the FRT/FLP system was used that allows the tissue specific induction of mitotic clones (Xu and Rubin 1993).

For labeling ORNs, the Flipase was expressed under the control of the *eyeless* promoter (*eyFLP*). Several experiments required specific labeling of only few cells, in this case a flipase under the control of the *hsp70* promoter was used (*hsFLP*) (Golic and Lindquist 1989). During mitosis FLP induced recombination leads to different outcomes. Either the cells remain heterozygous or one homozygous mutant cell and one homozygous wild type cell is generated. If these cells divide, they form homozygous patches in the adult animal. To increase the size of the homozygous mutant clones a cell lethal mutation was introduced on the counter-chromosome leading to cell autonomous cell death thus favoring the homozygous mutant cells (Shipman-Appasamy, Cohen et al. 1991)

The FRT/FLP system can also be combined with the heterologous UAS/Gal4 expression system (Brand and Perrimon 1993). In addition, introducing a Gal80 element that suppresses Gal4, it allows visualizing homozygous mutant cells in a heterozygous or homozygous wild type background. This method is called “mosaic analysis with a repressible cell marker” (MARCM) (Lee and Luo 1999) (Figure. 2.1).

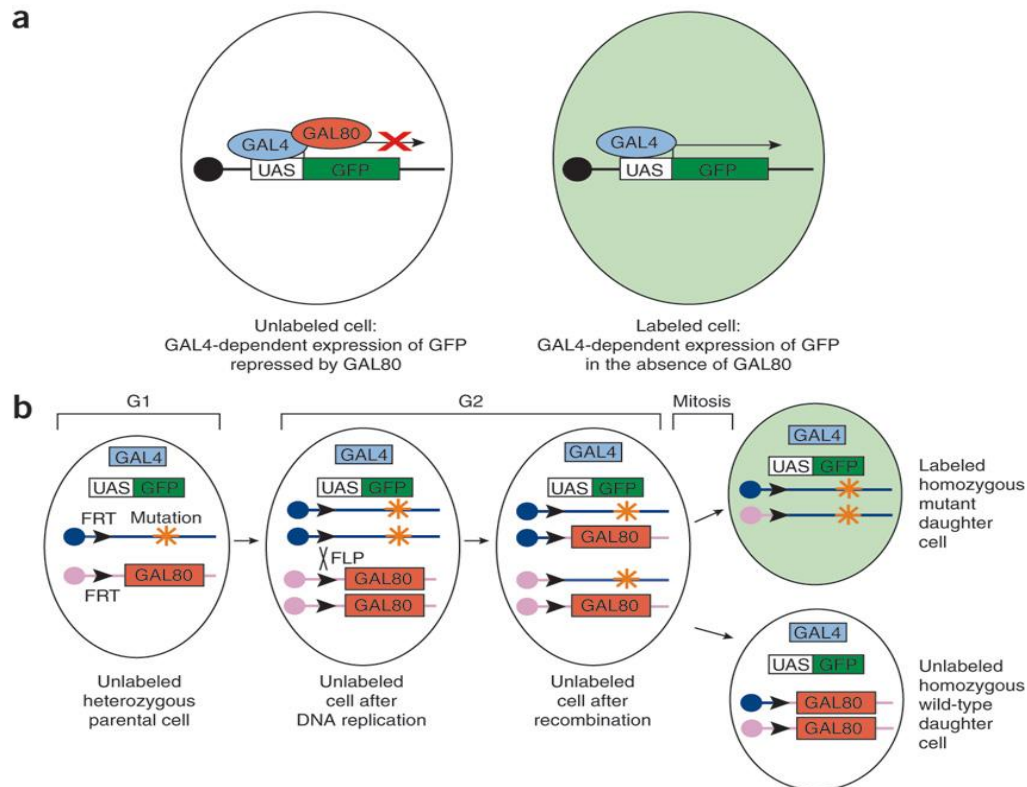


**Figure 2.1: Schematic of the GAL4–UAS system with GAL80 and the MARCM genetic system.**

(a) In cells containing the GAL80 protein, GAL4-dependent expression of a UAS–gene (GFP) is repressed. By contrast, cells containing GAL4 but lacking GAL80 will express the UAS–gene (GFP). (b) MARCM requires (i) two *FRT* sites located at the same position on homologous chromosomes, (ii) *GAL80* located distal to one of the *FRT* sites, (iii) *FLP recombinase* located anywhere in the genome, (iv) *GAL4* located anywhere in the genome except distal to the *FRT* site on the *FRT*, *GAL80* recombinant chromosome arm, (v) *UAS–marker* located anywhere in the genome except distal to the *FRT* site on the *FRT*, *GAL80* recombinant chromosome arm, and optionally (vi) a mutation distal to *FRT*, in *trans* to but not on the *FRT*, *GAL80* recombinant chromosome arm. Site-specific mitotic recombination at *FRT* sites (black arrowheads) gives rise to two daughter cells, each of which is homozygous for the chromosome arm distal to the *FRT* sites. Ubiquitous expression of GAL80 represses GAL4-dependent expression of a *UAS–marker* (*GFP*) gene. Loss of GAL80 expression in homozygous mutant cells results in specific expression of GFP. (From Joy S Wu1 & Liqun Luo Nature Protocols, 2007)

## 2.2.2 Histological methods

### Preparation technique of adult brains

Flies of the desired phenotype are anesthetized with CO<sub>2</sub> and immediately killed in 70% EtOH. The dead flies are washed with PBS three times. The flies are transferred to a silicon plate and covered with a drop of PBS to prevent drying out. The dissection process is schematically shown in Figure. 2.2. To dissect the brain, first the



proboscis is removed by grabbing it (I) with one pair of tweezers and holding the head down with the other (II). This leaves a hole (III) which is used to grab both sides of the head exoskeleton (IV). By carefully pulling to one side the first half is removed (V), subsequently the other (VI). The brain is now freely accessible (VI) and can be detached from the body. Optionally remaining tracheae can be removed.

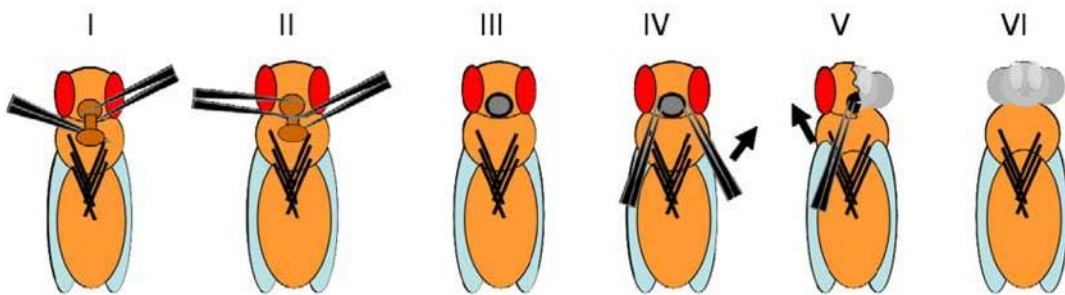


**Figure 2.2: Dissection method for adult brains ( from Christoph Scheper , 2009)**

### **Preparation of pupal brains**

To determine the age pupae have to be staged. The desired developmental stadium is selected. The pupae are carefully removed from the vial and transferred to a stripe of double sided adhesive tape. Next the operculum gets removed and the puparium gets cut longitudinally and carefully opened. The pupa is transferred carefully to a second stripe of tape and covered with PBT. Then a little hole is pinched in the anterior part of the pupae and slowly enlarged. The brain are picked out of the body and transferred to a fixation solution.

### **Antibody staining**

- 1) Fixate brains in 2% PFA for 90 minutes on a shaker
- 2) Remove fixation solution, add PBT

- 3) Wash 3x in PBT for 15 minutes
- 4) Block in 10% goat serum for 60min at room temperature -Incubate in first antibody at 4°C over night -Wash 3x in PBT for 15 minutes
- 5) Incubate in second antibody 3 hours at room temperature
- 6) Wash 3x in PBT for 15 minutes
- 7) Place specimen on a object slide, cover with a drop of VectaShield™ mounting medium
- 8) Put on cover slip with little rubber feet to prevent mechanical stress on the specimen
- 9) Store at 4°C

### **2.2.3 Biochemistry methods**

#### **Prepare membranes from fly heads**

- 1) Appropriate flies were decapitated and heads were collected
- 2) Put them into cold lysis buffer and broke by a dounce homogenizer with type B pestle until the pestle moved smoothly (approximately 8 times).
- 3) Homogenate was spun at 5000 rpm for 10 min at 4 °C to pellet nuclei, and the post-nuclear supernatant was collected, adjusted to 1.4 M sucrose, and distributed into TSL55 centrifuge tubes.
- 4) Post-nuclear supernatants were overlaid with 1.2ml of 1.22 M sucrose in TNE buffer and 0.6 ml of 0.1M sucrose in TNE buffer and then spun for 4hr at 50.000g at 4°C.
- 5) Membranes with a white, flocculent appearance were observed floating above the 1.22/0.1M interface, and membranes with a more yellowish homogeneous

appearance were observed at the 1.4/1.22M interface

- 6) Collect the membranes floating above the 1.22/0.1M interface .
- 7) The membranes were then resuspended in TNE buffer, aliquoted, and stored at  $-80^{\circ}\text{C}$ .

#### **Purification of detergent-insoluble membranes**

- 1) Membranes were thawed and washed in 3 volumes of TNE buffer to remove residual sucrose.
- 2) resuspend them in 350  $\mu\text{l}$  ice-cold TNE buffer to a phospholipid concentration of 880 nmol/ml.
- 3) Add an equal volume of prechilled 2% Triton X-100 , and the membranes were solubilized at  $0^{\circ}\text{C}$  for 30 min in TSL55 tubes.
- 4) After solubilization, adjust the membranes to a final concentration of 24% Optiprep<sup>TM</sup> (Nycomed Pharma AS); overlaid with 0.5ml of 21%, 0.7ml of 15% and 0.5ml 6% Optiprep in TNE buffer.
- 5) Centrifuge for 5 h at 45,000 g at  $2-4^{\circ}\text{C}$ .
- 6) Collect the insoluble membranes between the 6% and the 15% layers.

#### **SDS-Polyacrylamide gel electrophoresis (PAGE)**

Protein samples were dissolved in 1x SDS sample buffer and denatured at  $94^{\circ}\text{C}$  for 5min. 10 $\mu\text{l}$  sample and 2 $\mu\text{l}$  DualColor<sup>TM</sup> pre-stained protein standard (bio-rad) for estimation of protein sizes were loaded onto 10% tris-glycine acrylamide pre-cast gels and run at 100-140V . After completion, gels were prepared for western blotting.

**Western blotting**

Following SDS-PAGE, gels were blotted onto PVDF membrane (BioTrace) using the XCell II blotting module according to the manufacturer's manual (Invitrogen). To check transfer efficiency, blotted gels were subsequently stained with Coomassie Blue staining solution (BioRad) for 1h and de-stained with 7 % acetic acid. To detect blotted protein samples, PVDF membranes were blocked with 5% skim milk in 1xTBS/ 0.1%Tween-20 (TBST) for 1h and probed with primary antibody at 4°C overnight. Following overnight incubation the membrane was washed 5 times in 5% skim milk/TBST for 15min each. The membrane was subsequently probed with the secondary antibody anti-mouse IgG conjugated to horseradish peroxidase (HRP) at a 1:1500 dilution in 5% skim milk/TBST, at room temperature for 1h, rocking. After 5 repeated washes in 5% skim milk/TBST for 15min each, the blotted membrane was developed using the ECL Detection system (Amersham, BD Biosciences), according to the manufacturer's protocol. Kodak x-ray film was used for development in the AGFA Curix 60 developing machine.

### 3 RESULTS

#### 3.1 Identification of genes involved in olfactory targeting in *Drosophila*

To identify novel genes required for proper development and function of the olfactory system in *Drosophila*, a forward genetic screen was performed previously (Steffes 2007). In short, flies carrying a FRT cassette on the second chromosome (*FRT40/FRT42*) were fed with Ethyl methanesulfonate (EMS) and the mutagenized chromosomes were established. To circumvent homozygote lethality the FRT/FLP system was used for inducing mitotic clones in the developing eye-antennal imaginal disc. The mutant chromosomes were examined for the ORN axon innervations pattern visualized via multiple ORN-Gal4 driven synaptotagmin-GFP. In totally, about 5000 mutant lines were screened, of which about 5% showed innervation defects. Several complementation groups could be identified, indicating a high degree of saturation of the screen.

Two of the genes identified in the mosaic screen encode the subunits of *Serine palmitoyl CoA transferase (SPT)* (Steffes 2007). The *Drosophila SPT* is a membrane-bound heterodimer of *LCB1* and *LCB2*, which is the *de novo* sphingolipid biosynthetic enzyme (Figure 3.1 A). The *Spt-I* gene encodes the *LCB1* subunit, which locates at chromosomal position 49F4 on the right arm of the second chromosome. Totally, four *spt-I* alleles are used for my study. Two *spt-I* alleles, *spt-I<sup>IIIB2</sup>* (an EMS allele leading to the base exchange Gly127Glu) and *spt-I<sup>P1</sup>* (a P insertion at Glu295) were isolated from the mutagenesis screen (Steffes 2007). Another *P {lacW}*-insertion *l(2)<sup>SH1626</sup>* in the 5'UTR of *spt-I* is from Szeged *Drosophila* stock center. An additional allele, *spt-I<sup>Q90 stop</sup>* missense mutation was kindly provided by Dr. Sean T Sweeney

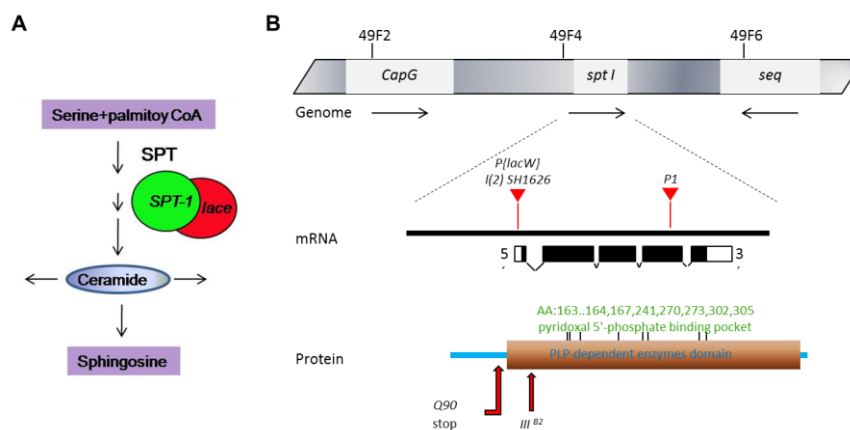


**Figure 3.1: Structural organization of the Serine palmitoyltransferase (SPT) enzyme and *spt-I* gene**

(A) Schematic of serine palmitoyltransferase (SPT) in sphingolipid metabolism pathway. SPT is a membrane-bound heterodimer of SPT-I and Lace in *Drosophila*, which is the *de novo* sphingolipid biosynthetic enzyme. (B) Schematic representation of the *spt-I* gene. It locates in 49F4. The arrows denote the transcriptional direction of each gene. The positions of the coding exons and noncoding introns (filled and open boxes, respectively) of the *spt-I* gene are indicated in the middle. The P insertion site in the *SH1626* and *P1* alleles are indicated by the inverted triangle. The protein structure is showing in lower diagram. The EMS alleles are marked by red arrows, including *Q90 stop*, and *III B2* missense mutations.

(unpublished). The *lace* gene encodes the *LCB2* subunit and maps to chromosomal region 35D1-4 on the left arm of the second chromosome. *lace* alleles used in this study include a *P{lacW}* insertion *l(2)<sup>k05305</sup>*, which inserts 8–10bp upstream of the *lace* transcription start site (Adachi-Yamada, Gotoh et al. 1999). Two additional *lace* EMS mutations, *lace<sup>U17</sup>* (Bernd Goellner, 2005) and *lace<sup>2</sup>* (Ashburner et al., 1990) have not been characterized molecularly yet.

All the *spt-I* and *lace* mutations described above are homozygous lethal at early larval stage. The four *spt-I* alleles (Figure. 3.1B) described above fail to complement each other. However, *lace<sup>k05</sup> / lace<sup>2</sup>* trans-heterozygotes grew into adults and show similar neuronal defects as homozygous *lace<sup>k05</sup>* clones. In contrast, *lace<sup>U17</sup>* failed to complement *lace<sup>k05</sup>* and *lace<sup>2</sup>*, indicating *lace<sup>U17</sup>* is a strong allele.

**Table 3.1: summary of *spt-I* and *lace* alleles used in this study**

<i>Spt</i> alleles	type	change ment	Phenotype					
			<i>21a</i>	<i>47a</i> (mistargeting/AL)	<i>47b</i>	<i>88a</i>	<i>46a</i>	<i>59c</i>
<i>spt-I</i> <sup>SH1626</sup>	P-Element	Insertion in 5' UTR	0 (n=16)	0.75 (n=16)	0 (n=12)	0 (n=12)	0 (n=14)	0 (n=10)
<i>spt-I</i> <sup>P1</sup>	P-Element	Insertion in Glu 295	n.d.	1.92 (n=24)	55% (n=20)	44% (n=18)	40% (n=15)	27% (n=18)
<i>Spt-I</i> <sup>Q90</sup>	EMS	Q90 stop	n.d.	2.6 (n=12)	81% (n=16)	n.d.	71% (n=24)	n.d.
<i>lace</i> <sup>2</sup>	EMS	n.d.	n.d.	n.d.	n.d.	n.d.	n.d.	n.d.
<i>lace</i> <sup>K05</sup>	P-Element	Insertion in 5' UTR	5/20	1 (n=16)	30% (n=10)	31% (n=16)	20% (n=10)	21% (n=14)
<i>lace</i> <sup>U17</sup>	EMS	n.d.	13/18	1.5 (n=30)	50% (n=10)	72% (n=16)	61% (n=18)	40% (n=10)
<i>lace</i> <sup>K/lace</sup> <sup>2</sup>	hypomorph	—	38% (n=8)	0.85 (n=14)	60% (n=10)	80% (n=10)	86% (n=14)	90% (n=10)

### 3.2 *spt* function in the *Drosophila* olfactory system.

#### 3.2.1 *spt* is required for class-specific ORNs targeting.

To test *spt* function in ORNs targeting, we first check antennal *ORN47a*, *47b*, *88a* and *21a* projections. In wild-type, *ORN47a* innervate the dorsally located DM3 glomerulus. Or47b and Or88a from the same sensillum project to neighbor glomeruli, VA1v and VA1d respectively. ORN21a project to the most ventrally located V glomerulus (Figure 3.2 B, E, H and K). In large *spt* mosaic clones (Minute technique, see M&M), the antennal Or47a show strong mistargeting defects (Figure 3.2 C-D) and this phenotype is highly penetrant (80%, n > 50). *Spt-I*<sup>P1</sup> and *lace*<sup>U17</sup> mutant Or47b axons innervate into VA1v in all samples, however mistargeting to dorsal regions and misshape glomerulus are frequently observed (Figure 3.2 F-G). Or88a localized in same sensillum with Or47b, has a very similar phenotype (Figure 3.2 I-J). For Or21a,

mutant axons leave the nerve, turn ventrally as in wild-type, but innervate ectopic positions within the ventral region of the antennal lobe (Figure 3.2 L). In some other samples, Or21a mutant axons do not turn ventrally and terminate more dorsally and central regions of the lobe. (Figure 3.2 M).

Next, we test the projections of two different classes of maxillary palp ORNs, Or46a, and Or59c, which extend their axons via the labial nerve and through the suboesophageal ganglion prior to entering the antennal lobe (Figure 3.2 O and R). Mutant *Spt-I*<sup>P1</sup> and *lace*<sup>U17</sup> ORNs of these two classes frequently terminated upon entering the ventral CNS before reaching the antennal lobe, either immediately prior to entering the suboesophageal ganglion or upon exiting it, just ventral to the antennal lobe (Figure 3.2 P, Q, S and T).

Taken together, *spt* mutant antennal ORNs appear to mistargeting when the axons are within the target region. In contrast, maxillary palp mutant ORN axons are pre-stopping before they reach the target.

### **3.2.2 *Spt-I* and *lace* mutations exhibited identical phenotypes in the olfactory system.**

We found *spt-I*<sup>P1</sup> and *lace*<sup>U17</sup> had identical phenotypes in ORNs targeting (Figure 3.2). It is interesting to compare all of the alleles mentioned above. We then compare antennal ORN47a and maxillary palp ORN46a for all of the *spt-I* and *lace* alleles. Mutant ORN47a axons mistarget to ventral, medial, and dorsal regions of the lobe, largely reflecting the distribution of ORN47a fibers as they project dorsally toward DM3 glomerulus (Figure 3.3 B-H). Moreover, this phenotype is highly penetrant (>75%, n=30) even in weak hypomorphic alleles *lace*<sup>K05</sup>, which indicate ORN47a phenotype is more sensitive for the loss of *spt* than other classes.



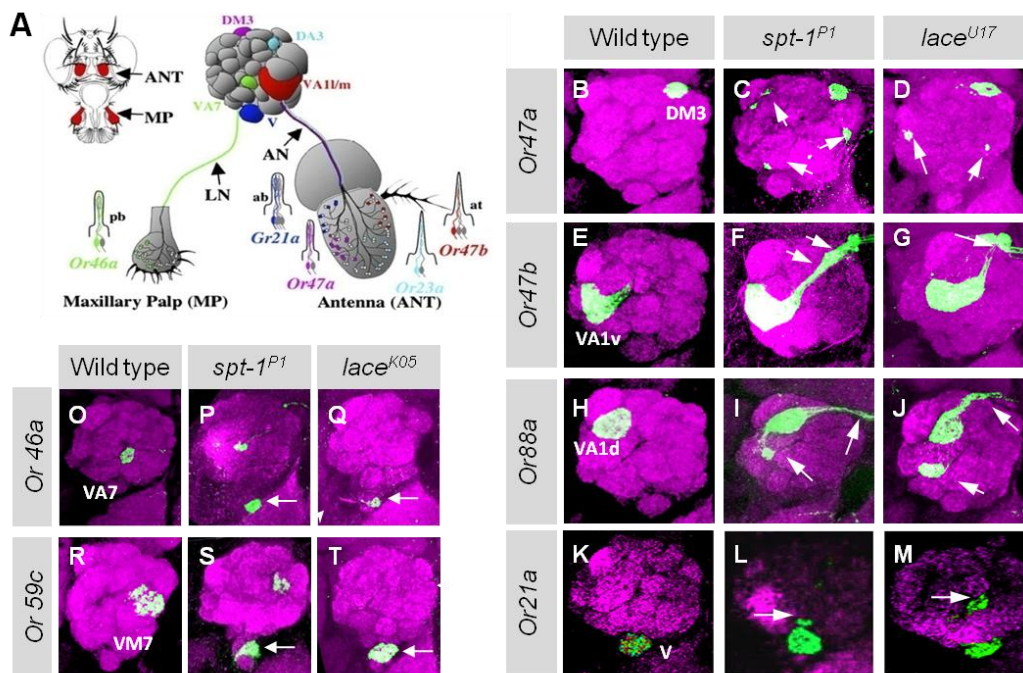


**Figure 3.2: Mutations of *spt-1* and *lace* disrupt ORN axon targeting**

(A) Organization of the *Drosophila* adult olfactory system. The two main olfactory organs, the antenna and the maxillary palps are covered with different types of sensilla, from which a subset of sensilla basiconica (ab and pb) and sensilla trichoid (at) are shown. Inside each sensillum, olfactory receptor neurons (ORNs) expressing specific odorant receptors (ORs) are housed. The sensilla of the same type (e.g., ab1) are distributed in a distinct antennal surface region and project their axons to a specific glomerulus in the antennal lobe (AL). (B, E, H and K) Targeting of wild-type multiple ORNs axons to their appropriate glomeruli. (C, F, I and L) *spt-1<sup>P1</sup>* and (D, G, J and M) *lace<sup>U17</sup>* antennal mutant ORNs Axons target to incorrect glomeruli in the antennal lobe. Genotype: (B, E, H, K, O and R) *eyFLP; FRT42/PCNA FRT42; ORN>sytGFP*. (C, F, I and L) *eyFLP; SPT-1<sup>P1</sup> FRT42/PCNA FRT42; ORN>sytGFP*. (D, G, J and M) *eyFLP; lace<sup>U17</sup> FRT40/cycE FRT40; ORN>sytGFP*. (D, H, L and P) *lace<sup>2</sup>/lace<sup>K05</sup>; ORN>sytGFP*. (P and S) *eyFLP; FRT42/PCNA FRT42; ORN>sytGFP*. (Q and T) *eyFLP; lace<sup>U17</sup> FRT40/cycE FRT40; ORN>sytGFP*. (Green: GFP; magenta: Ncad)

Mutant ORN46a axons were frequently stopping outside of AL in all the alleles (Figure 3.4 B-H). However, ORN46a did not stop prematurely within the labial nerve but terminated upon encountering neuropil and forming a structure with the appearance of a glomerulus within it (Figure 3.4 C), suggesting this phenotype does not simply reflect defects in axon outgrowth.

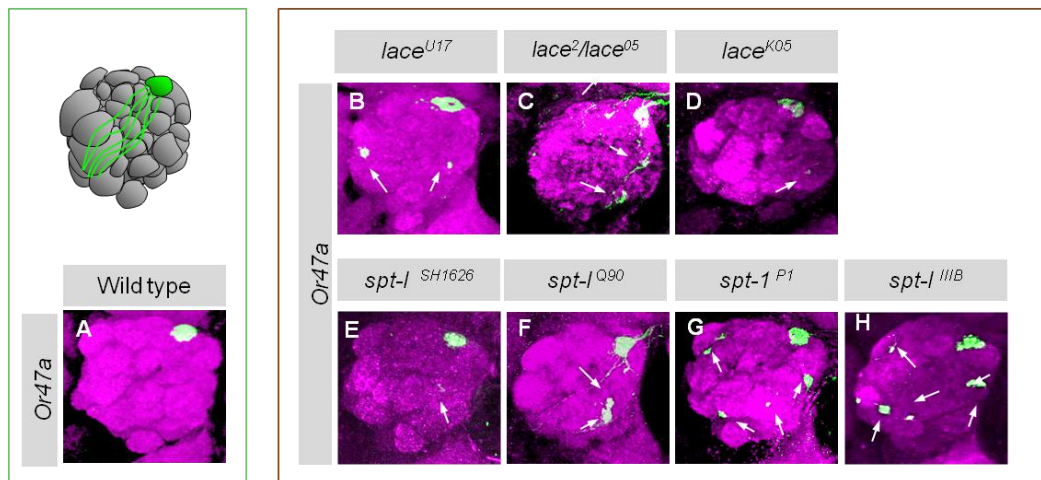


**Figure 3.3: *spt-I* and *lace* have similar ORN phenotypes for *ORN47a***

Mutant *ORN47a* axons mistarget to ventral, medial, and dorsal regions of the lobe. Genotype: (A) *eyFLP*; *FRT42/PCNA FRT42*; *Or47a Gal4 UAS sytGFP*. (B and D) *eyFLP*; *lace* alleles *FRT40/CycE FRT40*; *Or47a Gal4 UASsytGFP*. (C) *lace<sup>2</sup>/lace<sup>05</sup>*; *Or47a Gal4 UASsytGFP*. (E-H) *eyFLP*; *spt-I* alleles *FRT42/PCNA FRT42*; *Or47a Gal4 UAS sytGFP*. (Green: GFP; magenta: Ncad)

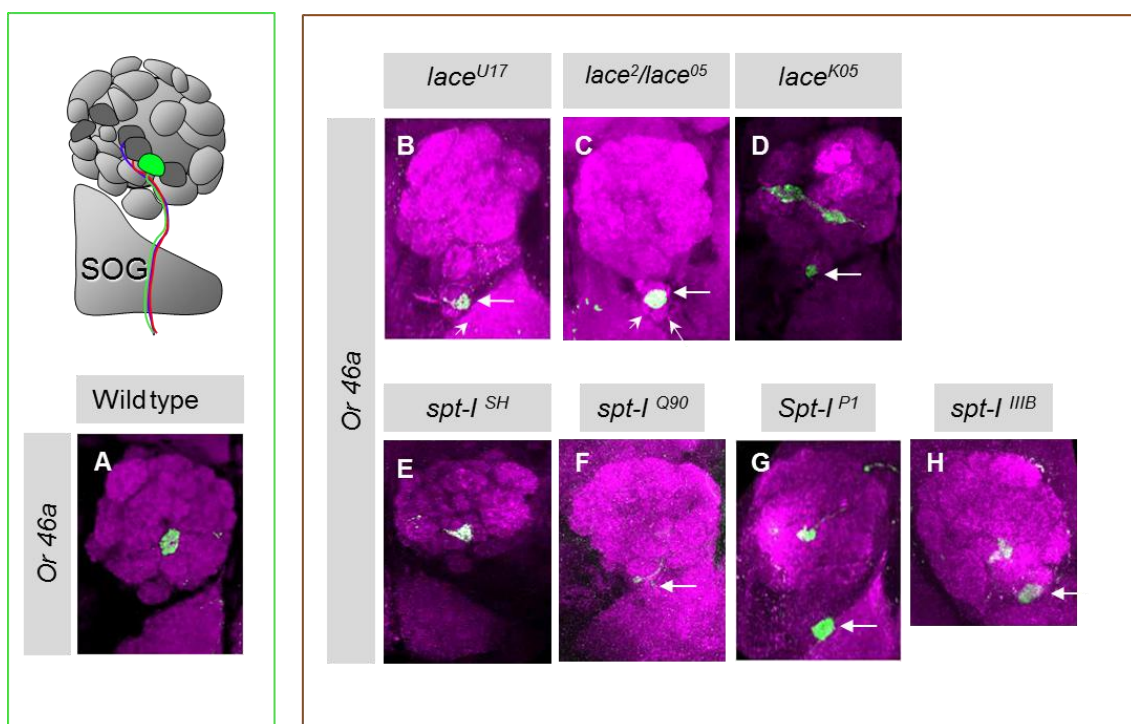


**Figure 3.4: *spt-I* and *lace* alleles have similar phenotypes for maxillary palp *46a* ORNs.**

ORNs from maxillary palp show short-stopping phenotypes in *spt-I* and *lace* mutants. Genotype: (A) *eyFLP*; *W+ FRT42/PCNA FRT42*; *Or46a Gal4 UASsytGFP*. (B and D) *eyFLP*; *lace* alleles *FRT40/CycE FRT40*; *Or46a Gal4 UASsytGFP*. (C) *lace<sup>2</sup>/lace<sup>K05</sup>*; *Or46a Gal4 UASsytGFP*. (E-H) *eyFLP*; *spt-I* alleles *FRT42/PCNA FRT42*; *Or46a Gal4 UASsytGFP*. (Green: GFP; magenta: Ncad)

As multiple ectopic glomerulus-like structures were seen with nc82 staining surrounding the ectopic glomerulus innervated by the labeled ORNs (Figure 3.4 C, arrows), it seems that different classes of maxillary palp *spt* mutant ORNs segregate into distinct ectopic glomeruli. Hence, *spt* acts in maxillary palp ORNs to prevent targeting to an inappropriate neuropil. Moreover, *lace* transheterozygotes show the highest penetrance of the ORN46a pre-stopping phenotype, indicating non-cell autonomous effect in *spt* mutants.

Overall, these results indicate all of *spt* alleles we test here have identical phenotypes, which suggest that *spt* plays an important role in ORNs targeting.

### 3.2.3 *spt* mutants do not affect axon sorting among maxillary palp ORNs

During the olfactory map formation, ORN axons project into a single glomerulus sorting out from the neighbor classes.

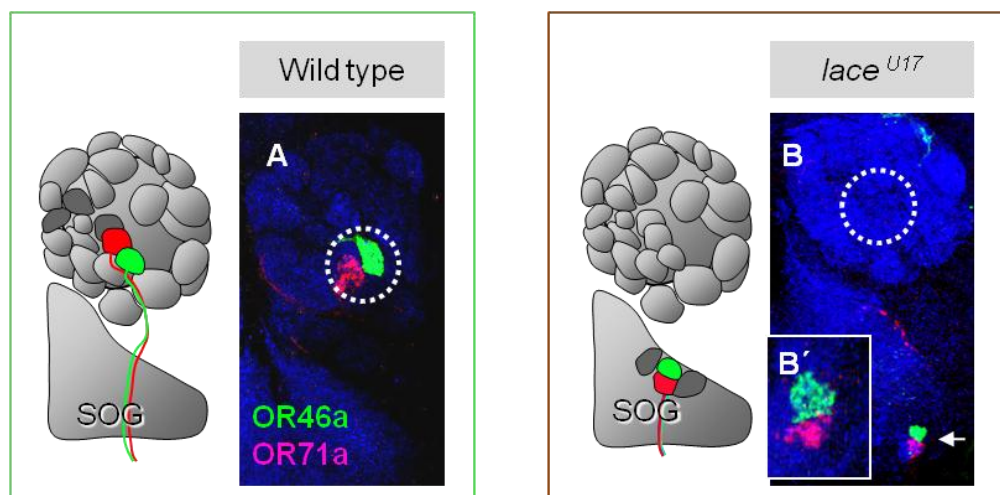


**Figure 3.5: *lace* does not affect axons sorting of maxillary palp ORNs**

Simultaneous labeling of the ORN classes 46a and 71a showed two distinct glomerular units in the wild-type AL (A) and this boundary is also cleared separated in *lace* mutant ALs (B and B'). Genotype: (A) *eyFLP; FRT40/cycE FRT40; Or46a::sytGFP 71a-Gal4 UAS-CD2*. (B and B') *eyFLP; lace<sup>U17</sup> FRT40/ cycE FRT40; Or46a::sytGFP 71a-Gal4 UAS-CD2*. (Green: Syt-GFP; red: CD2; blue: Ncad)

To test these sorting events in *spt* mutant, I perform double labeling of the maxillary ORN classes 46a/71a, which cohabit the pb2 sensillum and project their axons to the

---

neighbor glomeruli of VA7 and VC2. In wild type, *ORN46a/71a* project onto their target glomeruli with clear boundary (Figure 3.5 A). In contrast, *spt* mutant *ORN46a/71a* stops outside the AL, forming ectopic glomeruli. However, the boundary of these ectopic glomeruli is also clear. (Figure 3.5 B), indicating the sorting of *ORN46a /Or71a* axons are not affected.

### **3.2.4 ORNs targeting is not affected in MARCM clone, but the fine structure of individual mutant axon terminals within glomerulus is abnormal**

We observed that mutant *spt* ORNs targeting in MARCM are generally normal (Figure 3.6 compare A and B), indicating ORNs targeting phenotype only occur in large clone. I was curious about the single axon projection since it might be more sensitive to the whole projection change. To test targeting behavior of individual *spt* mutant axon, we generated small clones using FLP recombinase under the control of the heat shock-inducible promoter *hsp70* (see M&M). In wild type, single *ORN47b* axon reached VA1V and formed presynapse with normal morphology. In contrast, single *spt* mutant *ORN47b* terminals that reached their appropriate glomerulus failed to elaborate the thin arbors network. (Compare Figure 3.7 A' with B' and C'). The defects of *spt* mutant terminals in normal target glomeruli indicate that *spt* is required to form or maintain normal synapse morphology within the appropriate glomerulus. Also suggest that targeting defects happened in severe sphingolipid depletion, but synapse morphology is more sensitive.



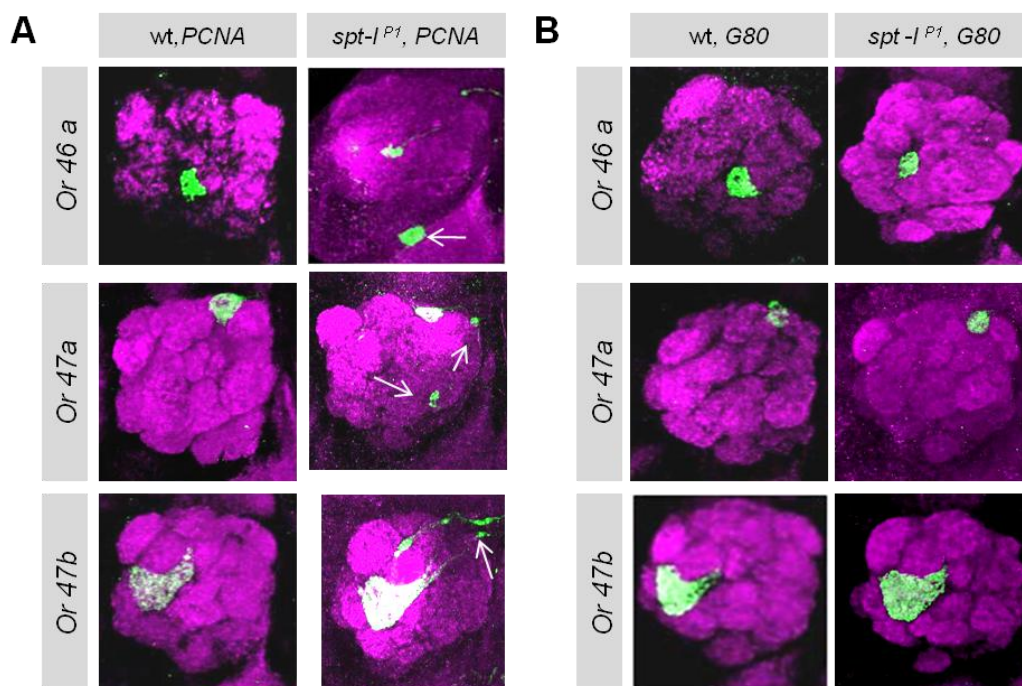


**Figure 3.6: ORNs targeting seems unaffected in *spt* MARCM clone**

(A) Mutant *spt* ORNs targeting in PCNA clones are affected. (B) Mutant *spt* ORNs targeting in MARCM are generally normal. Genotype: (Figure A. left column) *eyFLP; FRT42/ PCNA FRT42; ORN>syGFP*. (Figure A. right column) *eyFLP; Spt-I<sup>P1</sup> FRT42/ PCNA FRT42; ORN>syGFP*. (Figure B. left column) *eyFLP; FRT42/ G80 FRT42; ORN>syGFP*. (Figure B. right column) *eyFLP; Spt-I<sup>P1</sup> FRT42/ G80 FRT42; ORN>syGFP*. (Green: GFP; magenta: Ncad )

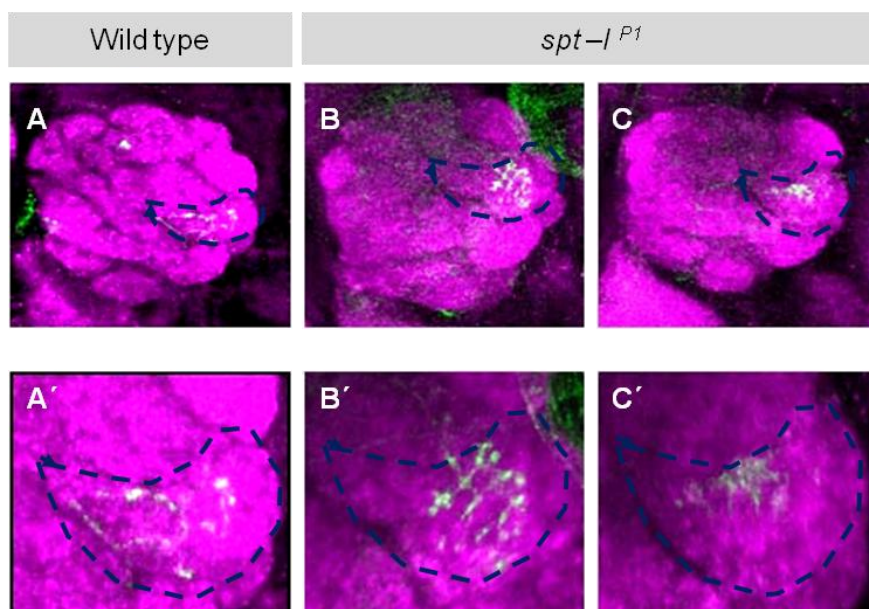


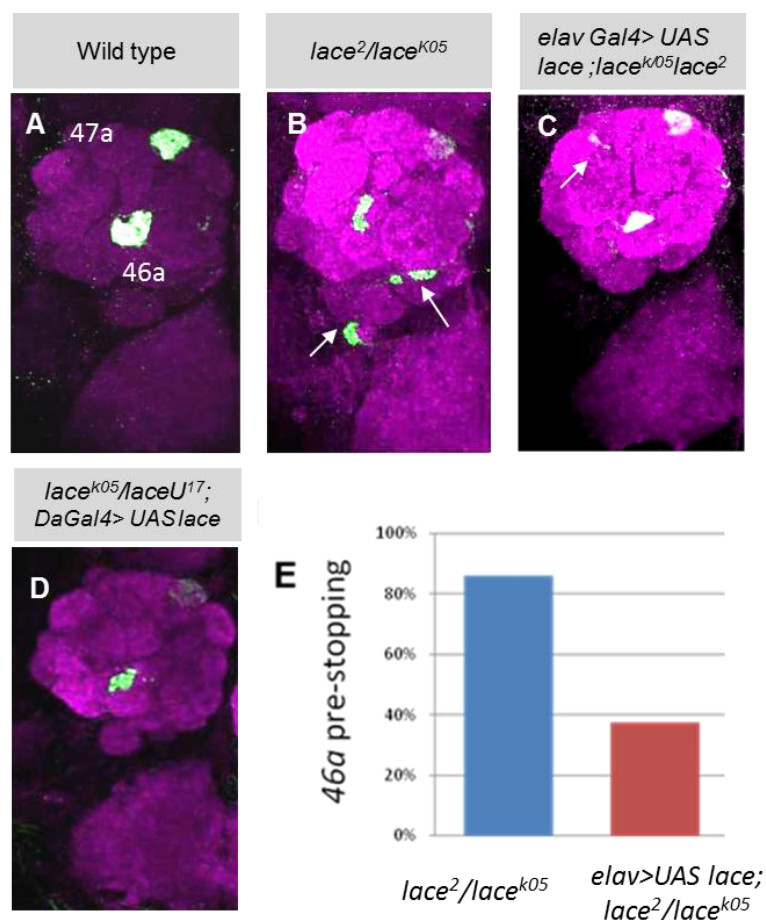
**Figure 3.7: *spt* mutant fibers have abnormal terminal morphology**

Single *spt* mutant *ORN7b* was generated by heat shock-induced mitotic recombination. Single axons are indicated with an arrowhead in the Figures. (A and A') Single wild-type ORNs shown for *ORN7b*, typically branch extensively throughout the target glomerulus. (B, B', C and C') *spt*

mutant *ORN47b* terminals did not extend processes throughout the glomerulus but remained restricted to small domains. Genotype: (A and D) *hsFLP; FRT42/ G80 FRT42; Or47b Gal4 UAS mGFP*. (B, B', C and C') *hsFLP; spt-I<sup>P1</sup> FRT42/G80 FRT42; Or47b Gal4 UAS mGFP*. (Green: GFP; magenta: Ncad)

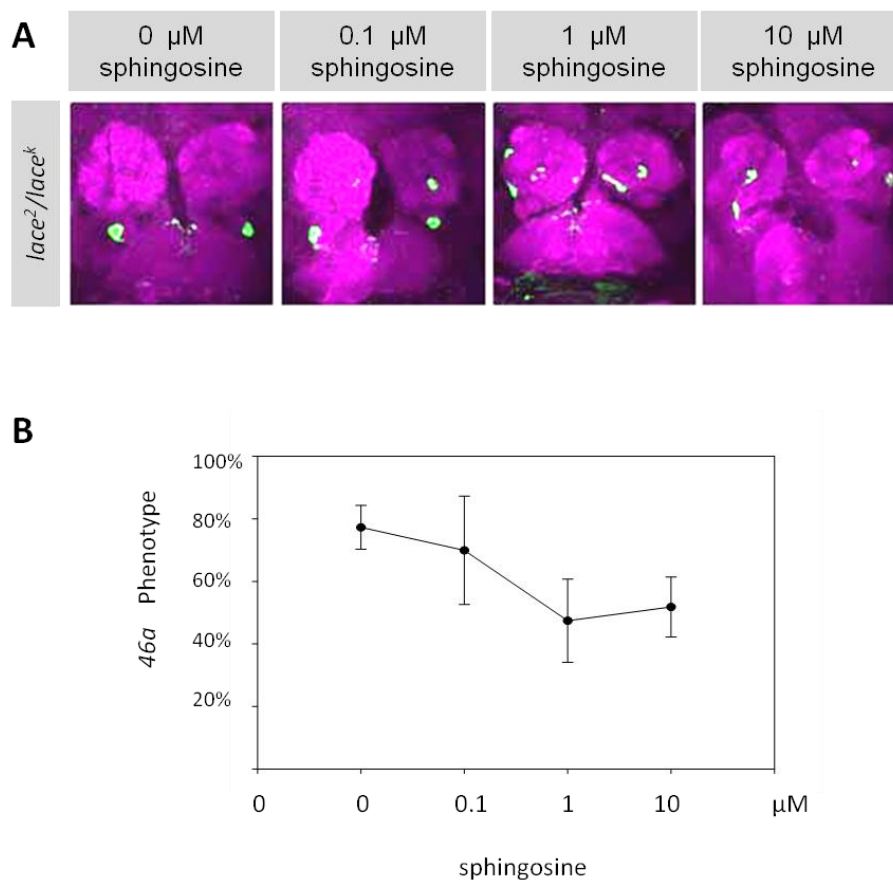
### 3.2.5 Rescue of the *lace* phenotype

To rescue *lace* phenotype, wild type *lace* was expressed in *lace<sup>K05</sup>/lace<sup>2</sup>* background driven by the pan-neural driver, *elav-GAL4* or *da Gal4*. In *lace<sup>K05</sup>/lace<sup>2</sup>* background, *ORN46a* pre-stopping phenotype was partially rescued by *elav-GAL4* driven wild type *lace* expression (Figure 3.8 C and E). Rescued by ubiquitous driver, *daGal4Not*, in the *lace<sup>K05</sup>/lace<sup>U17</sup>* background (*lace<sup>K05</sup>/lace<sup>U17</sup>* is lethal in first larvae stage), flies can grow up to adults with normal *ORN46a* projection (Figure 3.8 D).



**Figure 3.8: Genetic rescue of *lace* phenotype**

(A) *ORN46a* and *ORN47a* have normal projection pattern in Wild type. (B) *ORN46a* axon stop outside of antenna lobe under *lace<sup>2</sup> / lace<sup>K05</sup>* transheterozygots . (C) *ORN46a* axon pre-stopping is recovered when express *lace* by *elav Gal4* driver. (D) *lace<sup>K05</sup> / lace<sup>U17</sup>* survive to adult stage and with normal *ORN46a* projection when express *lace* by *Da gal4* diver.(E) quantification of *ORN46a* axon stopping phenotype in *lace<sup>2</sup> / lace<sup>K05</sup>* transheterozygotes and the rescue situation, indicating the phenotype can be rescued by genetic bring back a wild type *lace*. Genotype: (A) *46a:: sytGFP, 47a:: sytGFP*. (B) *lace<sup>2</sup> / lace<sup>K05</sup> ; 46a:: sytGFP, 47a:: sytGFP*. (C) *elav Gal4; lace<sup>2</sup> / lace<sup>K05</sup> UAS HA lace; 46a:: sytGFP, 47a:: sytGFP*. (D) *lace<sup>U17</sup> / lace<sup>K05</sup> UAS HA lace; 46a:: sytGFP, 47a:: sytGFP / Da Gal4*. (Green: GFP; magenta: Ncad )

**Figure 3.9: Rescue of *lace* mutants by feeding sphingosine**

When D-erythrosphingosine was added to the diet, *ORN46a* phenotype of the *lace* mutant was rescued at high concentration 1 $\mu$ M and 10 $\mu$ M sphingosine. Genotype in panel A: *lace<sup>2</sup> / lace<sup>K05</sup> ; 46a Gal4 UAS sytGFP*. (Green: GFP; magenta: Ncad )

A rescue of *lace* mutants has also been performed by feeding sphingosine.

*lace<sup>K05</sup> / lace<sup>2</sup>* heterozygotes larvae were reared on diets containing various

concentrations of sphingosine. *ORN46a* projection defects were counted. A partial rescue was found at the concentration of 1mM and 10mM sphingosine (Figure 3.9). The food rescue gives a hint that it is not the loss of the SPT protein itself leading the phenotype but one or several metabolic intermediate having important function in axon targeting.

### **3.2.6 *lace* mutations have weak phenotype at lower temperature**

The length and the degree of unsaturation of fatty acid chains of the membrane lipids have a profound effect on membrane fluidity. Sphingolipids contain long and saturated amide-linked fatty acyl chains and pack more tightly together, thus giving sphingolipids much higher melting temperatures than membrane glycerophospholipids. This tight acyl chain packing is essential for raft lipid organization.

The membrane lipid bilayer is normally highly fluid. But at low temperatures, bilayers exist in a frozen state. The frozen state is referred to as the gel, solid-ordered phase. I speculated that lost sphingolipids might affect the fluidity of cell membrane, which further affect membrane protein function. To test this hypothesis, I compared the *lace* phenotype in different temperature, I found that *lace* mutations have weak phenotype under 18 degree (Figure 3.10). Briefly, *lace* transheterozygotes progeny were raised under 18°C, 25°C and 29°C. Five ORNs (21a, 23a, 46a, 47a, 47b) were labeled in the mutants. At 29°C and 25°C, the ORNs projection pattern of *lace* were disrupted, and ORN46a pre-stopping was frequently observed. However, much weaker axonal defect was observed at 18°C (Figure 3.10 A and B). Therefore, *lace* mutant phenotype can be suppressed under lower temperature, suggesting that lost



sphingolipids might affect membrane function due to lost the solid organization region.

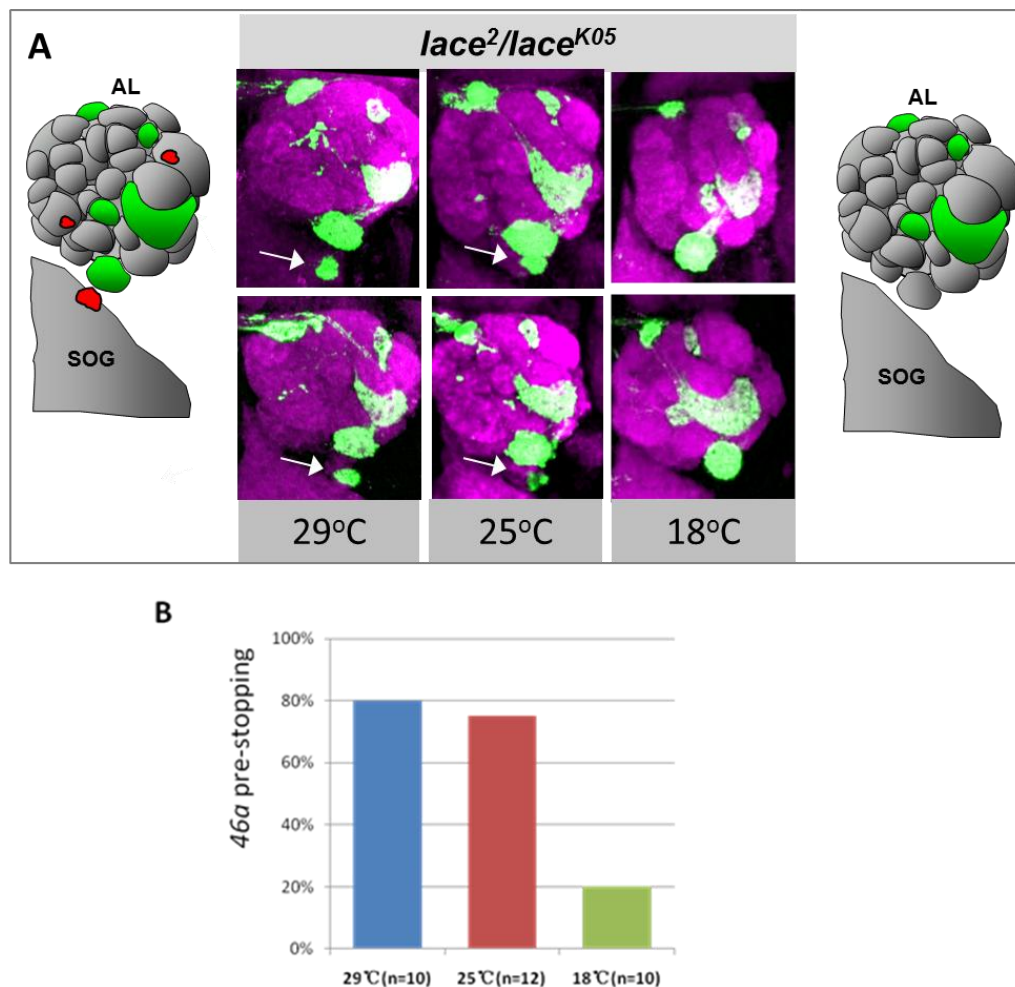


**Figure 3.10: Influence of the temperature on the *lace* phenotype**

(A) Compare the phenotype at different temperature. Five OR driven synaptotagmin-GFP give a normal projection pattern as shown in the right carton. Under 29°C and 25°C, whole projection pattern was disrupted. Additional OR positive glomeruli were innervated (shown as red spots in left carton) and *ORN46a* pre-stopping often observed (arrows). (B) Quantification of *ORN46a* phenotype under different temperature.

Genotype:*lace<sup>2</sup>/lace<sup>K05</sup>* multiple ORN (21a, 23a, 46a, 47a, 47b)-sytGFP. (Green: GFP; magenta: Ncad )

### 3.2.7 Genetic dissection of sphingolipid function in ORNs targeting

Sphingolipids are a family of phospholipids and glycolipids built upon sphingoid base backbones, including both the simple sphingolipids and the complex glycosphingolipids. Sphingolipids are important structural components of cellular membrane and they are also associated with the phase separation of plasma membrane into raft components (Hensel, Hermann et al. 1999). Sphingolipids involved in several biological processes such as signal transduction (Kitatani, Idkowiak-Baldys et al. 2007), cell survival (Obeid, Linardic et al. 1993) and migration (Hannun and Obeid 2008)

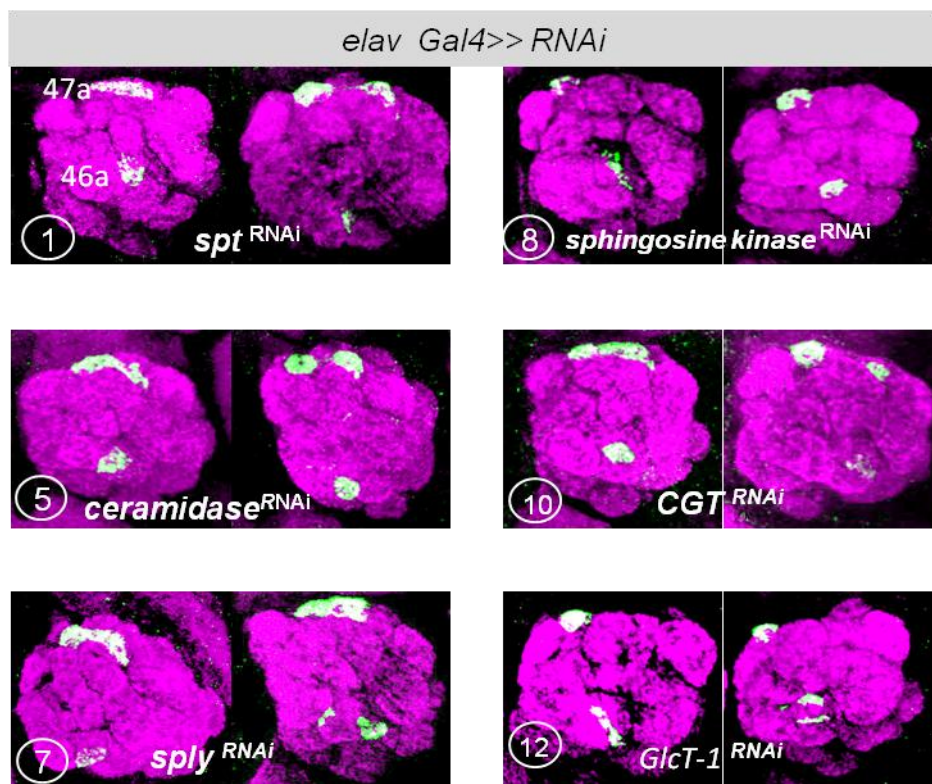


**Figure 3.11: Genetic dissection of *spt* defects in ORNs by *elav Gal4* driven RNAi**

Knockdown of different “sphingolipid synthesis enzymes” by *elav Gal4* driven RNAi. The number is corresponding to the Figure 1.3 Most of them give *ORN47a* phenotype, which is not identical to *spt* phenotype. And *ORN46a* projection looks normal. Genotype: *elavG4; enzyme RNAi*????

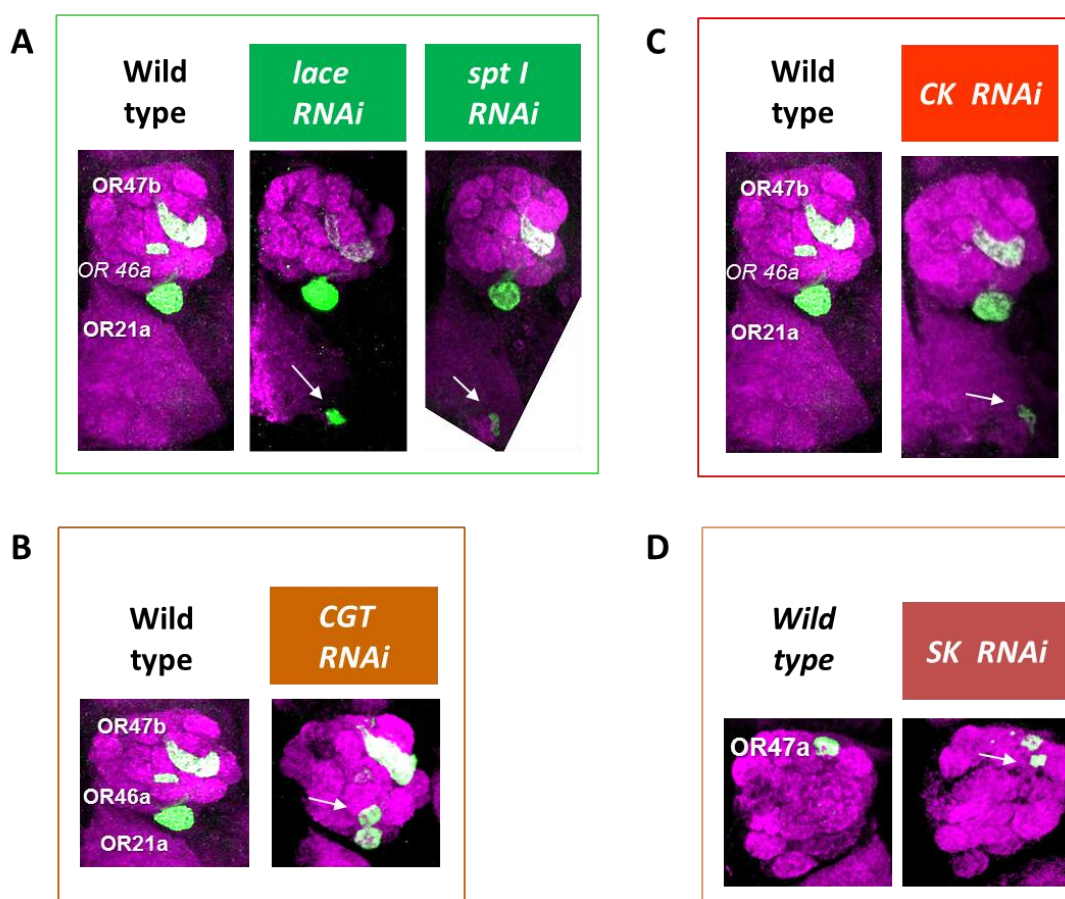
**Table 3.2: Genetic dissection of *spt* defects in ORNs**

<i>Gene</i>	<i>CG</i>	Trans- formant ID	on target	off target	Phenotype			
					<i>elav G4</i>		<i>elav G4+ ey G4</i>	
					<i>21a</i> (ectopic projection)	<i>46a</i> (stopping)	<i>21a</i> (ectopic projection)	<i>46a</i> (stopping)
<i>Spt-1</i>	<i>CG4016</i>	21805	1	0	0(n>10)	1/10	0(n>10)	1/8
<i>lace</i>	<i>CG4162</i>	1973	1	0	0(n>10)	0(n>10)	0(n>10)	3/16
<i>CDase</i>	<i>CG1471</i>	3129	1	0	0(n>10)	0(n>10)	0(n>10)	0(n>10)
<i>Ugt 86a</i>	<i>CG18578</i>	8573	1	1	0(n>10)	1/16	6/14	0(n>10)
<i>GlcT-1</i>	<i>CG6437</i>	44912	1	0	0(n>10)	0(n>10)	0(n>10)	0(n>10)
<i>sply</i>	<i>CG8946</i>	37974	1	1	0(n>10)	0(n>10)	0(n>10)	0(n>10)
<i>SK1</i>	<i>CG1747</i>	32930	1	0	0(n>10)	0(n>10)	0(n>10)	0(n>10)
<i>SK2</i>	<i>CG32484</i>	41905	1	0	0(n>10)	0(n>10)	0(n>10)	0(n>10)
<i>CK</i>	<i>CG16708</i>	43412	1	0	0(n>10)	0(n>10)	0(n>10)	3/22
<i>SMase</i>	<i>CG3376</i>	12227	1	1	0(n>10)	0(n>10)	0(n>10)	0(n>10)
<i>bbc</i>	<i>CG6016</i>	7989	1	0	0(n>10)	0(n>10)	0(n>10)	0(n>10)
<i>PE-Cyt</i>	<i>CG5547</i>	27460	1	0	0(n>10)	0(n>10)	0(n>10)	0(n>10)

In our studies, we found *spt* mutants have the ORNs targeting defects and we speculated that one or several sphingolipids are important for the neuronal guidance. However, the *de novo* sphingolipid biosynthetic pathway is not a simple linear sequence of enzymatic reactions responsible for generating the products ceramide, sphingosine, sphingosine 1-phosphate and complex sphingolipids.

To identify the critical component in the sphingolipid biosynthesis, taken the advantage of RNA interference, I tried to decipher the sphingolipid function in neuronal targeting, by knocking down the enzymes in the sphingolipid metabolism pathway. First, by *elavGal4* driven the RNAi, I found *ORN47a* was defected in all depleted enzymes (Figure 3.11). However, this phenotype is not identical to *ORN47a* ectopic projection phenotype in *spt* mutants. In contrast, *ORN46a* has a lower

penetrance of pre-stopping phenotype for *spt-1* RNAi (10%, n=10). *ORN46a* targeting is unaffected in all the downstream enzymes RNAi. One explanation of this normal axon targeting in the *elavG4* driven RNAi might be because that the metabolism enzymes or the products are quite 'longevity' (stable in the cell) (Holthuis, Pomorski et al. 2001). Therefore, to improve the RNAi efficiency, we performed RNAi driven by *ey Gal4*, an earlier expressed driver, together with *ealv Gal4*. Interestingly, double driven RNAi can phenocopy *spt* mutant phenotype. I found the similar *ORN47a* phenotype in sphingosine kinase RNAi, *ORN21a* phenotype in ceramide galactosyl transferase RNAi and *ORN46a* phenotype in ceramide kinase RNAi (Figure 3.12).



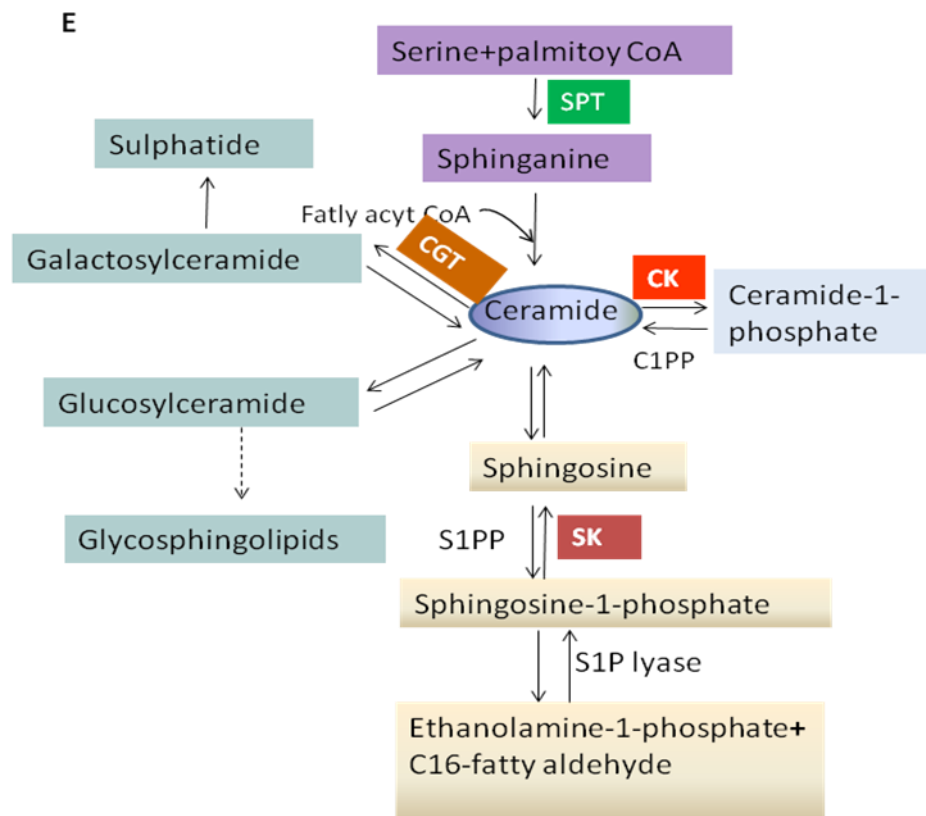


### Figure 3.12: Genetic dissection of *spt* defects in ORNs

Knockdown different sphingolipids synthesis enzymes by double driver (*elavGal4* and *eyGal4*) RNAi. (A) Knockdown *lace* and *spt-1* give the *ORN46a* phenotype (arrows), which is identical to *spt* mutants. (B) Knockdown *ceramide galactosyl transferase* leading *ORN21a* phenotype. (C) Knockdown *ceramide kinase* showing *ORN46a* phenotype. (D) Knockdown *sphingosine kinase* leading *ORN47a* phenotype. (E) A schematic to show these three enzymes in sphingolipid metabolism pathway. Genotype: (A, B and C) (Wild type) *elavGal4; eyGal4; OR::sytGFP*. (A) (*lace* RNAi) *elavGal4; eyGal4; lace* RNAi/ *OR::sytGFP*. (*spt* RNAi) *elavGal4; eyGal4; lace* RNAi/ *OR::sytGFP*. (B) (*CGT* RNAi) *elavGal4; eyGal4; CGT* RNAi/ *OR::sytGFP*. (C) (*CK* RNAi) *elavGal4; eyGal4; ceramide kinase* RNAi/ *OR::sytGFP*. (D) (Wild type) *elavGal4; eyGal4; Or47a::sytGFP*. (*SK* RNAi) *elavGal4; eyGal4; sphingosine kinase* RNAi/ *Or47a::sytGFP*. (Green: GFP; magenta: *Ncad*)

Therefore, the complex sphingolipids synthesis pathway were narrowed down into single branch, which suggests particular sphingolipid such as sphingosine-1-phosphate, ceramide-1-phosphate and galactosylceramide may lead the *ORN47a*, *ORN46a* and *ORN21a* defects in *spt* mutants.

### 3.2.8 Detergent-resistant membrane (DRM) components do not change in *lace* hypomorphic mutants.

Lipid rafts are liquid-ordered phase microdomains proposed to exist in biological membranes, which are enriched in cholesterol and sphingolipids (Brown and London 1998; Simons and Toomre 2000). These raft domains contain a particular set of associated proteins, especially glycosyl-phosphatidylinositol (GPI)-anchored proteins and certain transmembrane proteins including the flotillin. Their insolubility in non-ionic detergents such as Triton X-100 at 4°C allows them to be recovered in a low-density fraction on sucrose gradients (Brown and Rose 1992) have been involved in various cellular functions including signal transduction, immunological response and membrane trafficking (Tsui-Pierchala, Encinas et al. 2002). *spt* mutant has reduced amount of sphingolipid (Acharya and Acharya 2005). One speculation is *spt* phenotype could be a result of DRM depletion due to the reduction of sphingolipid.

To test this hypothesis, we examined whether the lipid rafts is changed in *spt* mutants or not. Briefly, membrane fractions were prepared from the heads lysis of *lace* transheterozygotes by Density gradient centrifugation.

Four fractions were collected from the top of the gradient to bottom and then subjected to SDS-PAGE and probed with antibodies using a standard immunoblot procedure. The top fraction contains flotilin-2, a DRM marker, thus designated as the lipid raft fraction (Figure 3.13 A and B line1), and the last two fraction contain Na-K<sup>+</sup> ATPase, a non-rafts plasma-membrane marker, therefore designated as the non-raft fraction (Figure 3.13 A and B lane3 and 4). Comparing Flot2 in wild type with *lace* mutant, first it is only restricted to rafts fractions, second the total amount of Flot2

protein is no difference in Wild type and *lace* mutant. This suggest that at least in *lace* transheterozygotes, defining a hypomorphic *spt* function, the general amount of Flotilin protein located in DRM fraction are not changed and Flotilin2 is not mislocalized into non-raft fractions.

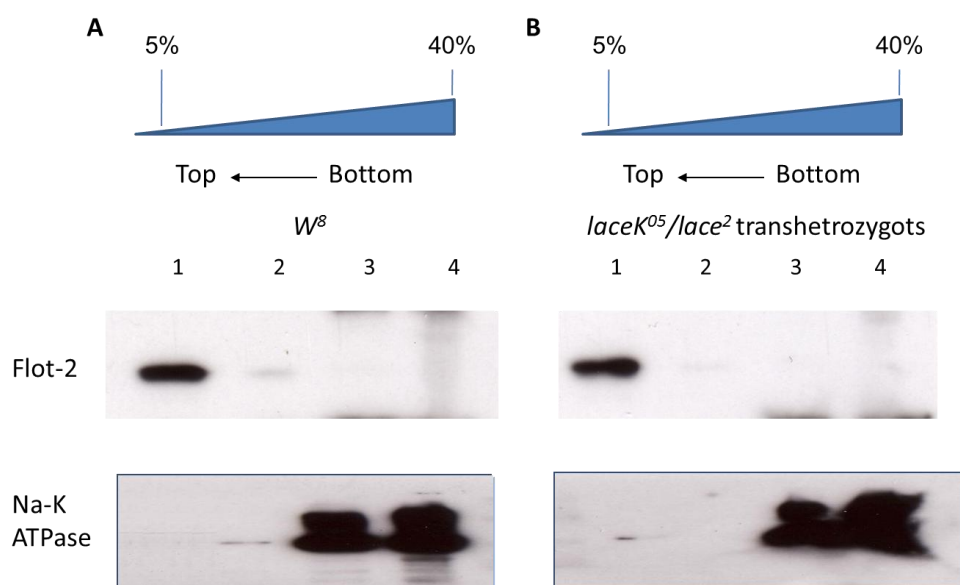


**Figure 3.13: DMR components are not changed in *lace* hypomorphic mutants**

(A) Membrane fractions from *W<sup>8</sup>* and *lace<sup>K05</sup>/lace<sup>2</sup> transheterozygotes* flies head lysis separated as raft and non-raft fractions in 5%-40% sucrose gradient. Flot2 mainly located in the first fraction which is the raft fraction and Na-K<sup>+</sup>ATPase located at the last two fractions which are the non-raft fractions. (B) In *lace<sup>2</sup>/lace<sup>K05</sup>* transheterozygotes, this fraction pattern is generally not changed.

### 3.2.9 Genetic interaction between *Spt* and *Dscam*

*Drosophila* Down Syndrome cell adhesion molecule (*Dscam*) is a transmembrane protein, which belongs to the immunoglobulin (Ig) superfamily. It is known that *Dscam* is essential for diverse neuronal morphogenetic processes, including axon guidance, branch segregation, and dendritogenesis. *Dscam* is required for the axon path-finding both in the olfactory system and mushroom body (Zhan, Clemens et al.



2004). When we compared the phenotype between *spt* and *Dscam*, similar phenotypes exist both in the olfactory system and MBs (see below). This phenotype similarity inspired us to speculate that *Dscam* function may depend on sphingolipid. To test this hypothesis, we made double mutants of *Spt* and *dscam* and analyzed the ORNs targeting in mosaic clone. To our surprise, the penetrance of the phenotype in double mutants was reduced (Figure 3.14). The *ORN46a* pre-stopping phenotype was 10% (n=14) in *spt-I<sup>P1</sup>-dscam<sup>21</sup>* double mutants, comparing with single mutant, *spt-I<sup>P1</sup>*, (30%, n=16) and *dscam<sup>21</sup>* (50%, n=16) (Figure 3.14 J). As for the *ORN47a* neurons, the ectopic projections per AL was counted, which was lower in double mutant *spt-I<sup>P1</sup>, dscam<sup>21</sup>* (1.25/AL, n=12) and double mutant *spt-I<sup>P1</sup>, dscam<sup>23</sup>* (1.65/AL, n=12) than in *spt-I<sup>P1</sup>* (2.22/AL, n=12) and *Dscam<sup>21</sup>* (2.07/AL, n=12) (Figure 3.15 K). Taken together, *spt* suppress *dscam* mutant defects in ORNs targeting.

### 3.2.10 Misexpression *Dscam* in *Spt* background does not suppress the phenotype

To further analyze the genetic interaction between *spt* and *dscam*, *Dscam* was misexpressed in the *spt* background. As described earlier, *Drosophila dscam* can encode thousands of isoforms through alternative splicing involving many choices of exon 4, 6, 9 and 17. Distinct *Dscam* isoforms are targeted to dendrites or axons, depending on which of the two transmembrane-domain-encoding exon 17 alternatives, 17.1 or 17.2, is utilized. *Dscam* isoforms carrying exon 17.1 (*Dscam* [TM1]) are largely restricted to dendrites, while *Dscam* isoforms with exon 17.2 (*Dscam* [TM2]) are enriched in axons. Thus, we expressed *dscam 17.1* and *17.2* respectively in MARCM clone.

It is known that misexpression leads ORNs targeting defects (Hummel, unpublished).



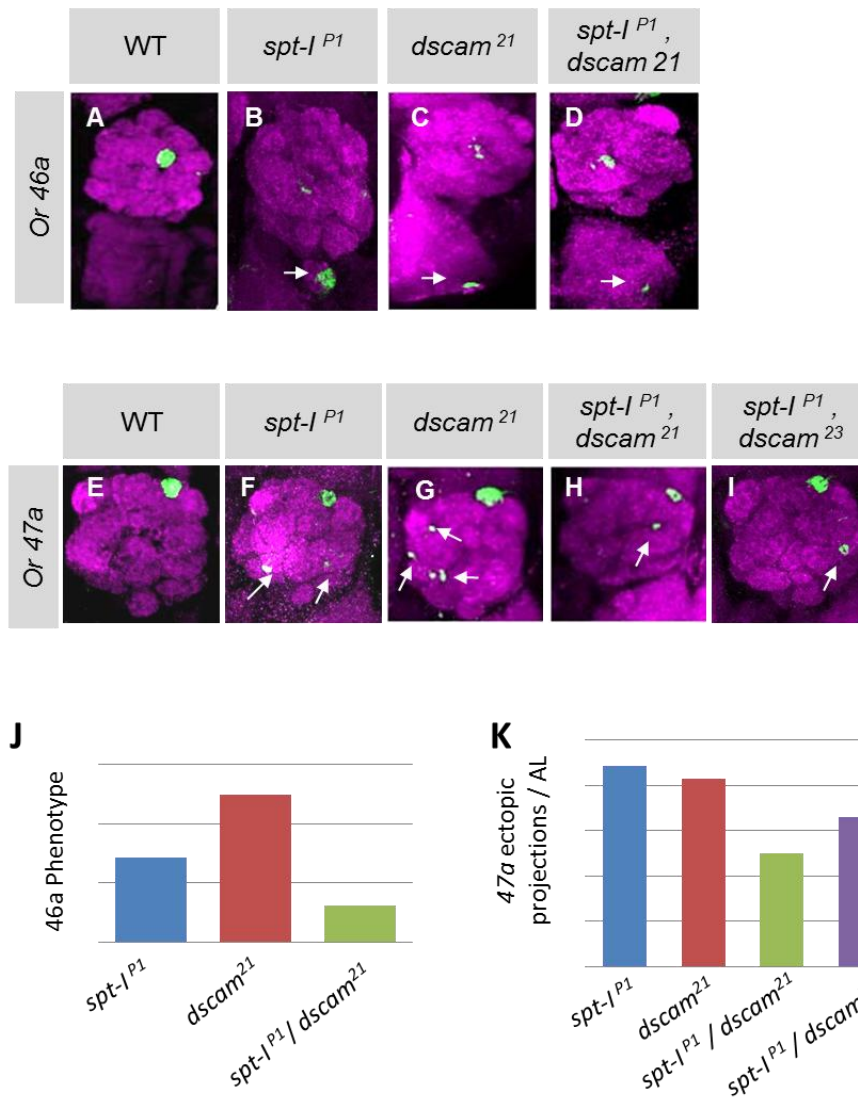


### Figure 3.14: Genetic interaction between *Spt* and *Dscam*

ORN 46a and ORN 47a phenotype were counted in Single and double mutants clones. (A and E) Wild type ORN 46a and ORN 47a projections. (B and C) *spt-I<sup>P1</sup>* and *dscam<sup>21</sup>* single mutant ORN46a has pre-stopping phenotype respectively. (D) *spt-I<sup>P1</sup>, dscam<sup>21</sup>* double mutant ORN46a showing pre-stopping phenotype. (F and G) *spt-I<sup>P1</sup>* and *dscam<sup>21</sup>* single mutant ORN47a has ectopic projection phenotype respectively. (H) *spt-I<sup>P1</sup>, dscam<sup>21</sup>* double mutant ORN47a has ectopic projection. (I) *spt-I<sup>P1</sup>, dscam<sup>23</sup>* double mutant ORN47a also has ectopic projection. (J and K) quantification of ORN46a and ORN47a phenotype, which indicate there is a genetic suppression between *spt* and *dscam*. Genotype: (A and E) *eyFLP; FRT42/ PCNA FRT42; OR>sytGFP*. (B and F) *eyFLP; spt-I<sup>P1</sup> FRT42/ PCNA FRT42; OR>sytGFP*. (C and G) *eyFLP; dscam<sup>21</sup> FRT42/ PCNA FRT42; OR>sytGFP*. (D and H) *eyFLP; spt-I<sup>P1</sup>, dscam<sup>21</sup> FRT42/ PCNA FRT42; OR>sytGFP*. (I) *eyFLP; spt-I<sup>P1</sup>, dscam<sup>23</sup> FRT42/ PCNA FRT42; OR>sytGFP*. (Green: GFP; magenta: Ncad)

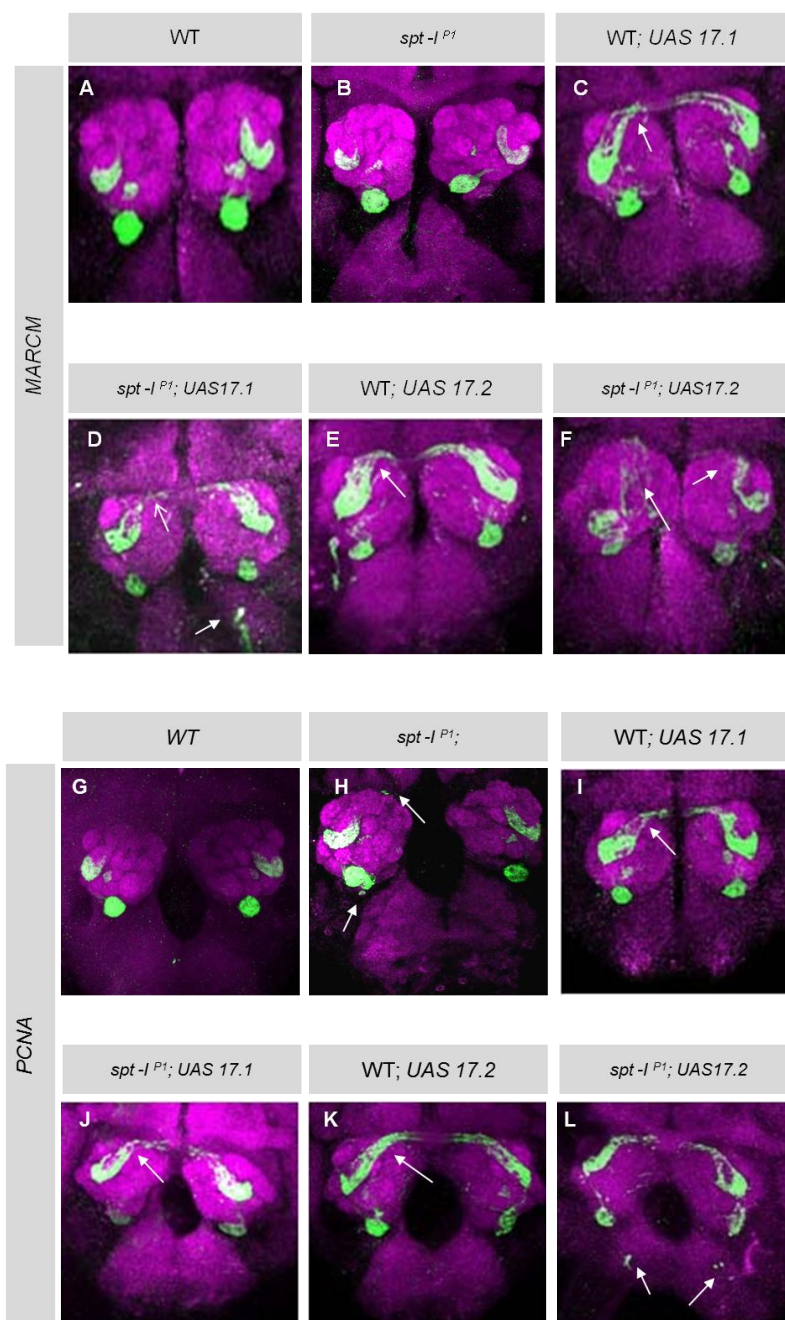


**Figure 3.15: Misexpression of *Dscam* in *spt-I* background**

These classes of ORNs (*21a*, *46a* and *47b*) were labeled in MARCM (A-F) and PCNA clones (G-L). (A and G) Wild type projections in MARCM and PCNA clone respectively. (B) *spt-I<sup>P1</sup>* mutant ORNs has normal pattern in MARCM. (C) Misexpress *dscam 17.1* has mild defects of *ORN47b*. (D) *Dscam 17.1* in *spt* background has stronger phenotype. (F) Overexpress *Dscam 17.2* in *spt* background also has stronger phenotype than wild type background (E). (H) *spt-I<sup>P1</sup>* mutant ORNs has phenotype in PCNA clone (arrows). Misexpress *dscam 17.1* under *spt* background (J) has stronger phenotype than wild type background (I). Overexpress *Dscam 17.2* in *spt* background (L) also has stronger phenotype than in wild type background (K). Genotype: (A) *eyFLP, elav Gal4; FRT42/ Gal80 FRT42; ORs :: sytGFP*. (B) *eyFLP, elav Gal4; spt-I<sup>P1</sup> FRT42/ Gal80 FRT42; ORs :: sytGFP*. (C) *eyFLP, elav Gal4; FRT42/ Gal80 FRT42; UAS*

*dscam* 17.1 /ORs :: sytGFP.(D) *eyFLP, elav Gal4; spt-I<sup>P1</sup> FRT42/ Gal80 FRT42; UAS dscam 17.1 /ORs :: sytGFP.(E) eyFLP, elav Gal4; FRT42/ Gal80 FRT42; UAS dscam 17.2 /ORs :: sytGFP.(F) eyFLP, elav Gal4; spt-I<sup>P1</sup> FRT42/ Gal80 FRT42; UAS dscam 17.2 /ORs :: sytGFP.(H) eyFLP, elav Gal4; spt-I<sup>P1</sup> FRT42/ PCNA FRT42; ORs :: sytGFP.(I) eyFLP, elav Gal4; FRT42/ PCNA FRT42; UAS dscam 17.1 /ORs :: sytGFP. (J) eyFLP, elav Gal4; spt-I<sup>P1</sup> FRT42/ PCNA FRT42; UAS dscam 17.1 /ORs :: sytGFP.(K) eyFLP, elav Gal4; FRT42/ PCNA FRT42; UAS dscam 17.2 /ORs :: sytGFP. (L) eyFLP, elav Gal4; spt-I<sup>P1</sup> FRT42/ PCNA FRT42; UAS dscam 17.2 /ORs :: sytGFP. (Green: GFP; magenta: Ncad )*

If *Dscam* function depends on *spt*, then we expected to see a suppression of *Dscam* phenotype in *spt* background. Expression of *Dscam 17.1* in the wild type background has mild effects on *ORN47b*, including glomeruli mis-shape and mis-projection to more anterior-dorsal region of the antennal lobe (Figure 3.15 C). In contrast, *Spt-I<sup>P1</sup>* mutant ORNs are normal in MARCM clone (Figure 3.15 B). The phenotype is enhanced when express *Dscam 17.1* in *spt* background. Moreover, *ORN46a* had pre-stopping phenotype, which is usually normal in *Dscam 17.1* overexpression. In parallel, overexpress *Dscam 17.2* in *spt* background (Figure 3.15 F) also showed a stronger phenotype than that in wild type background (Figure 3.15 E). These data together with the double mutant experiments suggest *spt* suppress *dscam* mutant defects, however, *spt* does not function downstream to *dscam*.

### 3.3 *spt* function in mushroom body (MB) development

Previous studies proved *Dscam* to be important for MB neuron development (Wang, Zugates et al. 2002; Wang, Ma et al. 2004; Zhan, Clemens et al. 2004). And distinct *dscam* juxtamembrane isoforms, *Dscam*[TM1] and *Dscam*[TM2] located to axon and dendritits , also function respectively. We found *Dscam* and *spt* have very similar phenotype in olfactory system, interestingly, this similarity is also found in MB.

#### 3.3.1 MB development and structure

The MBs are paired structures, one in each brain lobe, and each MB is derived from four neuroblasts (Nbs). Axon fascicles within the developing peduncle and lobes show a highly characteristic organization with axons from newly generated neurons in the center (forming a core fiber) and those from progressively older neurons in sequentially arranged concentric rings (Kurusu, Awasaki et al. 2002).

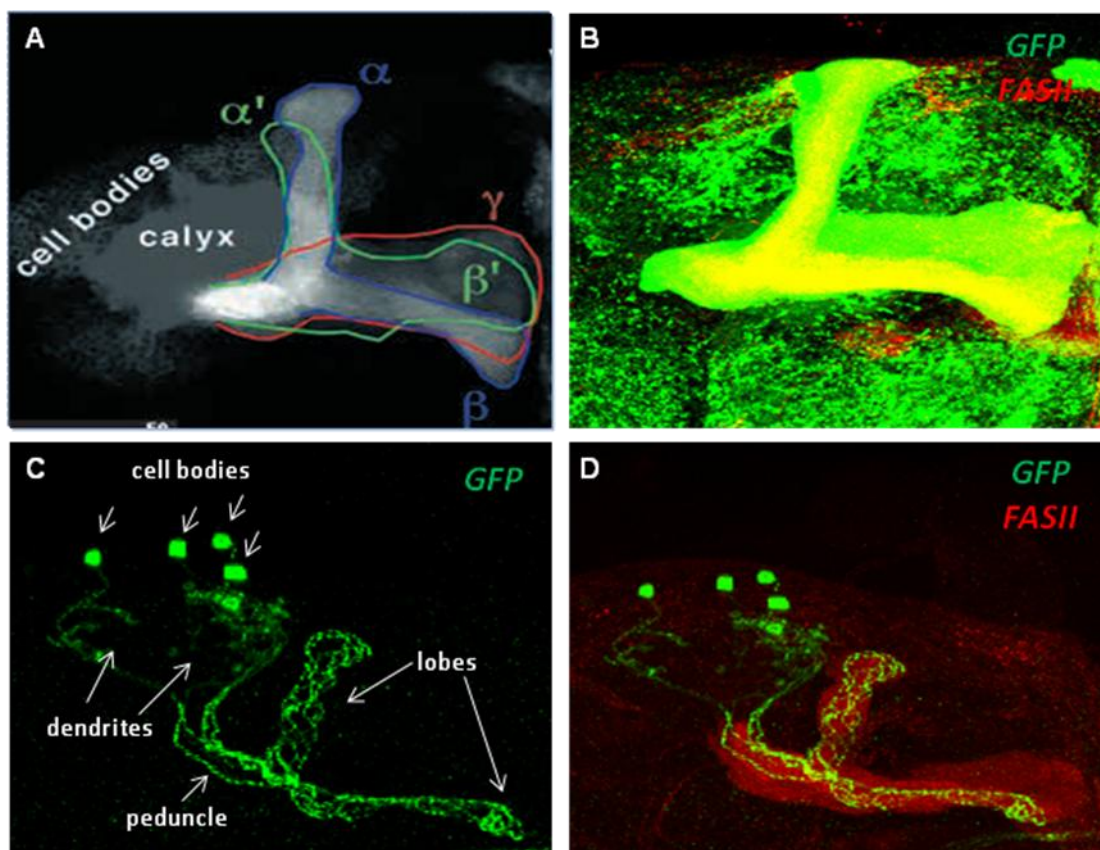


**Figure 3.16: Mushroom body structure**

(A) MB neurons on each side of the brain are derived from four neuroblasts (Nbs) (adapted from LQ Luo, 2000) five Individual axonal lobes are outlined with solid lines:  $\gamma$  in red,  $\alpha' / \beta'$  in green and  $\alpha / \beta$  in blue. (C and D) The MB cell bodies, Kenyon cells, are located at the dorsal cortex, extending their dendrites into the calyx and their axonal projections form a thick nerve bundle referred to as the peduncle. The axons bifurcate at the base of the peduncle, and then project into dorsal and medial lobes respectively. (B and D) This organization can be visualized in developing MBs with a variety of markers, for instance, Fasciclin II (Fas II), the fly homolog of N-CAM selectively express in  $\alpha / \beta$  lobes and  $\gamma$  lobe, but not in  $\alpha' / \beta'$  lobe. Genotype: (B) *UASsytGFP; OK107 Gal4*. (C and D) *hsFLP; FRT42, UAS-mCD8-GFP/ FRTG42, tubP-GAL80; OK107 Gal4*

The MB structure can be visualized by MB specific enhancer trap line such as *OK107-Gal4* or *201Y-GAL4*. *OK107-Gal4* is highly expressed in all MB neurons and

their neuroblasts. In contrast, Gal4-201Y is expressed in postmitotic  $\gamma$  neurons and in a subset of later-born  $\alpha/\beta$  neurons. In addition, The MB structure also can be labeled by chemical or antibody including phalloidin highlighting the youngest fibers in the core axons and fasciclin II (Fas II) selectively high expressed in  $\alpha/\beta$  lobes, but not in  $\alpha'/\beta'$  lobe (Figure 3.16 B and D).

### 3.3.2 *spt* mutations have mushroom body defects.

When I visualized MB organization in *lace* transheterozygotes, I found normal shape of the  $\gamma$  lobes (Figure 3.17B). In contrast,  $\alpha$  and  $\beta$  lobes which are morphologically distinguishable by FasII staining had defects. In wild type individual  $\alpha/\beta$  axons bifurcate into two branches that project away from each other into the  $\alpha$  and  $\beta$  lobes, respectively (Figure 3.17A).

In *lace* mutant, several defects are observed, including the loss of the  $\alpha$  lobe (Figure 3.17 B and C') (38%, n=50), the loss of both lobes (18%), and sometimes the lobes are reduced either in the length or the thickness (Figure 3.17 C') (18%). It is interesting that the lost of the  $\beta$  lobe is not frequent in *lace* transheterozygote.

Moreover, when the  $\alpha$  lobe is lost, the  $\beta$  lobe is much thicker and denser than in wild type (Figure 3.17 B), indicating the bifurcation of  $\alpha/\beta$  axons is normal, but two branches projecting into one direction. These defects can be fully rescued by the expression a wild type *lace* gene (Figure 3.17 C-E). Taken together, these abnormalities suggest that sphingolipids play an important role in MB neurons development, including the axon bifurcation and axon growth.



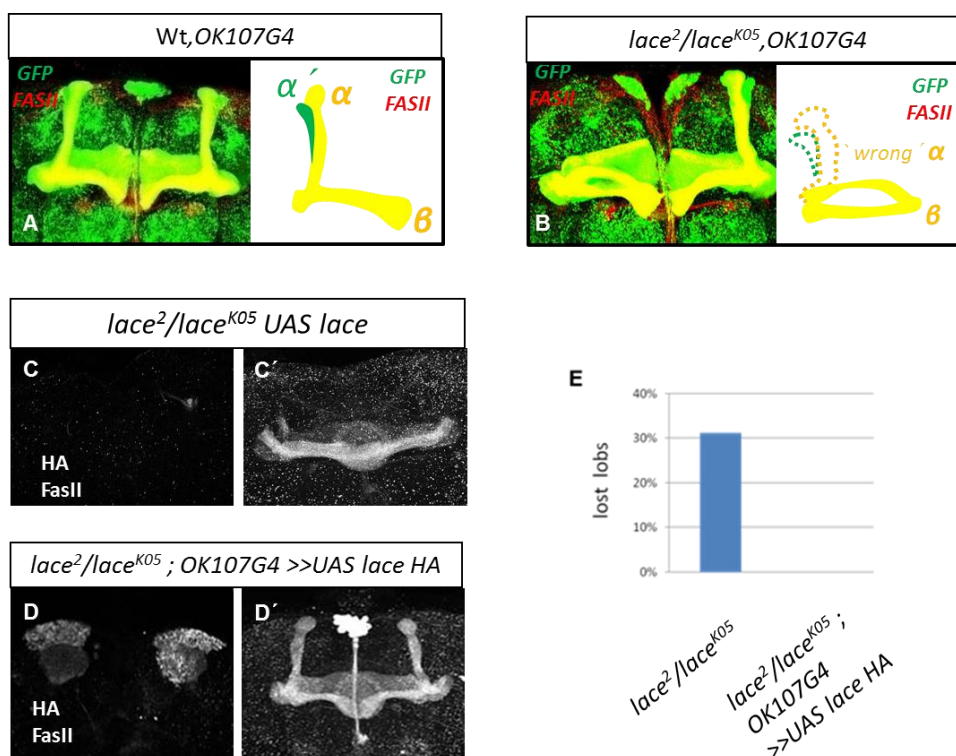


**Figure 3.17: *lace* mutation affect the formation of bifurcated axons in MB**

(A and B) Shown are composite confocal images of adult MB that were labeled by *Gal4-OK107* driven expression of mCD8-GFP, which is expressed in all the MB lobes, and endogenous FasII strongly located in  $\alpha/\beta$  and weakly located in  $\gamma$  lobe but not in  $\alpha'/\beta'$  lobes. In wild-type (A), we observe full  $\alpha/\beta$  lobes and  $\alpha'/\beta'$  lobes. Interestingly, in *lace* transheterozygotes mutant (B), the lobe is missing. In addition, two FasII positive branch bundles project to the middle. (C-E) Genetic rescue of *lace* defects in MB. MB were labeled by HA and FasII antibodies. In *lace* transheterozygotes mutant (C and C'),  $\alpha$  lobe was missing. (D and D'), the lost lobe phenotype is dramatic recovered (D'). Dorsal view to show the HA positive MB cell body and dendrites (D). (E) Quantification of the lost lobe phenotype indicate genetic rescue of *lace* defects in MB. For clarity, only the lobe regions are shown in Figure A-D. Genotype: (A) *UASmCD8-GFP; Ok107-Gal4*. (B) *lace*<sup>2</sup>/*lace*<sup>K05</sup>; *UASmCD8-GFP; Ok107-Gal4*. (C and C') *lace*<sup>2</sup>/*lace*<sup>K05</sup> *UAS-HA-lace*. (D and D') *lace*<sup>2</sup>/*lace*<sup>K05</sup> *UAS-HA-lace; OK107-Gal4*. (Green: GFP; red: FasII)

### 3.3.3 Genetic dissection of sphingolipid function in MB

Following the same idea in genetic dissection of sphingolipid function as described above for ORNs, sphingolipid synthesis enzymes were depleted by RNA interference to find the important candidate for MB neurons development (Figure 3.18). Using *OK107-Gal4* as the driver, knocking down *ceramidase*, *sphingosine kinase1*, *sply* and

*sphingomyelinase* showed  $\beta$  lobe lost phenotype respectively (Figure 3.18 B-E).

Moreover, the  $\beta$  lobe lost was often simultaneous with double thickness of  $\alpha$  lobe (Figure 3.18 C,D and E), indicating the branching of  $\alpha/\beta$  neurons are not defect but the two branches project into the same directing.

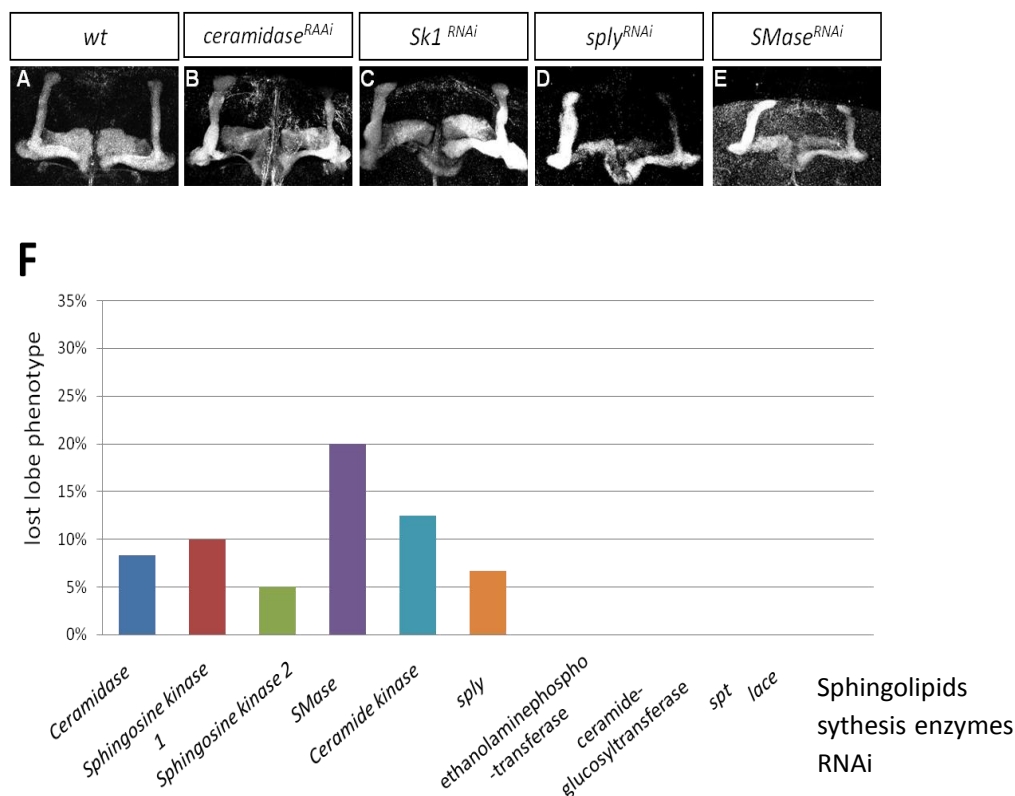


### Figure 3.18: Genetic dissection sphingolipid function in MB

Knockdown the sphingolipid synthesis enzymes by *OK107-Gal4 driven* RNAi. (A) Shown wild type MB structure, only  $\alpha/\beta$  and  $\gamma$  lobe can be visualized due to FasII staining. (B-E) Depletion of several enzymes give specific lost  $\beta$  lobe. (F) Quantification of RNAi results (n=20 at least /each), note that *spt-1* and *lace* RNAi do not show phenotype. Genotype: (A) OK107G4 (B) *ceramidase* RNAi; Ok107G4 (C) *sphingosine kinase1* RNAi; OK107G4 (D) *sply* RNAi; OK107G4 (E) *sphingomyelinase* RNAi; OK107G4.

Since knockdown of the five enzymes giving the same phenotype in MB, we proposed that one of the sphingolipid is critical and responding to the phenotype, which might be the membrane ceramide. At the first look, these results were confusing, because knockdown *SK1* and *ceramidase* increased ceramide amount, by

contrast, knockdown SMase decreased the ceramide. Moreover, *sply* depletion only directly decreased phospho-ethanolamine (Figure 3.19).

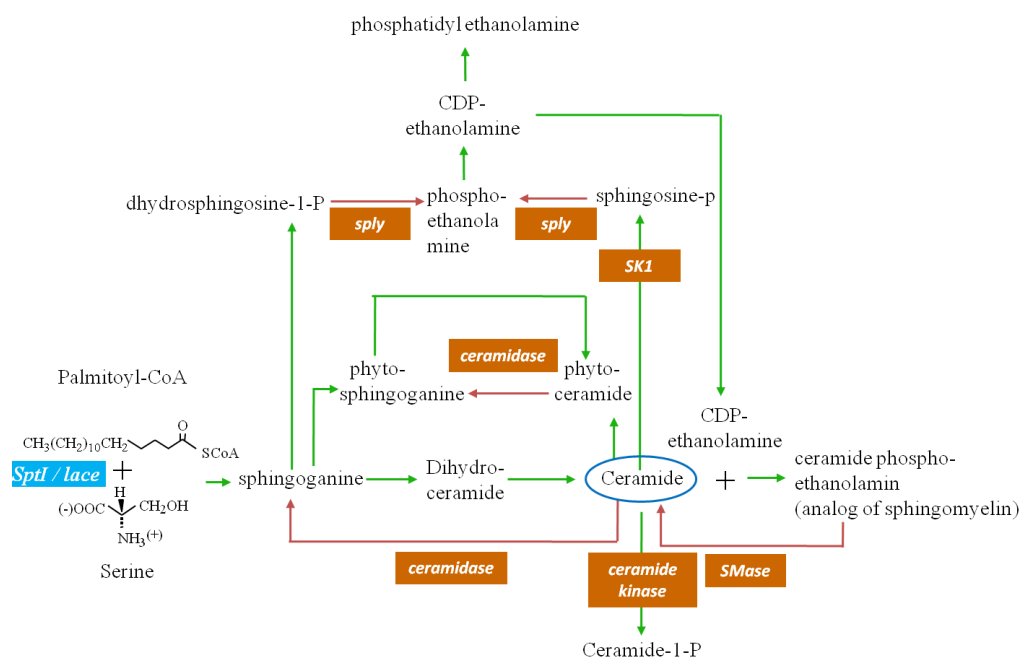


**Figure 3.19: Genetic dissection MB phenotype gives a hint that membrane ceramide is the candidate product responded to the lost lobe defect.**

*De novo* synthesis of sphingolipids (green). Sphingolipid degradative pathway (red). enzyme is shown in filled yellow square. Depletion either of these enzymes gives lost lobe phenotype in MB. The diversity branches can converge into one branch that is membrane ceramide produced by ceramide phospho-ethanolamine (*Drosophila* analog of Sphingomyelin) degradation.

However, there are two types of ceramides in the cell, cytoplasm ceramide and membrane ceramide. Membrane ceramide is mainly produced by the Sphingomyelin catalyzed by SMase, thus, SMase RNAi directly decreased the membrane ceramide. Oppositely, knockingdown *ceramidase*, *sphingosine kinase 1*, and *sply* decreased the sphingolipid intermediants such as CDP-ethanolamine, which is a substrate for Sphingomyelin synthesis, therefore, the membrane ceramide was decreased in an indirectly manner (Figure 3.19). Taken together, genetic dissection of the



sphingolipid function in MBs suggests that membrane ceramide play an important role in MB neuron development.

### 3.3.4 *Dscam* mutants have MB phenotype

It is known that *Dscam* is important for MB development (Zhan, Clemens et al. 2004). To compare *spt* and *dscam* phenotype, I confirmed the *dscam* phenotype in MB. First, *Dscam* RNAi give severe lost lobe phenotype (Figure 3.20), including lost  $\alpha$  lobe (22%, n=18), lost  $\beta$  lobe (28%) and lost  $\alpha/\beta$  (39%). In addition to the lobe defects, the bifurcation defects can be visualized in single MARCM clone (Figure 3.20). Single neuron analysis reveals individual axonal branches and their trajectories, which is essential for detailed morphological analysis of *Dscam* mutant neurons. To label a small number of the late born  $\alpha/\beta$  neurons, clones were generated by inducing mitotic recombination after pupa formation (PF). To compare the projections of MARCM-labeled  $\alpha/\beta$  axons with the projections of other  $\alpha/\beta$  axons in the same MB, we selectively stained the entire  $\alpha/\beta$  lobes using the anti-FasII monoclonal Ab 1D4. In wild type, labeled  $\alpha/\beta$  neuron project through the peduncle then bifurcate and form two axonal branches to dorsal and middle respectively (Figure 3.20 A). In *Dscam* mutant clones, the bifurcation is normal but two axon branches project into one direction (Figure 3.20 B and C). These 'wrong' branches still acquire their cell type-specific morphological features, and mutant  $\alpha/\beta$  axons are never incorporated into the  $\alpha'$ ,  $\beta'$ , or  $\gamma$  lobes, suggesting no cell fate change in *Dscam* mutant neurons.

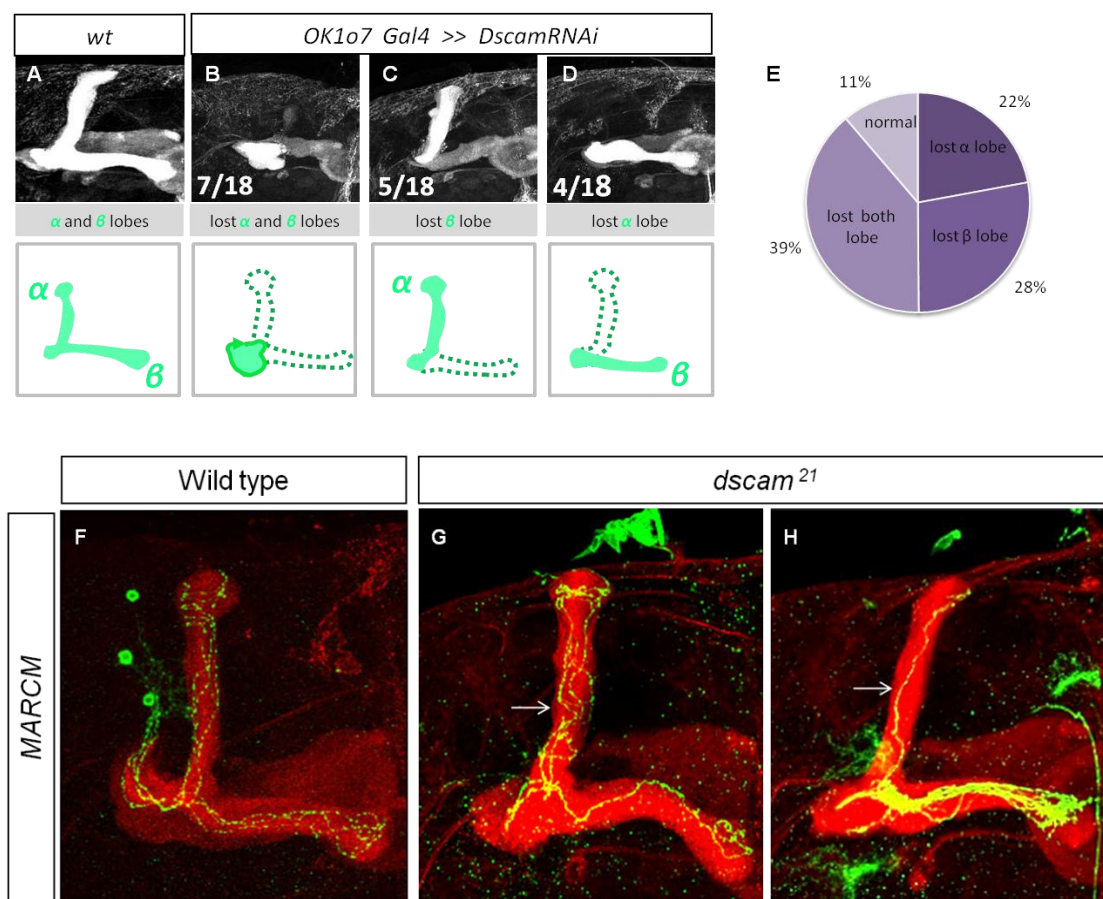


### Figure 3.20: *Dscam* mutants show MB phenotypes

(A-E) Knockdown *dscam* by RNAi leading to lost lobe phenotypes. (A) The Wild type MB with the normal  $\alpha$  and  $\beta$  lobes stained by FasII antibody. (B) Shown the severe phenotype, both  $\alpha/\beta$  are missing. (C) Only  $\beta$  lobe missing. (D) Only  $\alpha$  lobe missing. (E) Quantification of the lost lobe phenotypes. (F-H) *dscam* single MB axon shows bifurcation phenotype. (F) Wild-type clones of the  $\alpha/\beta$  axons bifurcate into two bundles, one projects dorsally and the other projects toward the midline. Since three cells are labeled in this sample, so three axons project to  $\alpha$  lobe and three axons to the  $\beta$  lobe are distinguishable. (G and H) *Dscam* mutant clones fail to project axons in divergent directions. (G) There axons project dorsally and one medially. (H) Multiple axons project medially and only one medially. *Genotype*: (A) *OK107G4*. (B-D) *Dscam RNAi/+; OK107G4/+* (F) *hsFLP; FRT42, UAS-mCD8-GFP/FRTG42,tubP-GAL80;; GAL4-OK107/+*; (G and H) *hs-FLP; FRT42,dscam*<sup>21</sup>,*UAS-mCD8-GFP/FRTG42,tubP-GAL80;; GAL4-OK107/+*; (Green: GFP; red: FasII)

### 3.3.5 *spt* mutant axons are normal in MARCM clones.

Single MB neuron analysis was also performed for *spt* mutants. In MARCM clone I could not find axon branching defects (Figure 3.21 A-D). The bifurcation of  $\alpha/\beta$  neuron is normal in single cell clones (Figure 3.21 D), medium size clones (Figure 3.21

B), and even in neuroblast clones (Figure 3.21 C).

This is consistent with the results in olfactory system, which again suggests the depletion of sphingolipid can be rescued by the surrounding environment.

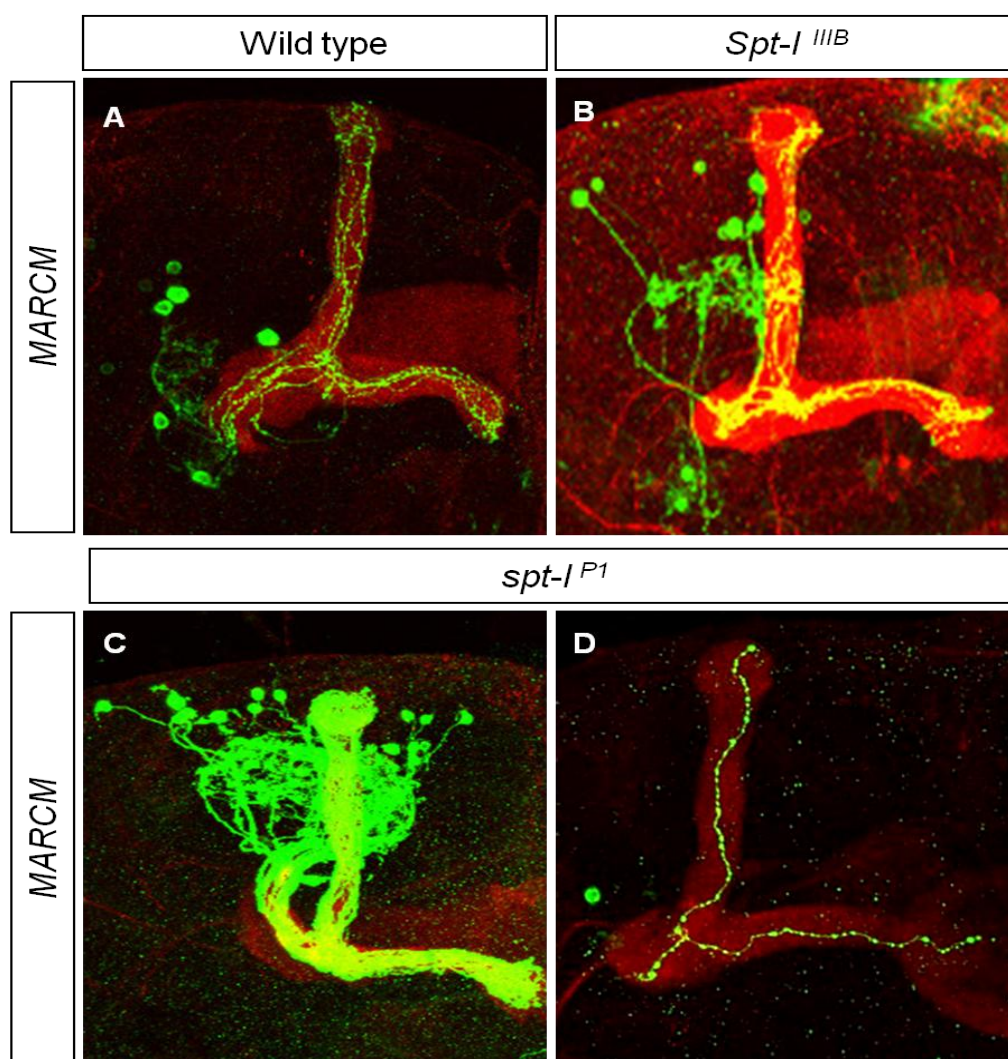


**Figure 3.21: *spt* mutant axons are normal in MARCM clones**

(A) Wild type of MB MARCM clone (B-D) *spt* MARCM do not give phenotype either in single cell clone (D), small clone (B) or neuroblast clone (C). (Wild type of MB PCNA clone, shown equal axon bundles project to dorsal and medial lobe, which indicate the normal bifurcation of MB neurons. Genotype: (A) *hs-FLP; FRT42, W<sup>f</sup>, UAS-mCD8-GFP/FRT42, tubP-GAL80;; GAL4-OK107/+*. (B) *hs-FLP; FRT42, spt-I<sup>P1</sup>, UAS-mCD8-GFP/FRT42, tubP-GAL80;; GAL4-OK107/+* (C and D) *hs-FLP; FRT42, Spt-I<sup>III B 2</sup>, UAS-mCD8-GFP/FRT42, tubP-GAL80;; GAL4-OK107/+*.

### 3.3.6 Genetic interaction between *spt* and *dscam* in MB

Follow the same idea as in olfactory system, we suspect there is a relationship between *spt* and *dscam* due to the very similar MB phenotypes. Therefore, we perform a genetic interaction experiment to test this hypothesis in MB.

#### 3.3.6.1 Overexpression of Dscam [TM1] and Dscam [TM2] isoforms in MB.

Distinct Dscam isoforms targeted to dendrites or axons, depending on which of the two transmembrane-domain-encoding exon 17 alternatives, 17.1 or 17.2, is utilized. Dscam isoforms carrying exon 17.1 (Dscam [TM1]) are largely restricted to dendrites, while Dscam isoforms with exon 17.2 (Dscam [TM2]) are enriched in axons. Further, depleting Dscam [TM1] or Dscam [TM2] blocks morphogenesis of dendrites versus axons (Shi, Yu et al. 2007)

We express Dscam [TM1]-GFP and Dscam [TM2]-GFP in developing MB by *Gal4-201Y* and *Gal4-OK107* respectively (Figure 3.22). In both situations, Dscam [TM1] are largely restricted to dendrites (Figure 3.22 A-C; G-H) and Dscam [TM2] are positive *in dendrites* and axon (Figure 3.22 D-F; J-L). However, *Gal4-OK107* driven expression of the Dscam [TM1] or Dscam [TM2] give severe phenotypes as abnormal morphology of dendrites (Figure 3.22 G-I) and lost axon lobes (Figure 3.22 J-L) respectively. In contrast, *Gal4-201Y* driven expression dscam largely keep normal (Figure 3.22 A-F), although overexpression of Dscam [TM2] leading the reduction of  $\alpha/\beta$  lobe and segregation of peduncle axon bundle, (Figure 3.22 D-F).

#### 3.3.6.2 Mislocalization of Dscam [TM1] in *lace* mutant

When we express Dscam [TM1] in *lace* background, misdistribution of dendritic Dscam [TM1] to axons was observed (Figure 3.23). In contrast to the expression

Dscam<sup>TM1</sup> in wild type restricted to dendrites (Figure 3.23 A-C), TM1 is mistargeting to the axons, both in  $\alpha$  and  $\beta$  lobes (Figure 3.23 D-F). It is interesting that the mislocalization happened in  $\alpha/\beta$  and  $\alpha'/\beta'$  lobes but never in or  $\gamma$  lobe. Moreover, mislocalization of TM1 in *lace* background modifies the *lace* phenotype from lost  $\alpha$  lobe to lost  $\beta$  lobe (Figure 3.23 D-F).

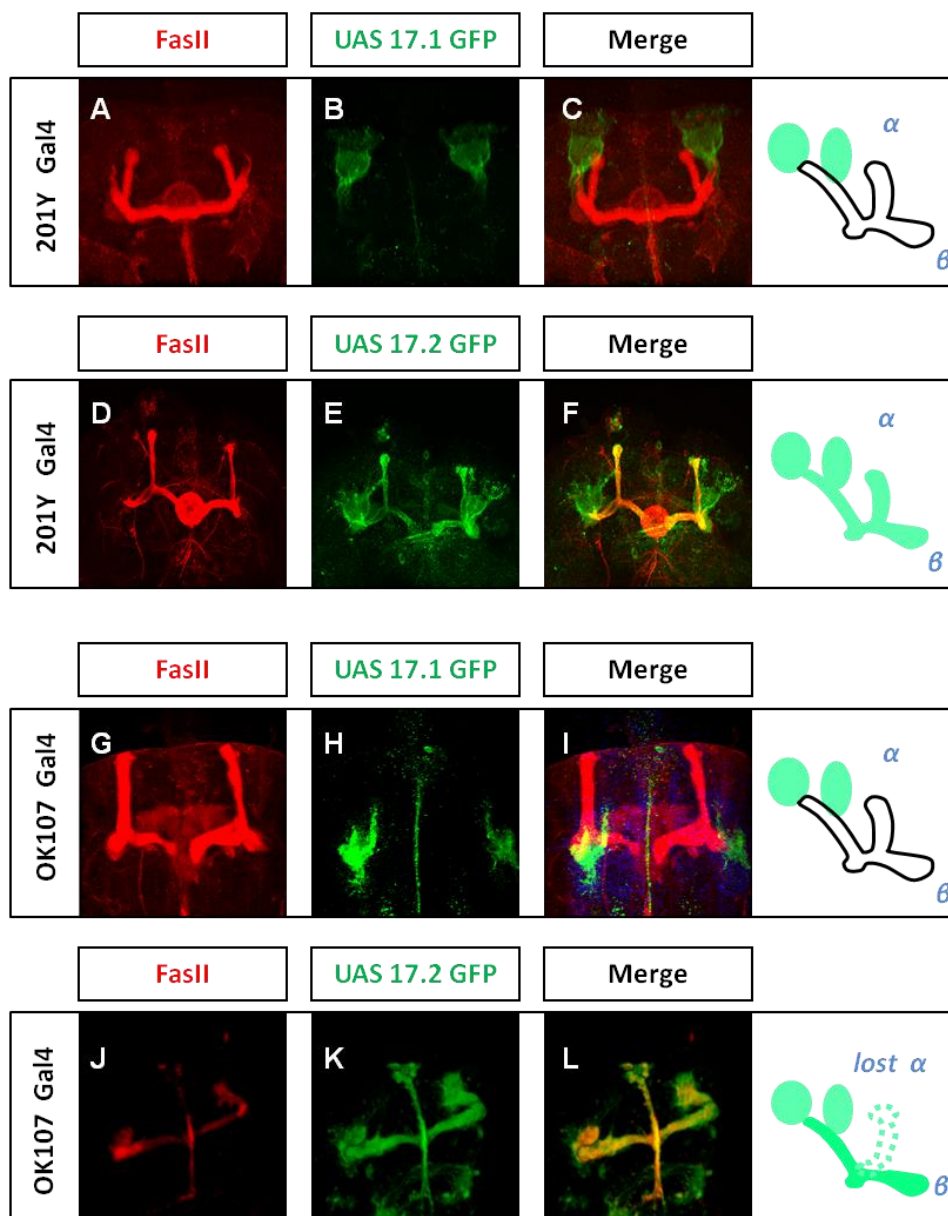


**Figure 3.22: Overexpression of Dscam [TM1] and Dscam [TM2] isoforms in MB by *Gal4-OK107* and *Gal4-201Y***

(A-C) Overexpression of Dscam [TM1] by *Gal4-201Y*. Shown the dendritic targeting of [TM1] and the normal dendritic morphology. (D-F) Overexpression of Dscam [TM2] by *Gal4-201Y*, which localize to the whole MB. The MB morphology is largely normal, although the axons



are reduced comparing with [TM1] overexpression. (G-I) Overexpression of Dscam [TM1] by Gal4-OK107, which restrict to dendrites. Note the abnormal morphology of dendrites (H). (J-K) Overexpression of Dscam [TM2] by Gal4-OK107, which localizes to the whole MB and disrupts the axon morphology. Genotype: (A-C) *Dscam [TM1]::GFP; Gal4-201Y*. (D-F) *Dscam [TM2]::GFP; Gal4-201Y* (G-H) *Dscam[TM1]::GFP; Gal4-OK107*. (J-L) *Dscam[TM2]::GFP; Gal4-OK107*. (Green: GFP; red: FasII)

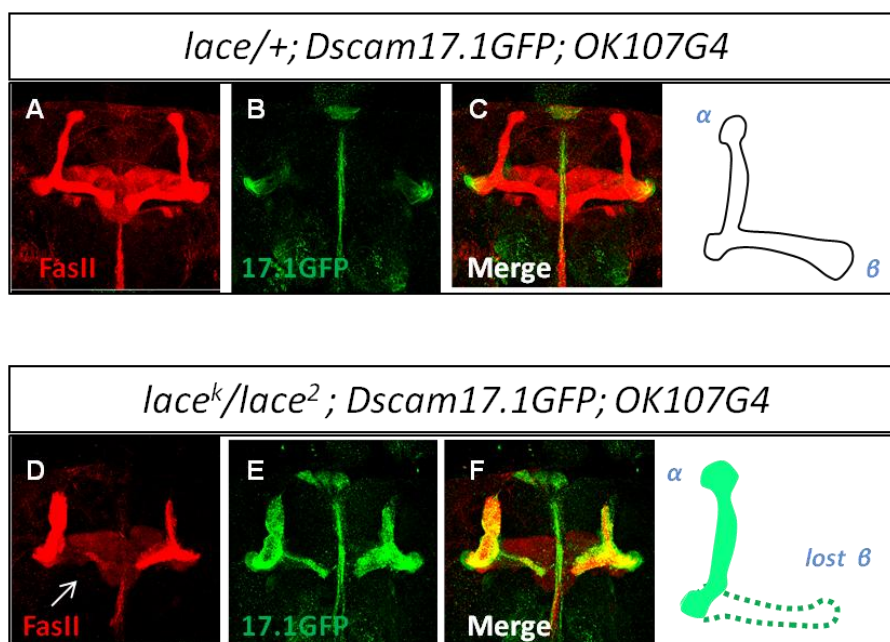


**Figure 3.23: Dscam [TM1] mistargeting in *lace* mutant background**

(A-C) In *lace*<sup>+/+</sup>, overexpression of Dscam [TM1] by *Gal4-OK107* is largely restricted to dendrites. (D-F) In *lace* transheterozygote mutant, TM1 is mistargeting to the axons, both in  $\alpha$  and  $\beta$  lobes. And the bifurcated axons project to  $\alpha$  lobe since the twice thickness of  $\alpha$  lobe. (A-C) *lace*<sup>+/+</sup>; *Dscam[TM1]::GFP; Gal4-OK107G4*. (D-F) *lace*<sup>K05</sup>/*lace*<sup>2</sup>; *Dscam[TM1]::GFP; Gal4-OK107G4*. (Green: GFP; red: FssII)

These observations indicate that sphingolipid might play a role in controlling dendritic distribution of Dscam [TM1]. Moreover, the modification of *lace* phenotype in above experiments, indicate a genetic interaction between *spt* and *dscam*.

### 3.3.6.3 Overexpression of Dscam [TM1] in *lace* background enhances the MB phenotype

To test this interaction, we overexpress Dscam TM1 in *lace* background and focused on the MB lobe phenotype (Figure 3.24). *lace*<sup>K05</sup>/*lace*<sup>2</sup> transheterozygote show the

“lost lobe” phenotype (33%,n=20). Expression of Dscam [TM1] by *OK107G4* in wild type has lower penetrant of the lost lobe phenotype (7%, n=24), however, overexpression of Dscam TM1 in *lace* background increase the penetrance of the phenotype (58%, n=24) (Figure 3.24 G).

Taken together, there is a genetic interaction between *dscam* and *lace* in MB development. The overexpression of the dendritic isoform Dscam [TM1], enhances *lace* phenotype in MB. This genetic enhancement is associate with mislocalization of Dscam [TM1] into axon, indicating Dscam [TM1] isoform mislocalization into axons in *lace* mutant disrupts MB axons development.

#### **3.3.6.4 The knockdown of Dscam [TM1] in *lace* background suppress MB phenotype**

The *lace* mutant phenotype might be caused by the mistargeting dscam TM1 into the MB axons. To test this hypothesis, I knockdown Dscam TM1 in *lace* background by Dscam TM1 specific RNA interference (kindly provide by Dr. Lee). Knockdown Dscam TM1 under wild type background does not affect the MB axon morphology (Figure 3.25 A). Since *Gal4-OK107* is highly expressed in all MB neurons, but *Gal4-201Y* is expressed in all  $\gamma$  and in a subset of late-pupal born  $\alpha/\beta$  neurons (Lee, Lee et al. 1999). Therefore, these results suggest that Dscam functions in early born  $\alpha/\beta$  neurons, which play a crucial role in shaping the projection patterns of later-born MB neurons. Knockdown Dscam TM1 under *lace* background decrease the “lost lobe” phenotype (Figure 3.25 E) (11%, n=20). It interesting that most axon processes do not reach the end of  $\alpha/\beta$  lobes (Figure 3.25 C and D), which is not so frequency in *lace* mutant. This indicate knockdown of Dscam TM1 suppress the axon bifurcation phenotype, but can not rescue the axon growth defects in *lace* mutant.

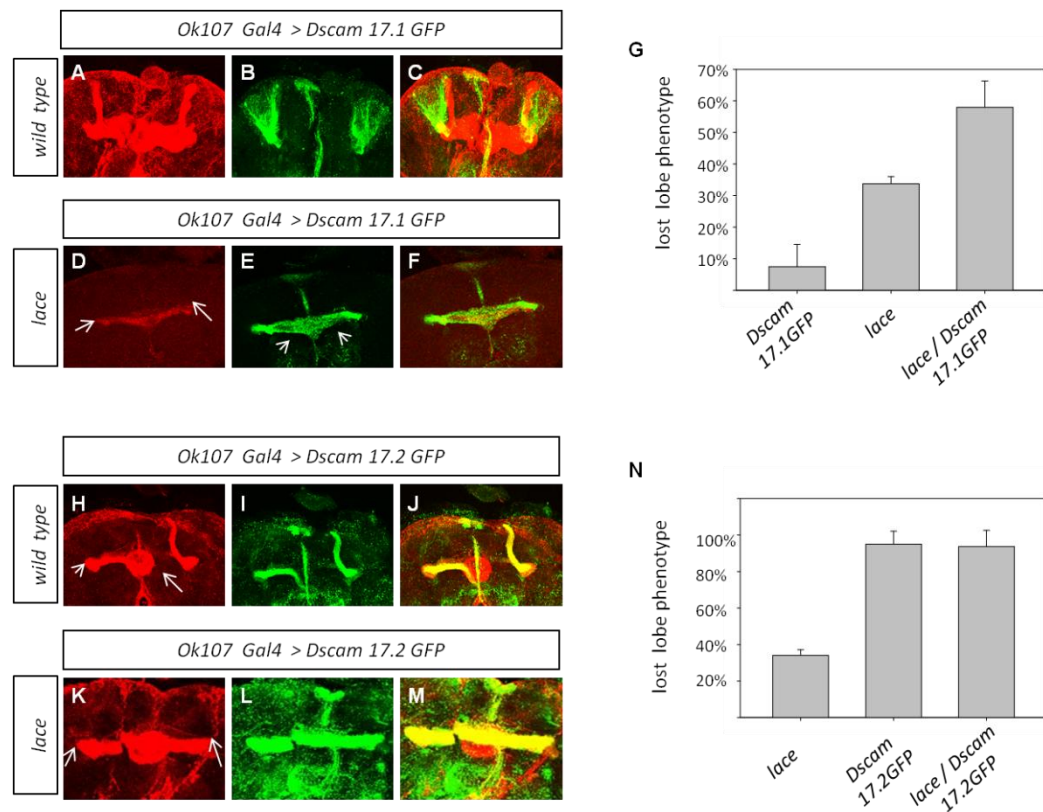


**Figure 3.24: Overexpression of Dscam TM1 in *lace* background enhances MB phenotype**

(A-C) In *lace*<sup>+/+</sup>, overexpression of Dscam [TM1] by Gal4-OK107 has a weak phenotype (around 5%). (D-F) In *lace*<sup>K05</sup>/*lace*<sup>2</sup> transheterozygote mutant, overexpression of TM1 enhances the lost lobe phenotype comparing with the *lace* mutant itself. (G) Quantification of Dscam [TM1] overexpression in *wild type* and *lace* background, shown TM1 enhance *lace* phenotype. (H-J) In *lace*<sup>+/+</sup>, overexpression of Dscam [TM2] by Gal4-OK107 has strong phenotype (around 90%). (K-M) *lace* transheterozygote mutant, overexpression of Dscam [TM2] by Gal4-OK107 also has strong phenotype. (N) Quantification of Dscam [TM2] overexpression in *wild type* and *lace* background, shown TM2 do not modify *lace* phenotype. (A-C) *Dscam*[TM1>::GFP; Gal4-OK107G4. (D-F) *lace*<sup>K05</sup>/*lace*<sup>2</sup>; *Dscam*[TM1>::GFP; Gal4-OK107G4 (H-J) *Dscam*[TM2>::GFP; Gal4-OK107G4. (K-M) *lace*<sup>K05</sup>/*lace*<sup>2</sup>; *Dscam*[TM2>::GFP; Gal4-OK107G4. (Green: GFP; red: FssII)



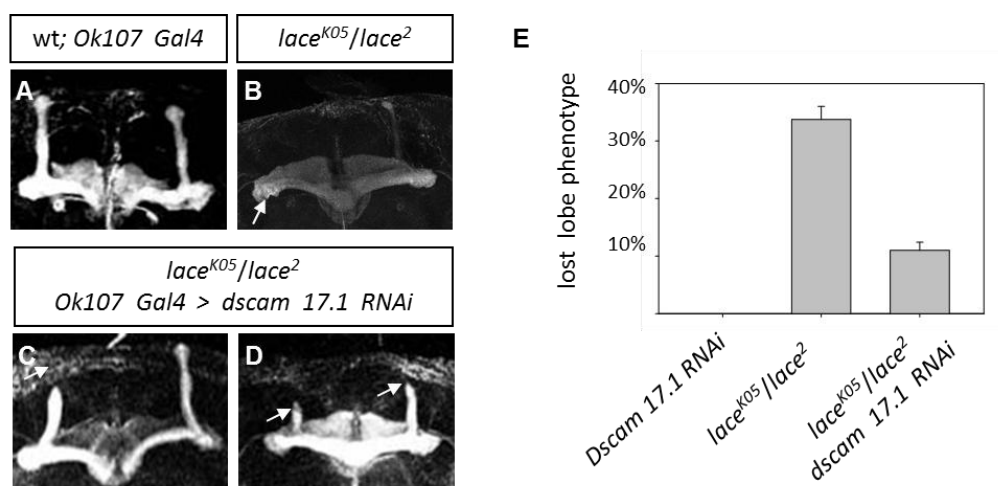


**Figure 3.25: Knockdown of Dscam TM1 in *lace* background suppress MB phenotype**

(A) Knockdown Dscam TM1 under wild type background does not affect the MB morphology. (B) *lace* transheterozygote mutant has lost lobe defect. (C and D) Knockdown Dscam TM1 under *lace* background decreases the lost lobe phenotype. (E) Quantification of phenotype (A) *Gal4-OK107G4*. (B) *lace<sup>2</sup>/lace<sup>K05</sup>; Gal4-OK107G4*. (C and D) *lace<sup>2</sup>/lace<sup>K05</sup>; DscamTM1 RNAi; Gal4-OK107G4*. (E) Quantification of Dscam [TM1] depletion in wild type and *lace* background, shown that knockdown TM1 suppress *lace* phenotype.

### 3.3.7 Dendritic proteins mistargeting in *lace* mutant

I next examined whether sphingolipids are required for proper localization of other dendritic proteins. Several documented dendritic markers *homer-GFP*, *Apc2-GFP*, *Act5C-GFP*, *Nod-GFP* and *Rdl-HA* (Sanchez-Soriano et al., 2005; Rolls et al., 2007) were expressed in the MBs using *GAL4-OK107* as the driver. In this condition, only *Nod-β-gal* and *Apc2-GFP* showed predominant somatodendritic distribution and were largely excluded from MB axon lobes (Figure 26 A, B and E).

Adenomatous polyposis coli tumor suppressor homolog 2 (*Apc2*), has been suggested to localizes with actin in multiple contexts in *Drosophila* embryos and epithelial cells regulate actin (reviewed by(Nathke 2004). In mushroom body neurons APC2-GFP mainly localized to the somatodendritic region and the very beginning of the peduncle (Figure3.26 A and B). In *lace* mutant, *Apc2 protein!* is localized to both

dendrites and axons. Interestingly, this mislocalized APC2 is strong in  $\alpha/\beta$  lobes, but not into  $\gamma$  lobe. This is similar to Dscam [TM1] mistargeting pattern.

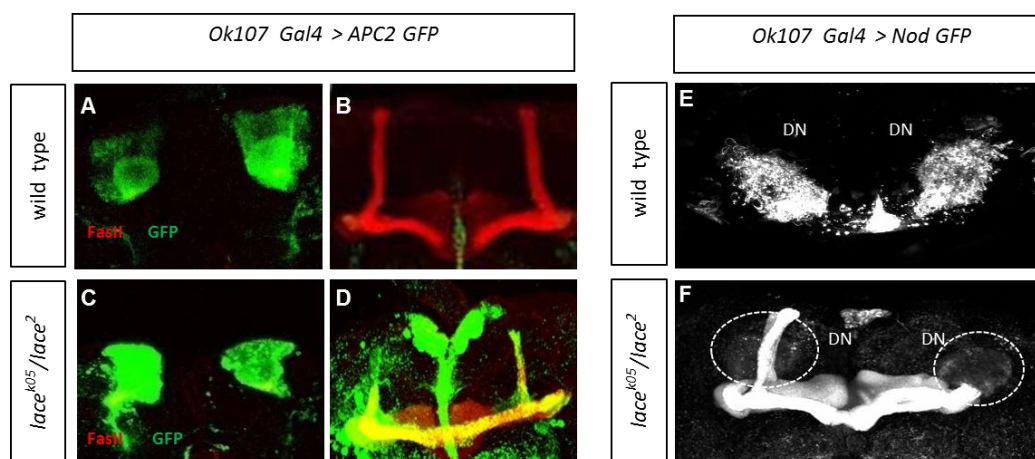


**Figure 3.26: MB dendritic proteins mistargeting in *lace* mutant**

(A and B) In wild type, Adenomatous polyposis coli tumor suppressor homolog 2 (*Apc2*) is localized to dendrites. *Apc2::GFP* is driven by *Gal4-OK107*. (A) Shown dendrites (B) shown axons. (C and D) In *lace* mutant, *Apc2* mistarget to axons. (C) Shown dendrites (D) shown axons. (E) In *wild type*, *Nod::GFP* is restrict to dendrites. (F) In *lace* mutant, *Apc2* mistarget to axons, including  $\alpha/\beta$ ,  $\alpha'/\beta'$  and  $\gamma$  lobe. Note the dendrites is lost *Nod::GFP* signal. Genotype: (A-B) *Apc2::GFP; Gal4-OK107G4*. (C-D) *lace<sup>K05</sup>lace<sup>2</sup>; UAS-Apc2::GFP; Gal4-OK107G4* (E) *Nod::GFP; Gal4-OK107G4*. (F) *lace<sup>K05</sup>lace<sup>2</sup>; UAS-Nod::GFP; Gal4-OK107G4*. (Green: GFP; red: FssII)

Another dendritic protein *Nod::GFP* is a fusion protein comprised of the motor domain of *Nod* and GFP, and has been shown to be a reliable minus-end reporter for microtubules in *Drosophila* (Andersen, Li et al. 2005). Microtubules in MB dendrites are bi-directional, but uniformly oriented with plus-end pointing distally in axons (Stone, Roegiers et al. 2008). Consistent with previous findings, *Nod::GFP* was highly enriched in dendrites, cell bodies and proximal region of peduncles, but largely absent from distal region of peduncles and axonal lobes in wild-type MB neurons (Figure 3.26 E). This dendritic distribution is totally disrupted in *lace* mutant (Figure 3.26 F). In contrast to the APC2 and Dscam[TM1], *Nod::GFP* mistarget to all the five lobes:  $\alpha/\beta$ ,  $\alpha'/\beta'$  and  $\gamma$  lobe. And dendritic targeting of *Nod::GFP* is totally lost in *lace*

mutant. It seemed that the polarity of the microtubule in MB dendrites and axons is reversed. It is very interesting to investigate how the microtubule polarity is controlled by sphingolipid and the general mislocalization phenotype is caused by the mis-polarity of microtubules or by other mechanisms.

### **3.3.8 Protein sorting and transport machinery disruption gives MB phenotype**

Since we found several MB dendritic proteins mislocalized into axons, indicating a general defects behind this phenotype. It is known that many dendritic proteins reach the somatodendritic membrane based on selective sorting and transport of carrier vesicles. Briefly, different cargo molecules segregation to tubular TGN subdomains according to the sorting signals in cargo molecules, then they interacts with a suitable motor and is extruded from the Golgi area, followed by the fission of these tubular precursors into centrifugally moving carriers ,which are sorted to different final destinations. Lots of factors involved in these progress, such as small GTPases of the ARF and Rab family, adaptors, GRIP-golgins and lipids, such as phosphoinositides, sphingolipids and cholesterol (De Matteis and Luini 2008). Generally, disruption of any of these factors could affect the protein transport.

I wondered if the protein sorting and transport machinery is important for the targeting of dendritic proteins in MBs. Following the knockdown of these candidate components by RNAi analyzed the MB morphology. Depletion of most of them gives MB defects (Figure 3.27). It is interesting that the phenotypes are not identical

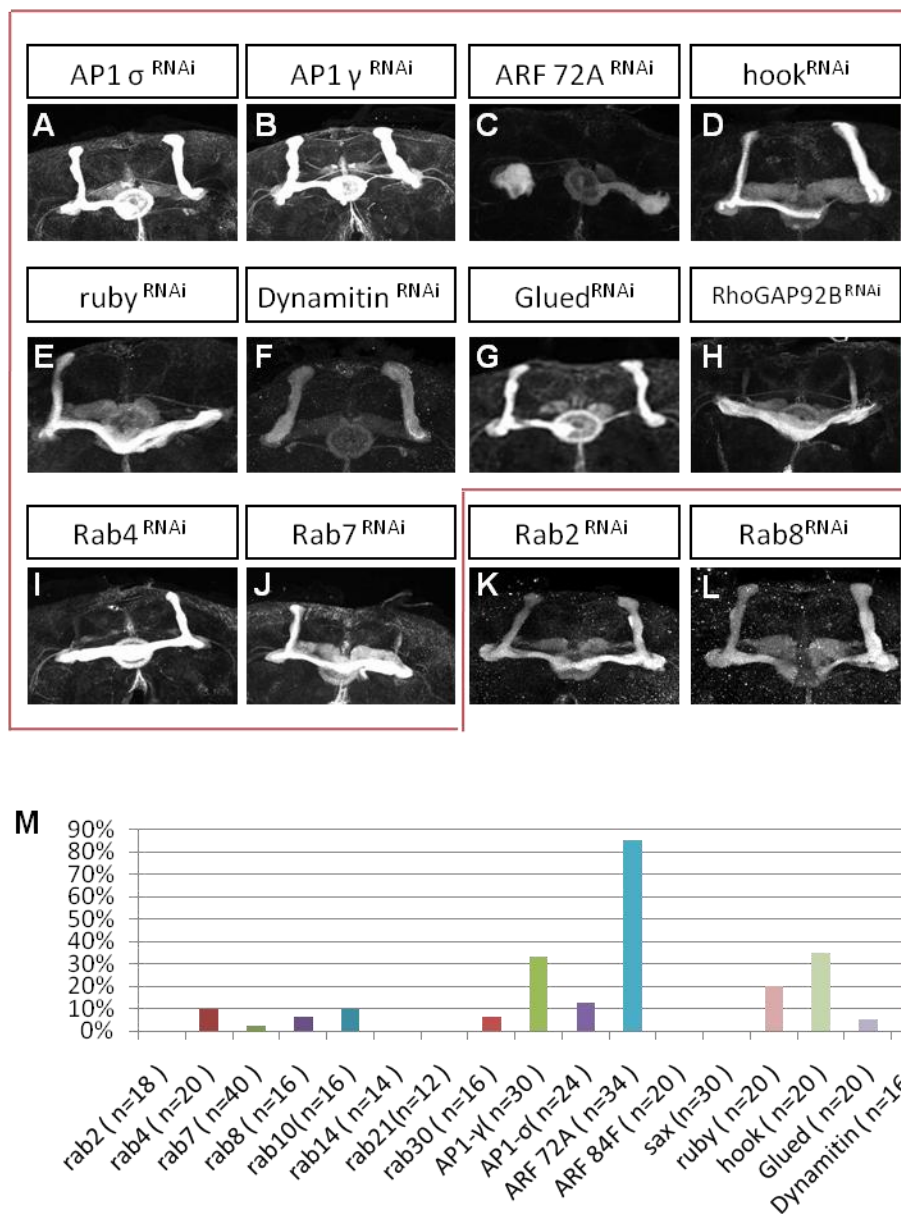


**Figure 3.27: Disruption of the protein sorting and transport machinery leads to MB phenotypes**

(A-L) Knockdown the genes of protein sorting and transport machinery in MB by Gal4-OK107. (A and B) AP-1 adaptor complex subunit  $\gamma$  and  $\sigma$ , lost  $\beta$  lobe and thicker  $\alpha$  lobe. (C) Arflike at 72A, severe lost lobe including  $\alpha/\beta$  and  $\gamma$  lobe. (D) hook, lost  $\beta$  lobe and thicker  $\alpha$  lobe. (E) ruby, lost  $\alpha$  lobe (F) Dynamitin, lost  $\beta$  lobe and thicker  $\alpha$  lobe. (G) Glued, reduce  $\beta$  lobe (H) RhoGAP92B, reduce  $\beta$  lobe. (I and J) Rab4 and Rab7, lost  $\alpha$  lobe. (K and L) Rab2 and Rab8, no obvious defect (M) Quantification of RNAi lost lobe phenotype.

among these genes. ARF72A (*Drosophila* Arl1-encoding ortholog) RNAi, give a severe axon guidance defect that axons stop growth at the end of the peduncle, therefore resulting in a lost  $\alpha/\beta$  and  $\gamma$  lobes in the FasII staining (Figure 3.27 C). AP1  $\gamma$  and  $\sigma$

(two subunit of AP-1 adaptor complex), hook (associated with early endosomes), and Dynamitin (one dynactin subunit) RNAi give the “lost  $\beta$  lobe” phenotype, meantime  $\alpha$  lobe is double thickness as wild type (Figure 3.27 A, B, D and F) which indicate two branches project into one direction after bifurcation. Ruby (the  $\beta$  subunit of the AP-3 complex), Rab4 and Rab7 RNAi give the lost  $\alpha$  lobe phenotype (Figure 3.27 E, I and J). Glued and RhoGAP92B RNAi give the lobe reduce phenotype (Figure 3.27 G and H). In contrast, Rab2 and Rab8 RNAi have largely normal MB morphology.

### **3.3.9 Rab4 and dscam 17.1GFP co-localize in MB neurons**

Although protein sorting machinery disruption give the MB morphology defects, this defects should be one of the broadly dysfunctions. To investigate the link among sphingolipid, protein mistargeting and sorting machinery, it is necessary to visualize dendritic proteins and sorting machinery colocalization in wild type and *lace* background. In wild type, Dscam [TM1] GFP and Rab4-RFP are colocalized in the somatodendritic region (Figure 3.28).

Rab4 localized to punctate structures throughout neurons in our study and a previous study (Sweeney, 2006) is consistent with endosome localization. It is interesting that only the big punctuate Dscam [TM1] colocalized with Rab4, the small dots of Dscam [TM1] are not overlapping with Rab4, indicating some Dscam [TM1] could be transport by other carriers. Rab4 is small GTPases belonging to the Ras superfamily and it is known that Rab4 labels the early endosomes. It is interesting to test the localization of Dscam [TM1] Rab4 and other endosomes producers under *lace* background in the future experiment.

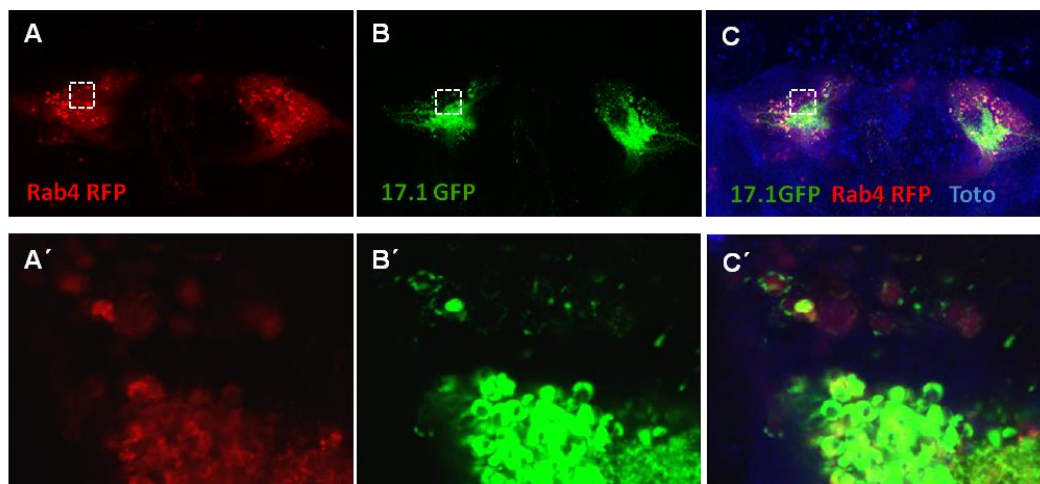


**Figure 3.28: Colocalization of Rab4 and dscam 17.1GFP in MB neurons**

Dscam [TM1] and Rab4 are co-labeled by GFP and RFP respectively. (A-C) and (A'-C') In *wild type*, Dscam [TM1] and Rab4 are colocalization in Somatodendritic region. (A and A') Rab4 localized in dendrites and axon (not shown) driven by Gal4-OK107. The small punctate structures are shown, which consistent with early endosomes. (B and B') Dscam [TM1] largely localized in cell body and dendrites. Both big and small punctate structures are seen (C and C') merge shown colocalization of Dscam [TM1] and Rab4. Note the small small punctate structures of Dscam [TM1] do not overlapping with Rab4. Genotype: (A-C) and (A'-C') *Rab4::RFP; Dscam [TM1)::GFP;OK107G4* (Green: GFP; red: FssII ; blue: Toto3)

## 4 DISCUSSIONS

Sphingolipids are enriched in the brain. Although it was assumed for many years that sphingolipids were mainly structural components of membranes, it is now clear that they participate in several cellular phenomena such as growth control, migration, differentiation, apoptosis, and senescence, crucial events that determine the normal development and fate of living organisms (Riboni, Viani et al. 1997; Stancevic and Kolesnick 2010).

In our study, we found that SPT (serine palmitoyltransferase), which catalyzes the first step of sphingolipid biosynthesis is required for olfactory neuron projection and Mushroom bodies (MBs) neurons development in *Drosophila melanogaster*. Mutants in two subunits of SPT, *spt-1* and *lace*, display identical ectopic ORNs targeting defects and *lace* mutant give a axon branching phenotype in MBs. *spt* and *dscam* have very similar phenotype and *spt* gene has a genetic suppression of *dscam* phenotype in ORNs projection based on the double mutants having a weaker phenotype. Moreover, several MBs dendritic makers such as APC2, Nod::*Khc*::GFP and Dscam[TM1] mislocalized to axons. Interestingly, ectopic expression of Dscam[TM1] in *lace* background enhance *lace* phenotype and depletion of Dscam[TM1] in MBs partially suppress the phenotype in MBs, indicating mislocalized Dscam[TM1] in *lace* mutant is contributing to the MBs defects. Moreover, Nod::*Khc*::GFP which is a minus-end microtubule binding protein localize in MB dendrites, mislocalized to axons suggest the microtubule polarity is mixed in MB axon in *spt* mutant. From these results I propose a model for *spt* function in mushroom body development (Figure 4.1). In wild type, the sphingolipids are highly enriched in trans-Golgi network(TGN) (De Matteis and Luini 2008), TGN has

classically been viewed as the main sorting node of the protein and lipid biosynthetic pathways. Enrichment of the sphingolipid in TGN provides a lipid environment that is substantially different from that of the earlier secretory compartments. These lipids have a tendency to coalesce and to form liquid-ordered membrane domains for which some proteins and have a specific cargo have a selective and distinctly higher affinity. This could therefore eventually lead to the segregation of sphingolipid-affinity cargo proteins from other cargo. Dscam[TM1] might be an example that has a higher affinity to sphingolipid and then selectively transported depend on sphingolipid enrichment environment. In addition, Dscam[TM1] selectively transported might via minus end directed motor depended mechanisms to the dendritic membrane in MBs. Unpacked Dscam[TM1] and Dscam[TM1] embedded vehicles might diffused to the axon initial segments(AIS), which is a distinctive region of the axon that is important for protein sorting within the neuron. Axon initial segments contain a specialized spectrin and ankyrin G submembrane skeleton that forms a diffusion barrier which isolates the plasma membrane in the axon from that in the soma. The diffused Dscam[TM1] are blocked by the AIS. Thus, DscamTM1 only target to dendrites membrane of MB in wild type.

In *spt* mutant, sphingolipids are reduced in TGN, which might affect the normal lipid environment, therefore affect the segregation of sphingolipid- affinity cargo proteins from other cargo. Moreover, reduced sphingolipids might lead to mispolarized microtubules in axon by unknown mechanisms. And reduced sphingolipids also



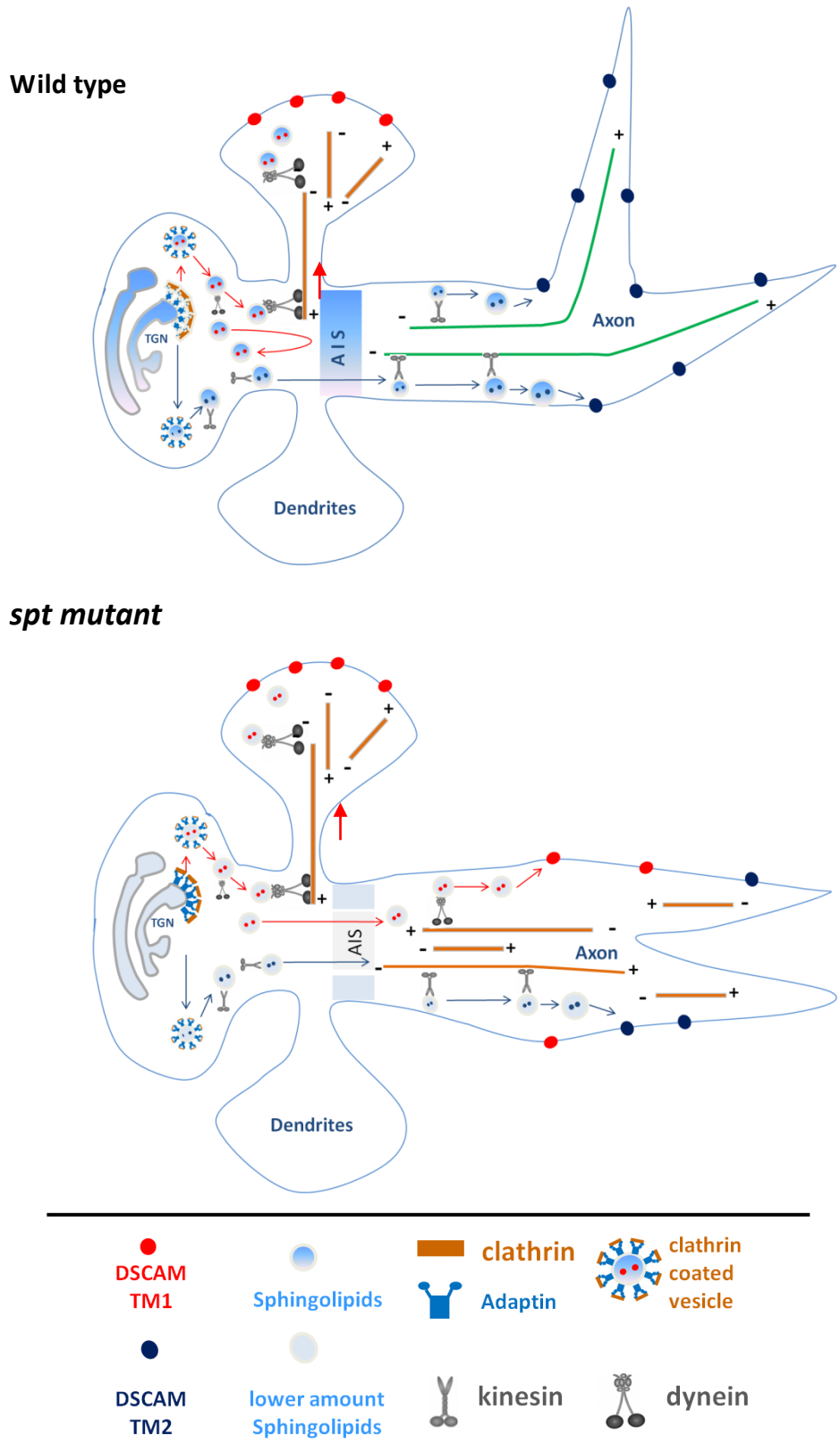


Figure 4.1: The model of *spt* function in Mushroom body

might disturbed AIS formation, since I found APC2 and EB1 protein, which localate mamlian AIS, had a abnormal pattern in *spt* mutant(see details in 4.4.2 and 4.4.3). The reduced sphingolipids vehicles can be transported to somadendretic membrane, but the selectivity of dendritic transporting is lost due to either the mispolarized microtubules, failed to recruit the proper transport machinery or disrupted AIS structure. Thus, Dscam TM1 mislocalize to axon and lead the MB phenotype in *spt* mutant.

#### **4.1 Non-cell-autonomous functions of *spt***

We found that *spt* and *lace* large clones produced by depletion the twin spot wild type cells with homozygous minute gene, have neuronal phenotype both in ORNs and MB neurons. However the MARCM clones are largely normal, which indicate only the large *spt* clones leading the defects. One speculation is that SPT proteins or the downstream products could be secreted from the neighbor wild type cells and taken though the endocytosis pathway by the mutant cells, thus the mutant cells in the bigger clone can not get enough materials from the environment. It is known that an isoform of sphingosine kinase 1 that acts on Sphingosine-1-phosphate (S1-P) is secreted and contributes to establishing the vascular S1-P gradient that regulates angiogenesis (Ancellin, Colmont et al. 2002). Ceramidase is secreted and can be internalized and localized to endosomes in the neighbor cells (Acharya, Dasgupta et al. 2008; Rigogliuso, Donati et al. 2010). Whether SPT proteins also could be secreted should be tested. In addition to the secreted enzymes, the secreted lipids are highly suspected candidates for the phenotypic difference between PCNA and MARCM clones. This is based on two points: first, it is known that several sphingolipids including sphingomyelin are shed from cells as membrane vesicles and could go into

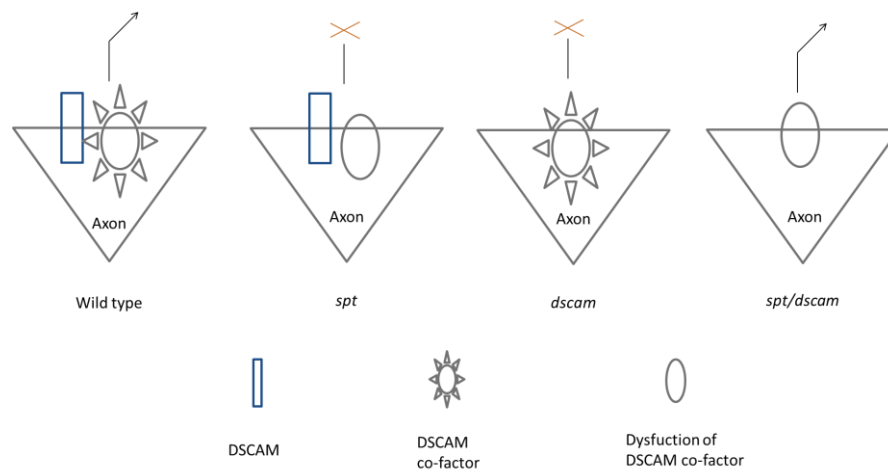
the cell by membrane internalization (Kim, Lee et al. 2002). Second, food supplying sphingosine can partially rescue the *lace* phenotype, indicating sphingolipid can be taken by the cell, and can transport through blood brain barrier to the nerve cell.

#### 4.2 Genetic interaction between *spt* and *dscam*

Our data suggest a genetic interaction between *spt* and *dscam* in ORNs targeting.

I supposed two possibilities for the *spt* and *dscam* suppression (Fig 4.2).

Model 1:



Model 2:

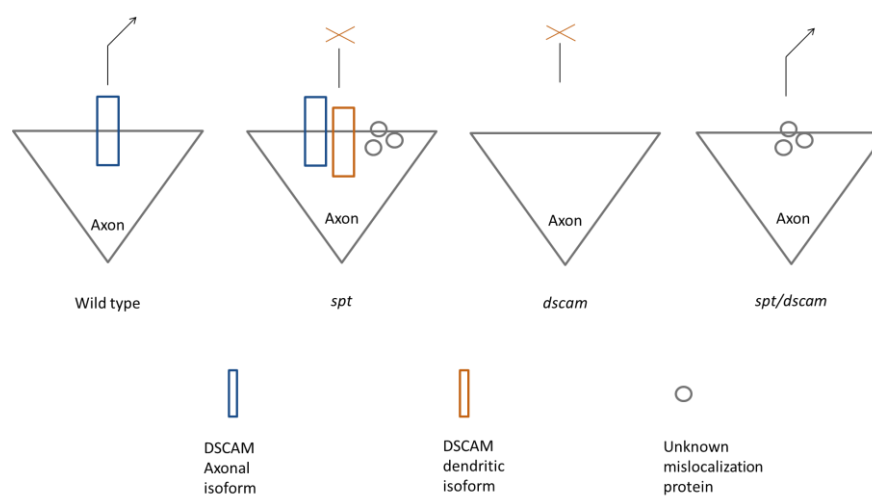


**Figure 4.2: Two models of *spt* and *dscam* genetic interaction**

First, *spt* may affect the function of a *dscam* co-factor that function together with *dscam*, but also can play an independent function when *dscam* depleted. Therefore, this dysfunction co-factor disturbs the *dscam* function in *spt* single mutant, but compensates *dscam* function in *dscam* and *spt* double mutant. Second, the suppression can also caused by accumulation of some products such as Dscam<sup>TM1</sup> and other proteins that are normally not accumulated in axon, these mix products affects *dscam* function in *spt* single mutant, but can compensate *dscam* function in *dscam* and *spt* double mutant.

#### **4.3 Genetic dissection of sphingolipid function by RNA interference**

To study complicated developmental processes, genes need to be inactivated in a tissue-specific manner in intact animals. This has become possible through the creation of a transgenic RNAi library targeting 88% of the *Drosophila* protein-coding genes (Dietzl, Chen et al. 2007). Taken the advantage of the RNAi tools, we did a genetic dissection of the sphingolipid function in ORNs and MB. I can phenocopy *spt* mutant phenotype in ORNs by the knocking down the downstream enzyme by *RNAi*. Similarly, I also observed MB phenotype by the knocking down the downstream enzymes. There are two limits in our experiments. First, the RNAi phenotypes are much weaker than the mutant in our experiments. Although it has been shown siRNA false-negative rate is about of 29.4% (Mummery-Widmer, Yamazaki et al. 2009), sphingolipid metabolism are very complex, and most of the biochemical reaction are located in an interconnected networks that many intermediates can be transformed each other. So, it is not surprise one enzyme depleted might have not decrease the product since blocking one branch could be bypass compensated by

other branches. Second, we did not check the RNA and protein expression in the RNAi experiments. However, we believe that most of them are functional constructs. since some of them had been used in a genome-wide analysis of Notch signaling in *Drosophila* and the constructs such as *spt* RNAi, *lace* RNAi, *sply* RNAi, and ceramidase RNAi are functional *in vivo*.(Mummery-Widmer, Yamazaki et al. 2009). Beside these limits, one advantage of the RNAi analysis of sphingolipid function in the full metabolism context is that we can get systematic information comparing with single mutant gene analyzing. For example, when I analysis the data of genetic dissection of MB phenotype, the data is confusing since each individual gene locate in different branches (Figure 3.21). However, focusing on the common product in different branches showed that different they converged to the membrane ceramide. Moreover, we also can make a new hypothesis from the systematic RNAi. For instance, *Drosophila* has been described as lacking sphingomyelin, but instead has phosphoethanolamine ceramide (CPE), where a phosphoethanolamine replaces phosphocholine in sphingomyelin (Bozidis, Williamson et al. 2007). We found SMase RNAi has a phenotype in MBs, based on the systematic RNAi data, which indicate *Drosophila* SMase could possible have the esterase activity to hydrolyze phosphoethanolamine ceramide, the fly substitute for sphingomyelin.

Although, the siRNA are powerful tools to investigate the sphingolipid function, it still needs other method to support the siRNA experiment. One expected experiment is that quantify different sphingolipid in the siRNA background by biochemistry methods, which can facilitate the genetic analysis and to find out the candidate sphingolipid.

## 4.4 Neuronal polarity and protein polarity localization in neuron

### 4.4.1 The mechanisms of protein polarity localization

The current knowledge of polarized localization of membrane proteins is primarily based on studies of biosynthetic and recycling pathways of apical and basolateral proteins in epithelial cells (Figure 4.3) (Rodriguez-Boulan and Musch 2005).

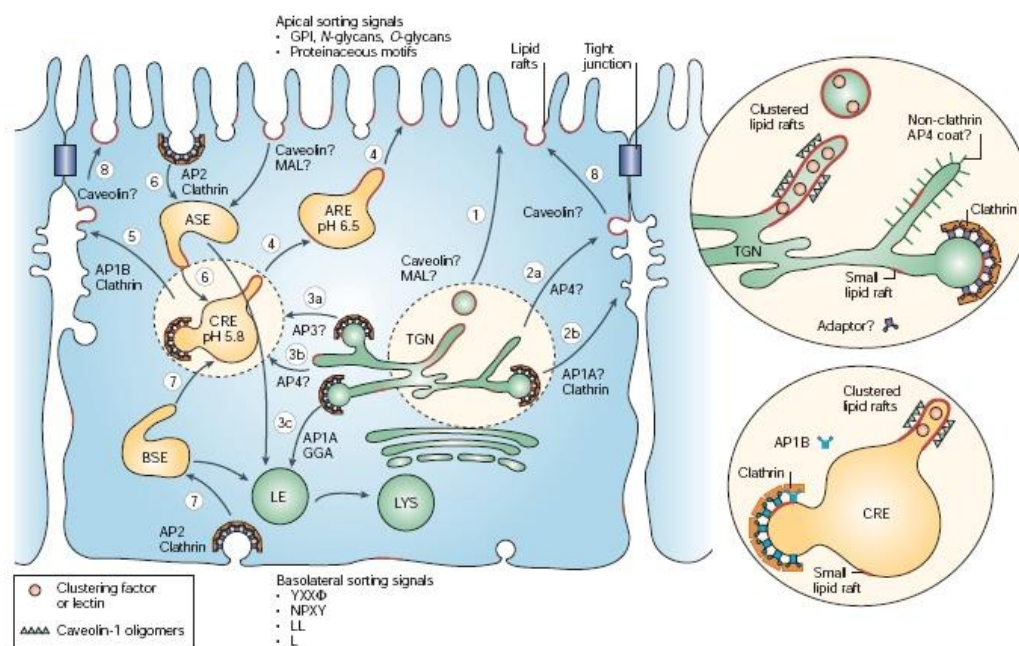


**Figure 4.3: Trafficking routes and sorting mechanisms in epithelial cells**

Apical exocytic routes (1 and 4): glycosylphosphatidylinositol (GPI) anchors, N-glycans and O-glycans sort apical proteins at the trans-Golgi network (TGN), common recycling endosomes (CREs) and apical recycling endosomes (AREs). This sorting might involve clustering small lipid rafts into larger functional lipid rafts. Basolateral exocytic routes (2 and 5): basolateral signals interact with adaptors of the clathrin (adaptor protein-1 (AP1), AP3, GGA (Golgi-localized,  $\gamma$ -earcontaining, Arf-binding protein)) or non-clathrin (AP4) type at the TGN or CREs. AP1B operates at the level of CREs (route 5; inset); membrane (route 2 followed by route 7 to basal sorting endosomes (BSEs), late endosomes (LEs) and lysosomes (LYS)), Endocytic routes (6 and 7): endocytosed apical (route 6) or basolateral (route 7) membrane proteins are internalized into apical sorting endosomes (ASEs) or BSEs by AP2, mix in CREs and are sorted into apical and basolateral exocytic routes by sorting signals that are similar to those used in the biosynthetic route (routes 4 and 5). Biosynthetic route through endosomes (routes 3a–c): some newly synthesized basolateral proteins reach CREs directly from the TGN (routes 3a and 3b; via unknown adaptors) from where they are sorted to the basolateral membrane via AP1B (route 5). Recycling and transcytosing apical membrane proteins transfer from CREs to AREs (route 4). Some GPI-anchored proteins seem to use a transcytotic route (route 8) in Madin–Darby canine kidney cells

One model to explain the differential distribution of membrane proteins is selective transport. Many basolateral plasma membrane proteins have targeting signals in their cytoplasmic domains, which consist of tyrosine- or dileucine-based motifs (Hunziker and Mellman 1991; Miranda, Khromykh et al. 2001). These motifs are recognized by clathrin adaptor protein (AP) complexes in the trans-Golgi network (TGN) or common recycling endosomes, and sorted to transport carriers destined for the basolateral domain (Mostov 2003; Folsch 2005). In contrast, apical targeting signals often reside in either the transmembrane domain or ectodomain of a protein (Lisanti, Caras et al. 1989; Gut, Kappeler et al. 1998). In addition to direct routes to the apical surface, some apical proteins are first transported to the basolateral membrane, and then sorted to the apical membrane via an indirect, transcytotic pathway (Bonilha, Marmorstein et al. 1997; Anderson, Maday et al. 2005; Weisz and Rodriguez-Boulan 2009). In neurons, the targeting of some somatodendritic plasma membrane proteins also depends on selective sorting and delivery from the TGN via the same cytoplasmic signals for basolateral sorting, including tyrosine- and dileucine-based motifs (Poyatos, Ruberti et al. 2000). Live-cell imaging studies have also revealed that the dendritic protein transferrin receptor (TfR) is directly transported into dendrites (Silverman, Kaech et al. 2001). In contrast, the polarization of some axonal proteins is dependent on an indirect pathway similar to epithelial apical proteins. It has been shown that axonal plasma membrane protein NgCAM reach the dendritic plasma membrane, then undergo endocytosis and travel to the axon (Yap, Nokes et al. 2008). Thus, current evidence suggests that direct sorting and delivery from the TGN is a predominant mechanism for dendritic targeting, while transcytosis and selective retention contribute to axonal targeting.

Besides selective transport, additional mechanisms may contribute to the polarized distribution by differential depletion or stabilization. For example, the steady-state axonal distribution of Nav1.2 and VAMP2 is primarily achieved through their selective removal by endocytosis from the dendritic plasma membrane (Garrido, Fernandes et al. 2003). Preferential fusion of vesicular cargos with different plasma membrane domains may mediate some polarized distribution as well.

#### **4.4.2 Dscam[TM1] and other dendritic proteins mislocalization**

Dscam [TM2] and [TM1] isoforms target to axon and dendrites respectively. It is known that an axonal targeting motif of Dscam is located in the cytoplasmic juxtamembrane region of TM2, which is dominant over the dendritic targeting motif, while dendritic targeting of Dscam relies on TM1 ectodomain (Wang, Ma et al. 2004; Shi, Yu et al. 2007).

In our study, we found Dscam [TM1] mistarget to the mushroom body axons. In addition, two other dendritic markers Nod and APC2 also mislocalized to axons indicating a general function of sphingolipid in the protein polarity targeting to the dendrites in MB neurons. One study shown that dynein-dynactin complex is essential for dendritic restriction of Dscam [TM1] (Yang, Bai et al. 2008). This study has uncovered that dynein-dynactin plays a role for maintaining dendritic distribution of Dscam[TM1] from axons by retrograde transport.

The TM1 mistargeting phenotypes in *dynein* and *spt* mutant are quite different. First, dynein/dynactin did not affect the initial dendritic targeting of Dscam [TM1], but disrupted the maintenance of its restriction to dendrites. In contrast, *spt* seems to affect the initial dendritic targeting based on the mistargeting phenotype in transient



expression TM1 (data not shown). Second, blocking dynein/dynactin function did not affect the distribution of two other dendritic markers, Nod- $\beta$ -gal and Rdl-HA. But, *spt* mutant lead to multiple dendritic makers mistargeting, include Nod and APC2. Nod- $\beta$ -gal is a reliable minus-end reporter of microtubules, and misdistribution of Nod- $\beta$ -gal in MB axons has been shown in *short stop* mutant clones, in which microtubule polarity is perturbed (Reuter, Nardine et al. 2003). Thus, Nod- $\beta$ -gal mislocalization in *spt* mutant suggests that dendritic Dscam mistargeting is due to abnormal microtubule organization. Taken together, dscam mistargeting in *spt* mutant is an early and general event.

As mentioned above, it has been demonstrated that different cargo proteins can segregate into different domains at the TGN and be subsequently incorporated into different transport carriers, even in a non-polarized cell (Keller et al. 2001). There are known mechanisms for this type of segregation in both polarized and non-polarized cells, such as selective interaction of a sorting signal with a coat protein or recruitment into lipid rafts. Determinants for separate axonal versus dendritic transport or targeting must occur downstream to this more general segregation process. There are two possibilities here: selective microtubule-based transport with 'smart' motor proteins that can distinguish different microtubules that lead to different destinations or selective fusion of carriers with specific plasma membrane domains. Both mechanisms may be utilized for any given carrier. It would be interesting to explore which mechanism that causes the phenotype in *spt* mutant.

For APC2 protein, it is known that there are two members of adenomatous polyposis coli tumor suppressor homolog in *Drosophila*. APC1 is strongly expressed in the CNS

and germline (Ahmed, Hayashi et al. 1998; McCartney, Dierick et al. 1999). APC2 is broadly expressed. APC1 and APC2 have different domain structures and subcellular localizations in embryo epithelia cell. In both mushroom body and projection neurons, Apc2-GFP was present in the cell body and dendrites. In mushroom body neurons it localized to just one region of the axons, near the beginning of the peduncle (Rolls, Satoh et al. 2007). No other report is available about the mistargeting of APC2 in MB. However, the polarity distribution of APC2 is related to microtubule in epithelial cell (Guerin and Kramer 2009). Since the Nod mistargeting suggest that microtubule polarity is affected, it is also possible that APC2 mistargeting is caused by the disturbed microtubules in *spt* mutant.

The Nod::Khc::GFP protein (Andersen, Li et al. 2005), as Nod-KHC- $\beta$ -Gal (Clark, Jan et al. 1997), is a reliable minus-end reporter of microtubules. It is known that MB dendrites microtubules are bi-directional (Hirokawa, Noda et al. 2009). In axons microtubules are uniformly oriented with minus-ends pointing to the cell body, so a minus-end-directed reporter can enter efficiently into the most distal parts of the dendrites, but cannot be efficiently transported along the axons since microtubules are oriented only plus-end distally and minus end point to cell body (Burack, Silverman et al. 2000). So, Nod chimera protein is restricted to the dendrites in wild type. In a previous study, misdistribution of Nod- $\beta$ -gal in MB axons has been shown in *short stop* mutant clones, in which microtubule polarity is perturbed (Reuter, Nardine et al. 2003). In *spt* mutant, we found a strong mislocalization of Nod::Khc::GFP in MB, indicating the polarity of microtubule is disturbed. Moreover, it is very interesting that MB dendrites are negative for Nod::Khc::GFP in the *spt* mutant, indicating the polarity of microtubule are mispolarity in dendrites and axon.

Little is known about the establishment of microtubule polarity differences in axons and dendrites during development. Although, disruption of CHO1/MKLP1, a kinesin protein, resulted in failure of dendritic differentiation in young hippocampal neurons and conversion of dendritic processes into axon-like processes in mature neurons, how can a motor protein, usually are thought to regulate organelle transport, reorganize the polarity of the microtubule are unknown (Sharp, Kuriyama et al. 1997; Yu, Cook et al. 2000).

In our study, *spt* mutants appear to have the opposite phenotype: conveying specific dendritic properties to axonal compartments. One report shown that ceramide is co-distribution with tubulin and aPKC in mouse ES cell, depletion of ceramide cause retraction of microtubules and membrane processes and lost aPKC polarity localization(Wang, Krishnamurthy et al. 2008), which indicate ceramide could be involved in cytoskeleton function. However, how can sphingolipid regulate microtubule polarity? It is still a puzzle need to be elucidated in the future.

#### **4.4.3 Axon initial segment (AIS), could MB as an in vivo model?**

The AIS is located at the most proximal part of the axon, where it functions as both a physiological and a physical bridge between the somatodendritic and axonal domains. In addition to its location, the AIS can be identified by ultrastructural features, such as fasciculated microtubules, by its molecular constituents and by its electrophysiological properties (Kole, Ilschner et al. 2008). Thus, the AIS functions as the nexus of neuronal polarity in the mature neuron (Figure 4.4).

The cytoskeletal scaffold protein ankyrin G is a master organizer of membrane domains and subcellular polarity. In neurons, AnkG is restricted to the AIS (Kordeli,

Lambert et al. 1995) and functions as a scaffold. Loss of AnkG blocks the subcellular polarization of the K<sup>+</sup> channels KCNQ2 and KCNQ3, the cell adhesion molecules neurofascin and neuronal cell adhesion molecule (NrCAM) and the cytoskeletal protein  $\beta$ IV spectrin (Pan, Kao et al. 2006; Hedstrom, Xu et al. 2007; Van Wart, Trimmer et al. 2007).

AIS play an important role in the establishment and maintenance of neuronal polarity due to its barrier function. Data support for the barrier model in vertebrates was provided in measured the diffusion of individual fluorescent phospholipid molecules in the axonal membrane and showed that their diffusion was blocked at the AIS (Nakada, Ritchie et al. 2003). The distribution of membrane proteins is also restricted by the AIS diffusion barrier (Winckler, Forscher et al. 1999). Many cytoplasmic proteins are also excluded from the axoplasm, indicating that the AIS barrier is not confined to the plasma membrane. The existence of a cytoplasmic barrier was confirmed in an experiment in which fluorescently labeled dextrans loaded into the soma of hippocampal neurons did not diffused into the axon (Song, Wang et al. 2009).

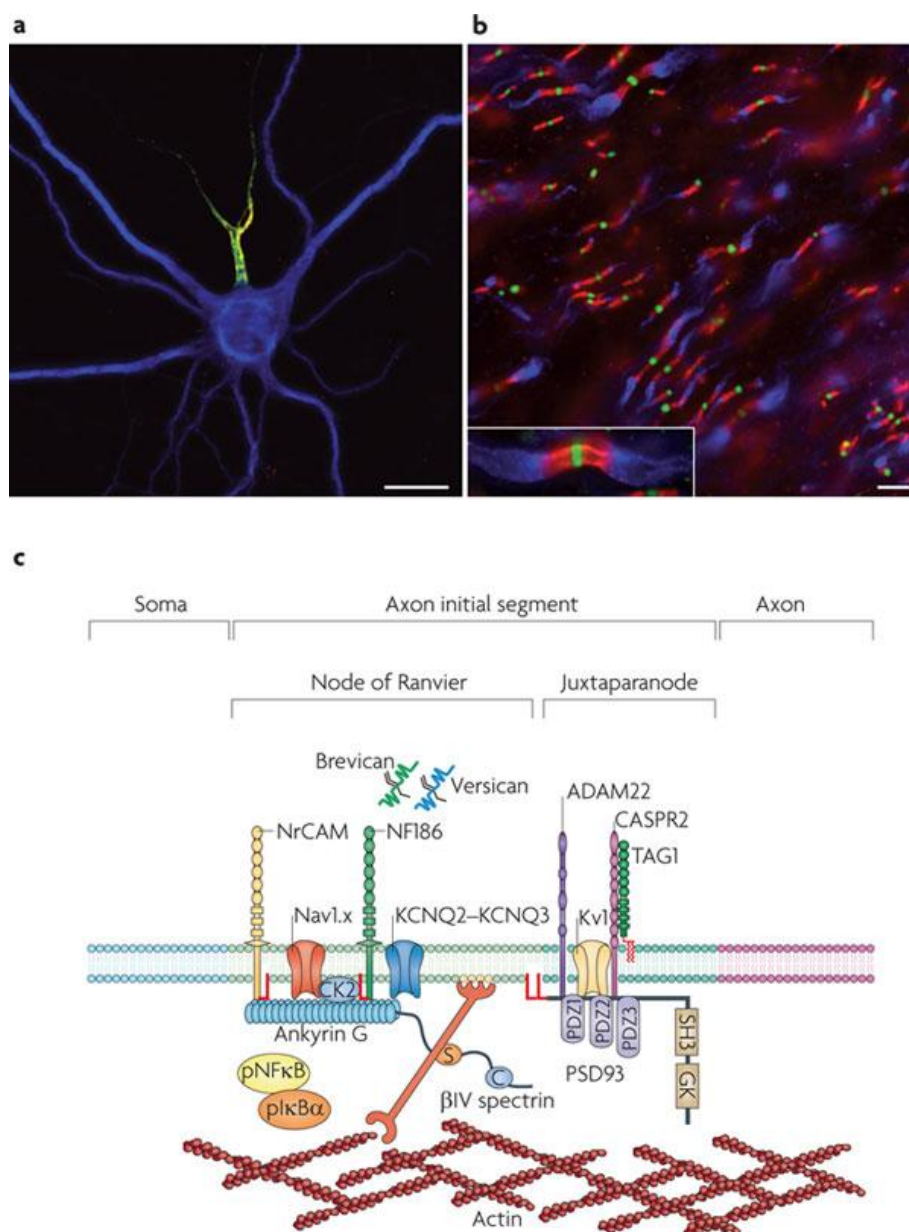


#### Figure 4.4: The organization of axon initial segment (AIS)

(a) A cultured hippocampal neuron with high densities of ankyrin G (AnkG, also known as ANK3) (green) and neurofascin 186 (NF186) (the overlap between AnkG and NF186 is shown in yellow) at the axon initial segment (AIS). Microtubule-associated protein 2 (MAP2) (blue) is confined to the somatodendritic domain. (b) Nodes of Ranvier show a highly polarized organization that includes nodal Na<sup>+</sup> channels (green), paranodal contactin-associated protein (Caspr) (red) and juxtapanodal K<sup>+</sup> channels (blue). (c) The molecular organization of the AIS, which has many features in common with nodes of Ranvier and juxtaparanodes (from M. N. Rasband; Nature Reviews Neuroscience 11, 552-562).

Furthermore, examining the movement of transport vesicles showed that vesicles

---

containing dendritic cargoes were excluded from the axon (Song, Wang et al. 2009). Taken together, these experiments provide support for the existence of a barrier that restricts lipids, cytoplasmic and membrane proteins and transport vesicles to distinct compartments of the polarized neuron.

In our study, we found a general mislocalization phenotype for the dendritic proteins in MB. It is interesting to mention that, in wild type, Apc2 is localized in the cell body and the proximal axon region, which is just distal to the stretch of proximal neuritis in which NgCAM was concentrate (Rolls, Satoh et al. 2007). It is also known that APC proteins bind a number of cytoskeletal proteins, including microtubules and the plus-end microtubule binding protein EB1 (Nathke 2004). It is known that overexpressed EB1-YFP localizes to the initial segment in hippocampal neurons, and may recognize a local microtubule specialization important for directional transport within neurons (Nakata and Hirokawa 2003). Thus, localization of two cytoskeleton-interacting proteins to the proximal axon in flies indicates that the *Drosophila* axon is divided into domains with specialized cytoskeletal properties. This proximal axon restriction of the dendritic protein is also true for dscam [TM1]. It will be interesting to determine whether this region is functionally similar to the vertebrate axon initial segment. Moreover, mushroom body could be a *in vivo* model for the AIS study due to its highly polarity structures and clearly distinguished dendritic and axon compartments.

Taken together, dendritic markers mislocalization in *spt* mutant suggest sphingolipid have general function in protein polarity targeting. We could not exclude any of the three models: the *spt* phenotype could be a result of the selective transport either directly by motor proteins or by vehicle carriers is defect; also could caused by the

dysfunction of selective excluding dendritic protein by retrograde and also could be led by the initial axon segment function defect due to depletion sphingolipid. However, based on the microtubule defects, it is plausible that the initial of polarity of microtubule are defect during the early development, this could happen simultaneously with the axon initial segment forming and link to each other. The disorder cytoskeleton is definitely leading the general protein sorting and transporting defects in *spt* mutant.

#### 4.4 Outlook

In our study, we found both ORNs and MB connectivity defects in *spt* mutant flies. It is clear that there is a genetic interaction between *spt* and *Dscam*. Loss of *spt* leads to disruption of *Dscam* function, so the phenotypes of *spt* and *dscam* are very similar. We also found that dendritic protein is mistargeting to axon in MB under *spt* mutant background, and it seemed to be a general mistargeting defects since several dendritic makers have this defects.

However, the sphingolipid synthesis are very complex, there are lots of unrevealed questions in our study.

First, how is the mislocalization of dendritic proteins happened in *spt* background? There are three possibilities. One is that some sphingolipid may regulate the general protein sorting machinery to dendrites. Another is sphingolipid keeping a special region between axon and dendrites, which is called the initial segment of axon having a barrier function that hold some proteins within the somadendritic region but allow axonal proteins travelling through. In addition, microtubule polarity seems to become disturbed in *spt* mutant, which lead the minus-end transport proteins (dendritic

proteins) transport to axon.

Second, we found the genetic interaction between *spt* and *dscam* both in olfactory system and mushroom body. We found that *spt* suppress *dscam* phenotype in ORNs targeting, and is it true in MB? Also, we found dendritic proteins mistargeting in MB, and is it true in ORNs?

Third, we do not know which kinds of sphingolipids function in Olfactory and mushroom body. Is it only one kind of sphingolipid function in the neuronal projection, or several kinds of sphingolipid function in several situations, or sphingolipid function in a network? And what is the molecular mechanism of the 'specific' sphingolipid function in neuronal guidance? All of these questions are very interesting and also challenging.



---

## 5 SUMMARY

A central question in neuronal development is how a combination of cell-intrinsic differentiation factors and extra-cellular signals specify axon and dendrite identity, eventually leading to distinct brain circuits. Using a genetic approach in the *Drosophila* brain, the goal of this thesis was the functional characterization of neuronal SPT, a key enzyme in the generation of membrane sphingolipids.

The loss of *spt-1* and *lace*, which encode the two subunits of SPT, leads to identical defects in the axonal projection of olfactory sensory neurons (ORN) as well as central brain mushroom bodies (MB). Genetic mosaic analysis, which showed a strong non-cell-autonomous effect, together with the rescue of the neuronal defects by feeding sphingosine, indicating that the reduction in sphingolipids is the main cause of the *spt* phenotype. Genetic dissection sphingolipids function by sphingosine kinase RNAi, ceramide galactosyl transferase RNAi and ceramide kinase RNAi have the similar phenotype as *spt* mutant, which also indicate that some sphingolipids are required for ORNs targeting. Interestingly, *spt* and *dscam* have very similar phenotypes. To investigate the relationship between *spt* and *dscam*, a genetic interaction study was performed and loss of *spt-1* partially suppresses *Dscam* mutant ORN phenotype, which indicates *spt* and *dscam* have a strong genetic interaction.

*Dscam* is well studied in mushroom body (MB) development. In order to address the relationship between *spt* and *Dscam*, I change to the MB system and found loss of *lace* leads to defects in the projection of MB axons. Following genetic dissection of the sphingolipid function in MBs by RNA interference give a hint that membrane ceramide playing an important role in MB neuron development. Again, the *spt*

---

phenotype in MB is very similar to *Dscam*. Loss of *lace* enhances the *Dscam*-TM1 overexpression phenotype in MB, suggesting *spt* and *Dscam* have a genetic interaction in MB. In addition, the dendritic isoform *Dscam*-TM1GFP was found mislocalized to MB axon. I suspected that the mislocalized *dscam* might disturb the function of normal axonal isoform of *Dscam*TM2. Later experiments showed that *lace*<sup>2</sup>/*lace*<sup>k</sup> phenotype in MB can be partially suppressed by Ok107 driving *Dscam*-TM1 RNAi, which support the hypothesis and indicate the mislocalization of *Dscam*TM1 affect MB neuron projection. Finally, I found other MB dendritic proteins, including APC2 and Nod, mistargeting to the axons, which suggest that the mislocalization of dendritic protein into axon in *spt* is unselective and general defects. Nod::*Khc*::GFP is a reliable minus-end reporter of microtubules, mislocalization of Nod indicate the polarity of microtubule is disturbed in axon.

These results therefore suggest sphingolipids are important for olfactory neurons and mushroom body neurons development. Decrease sphingolipids in the MB neurons leading the mislocalization of dendritic proteins, which may be the results of the mispolarized microtubule.

## 6 BIBLIOGRAPHY

Acharya, J. K., U. Dasgupta, S. S. Rawat, C. Yuan, P. D. Sanxaridis, I. Yonamine, P. Karim, K. Nagashima, M. H. Brodsky, S. Tsunoda and U. Acharya (2008). "Cell-nonautonomous function of ceramidase in photoreceptor homeostasis." Neuron **57**(1): 69-79.

Acharya, U. and J. K. Acharya (2005). "Enzymes of sphingolipid metabolism in *Drosophila melanogaster*." Cell Mol Life Sci **62**(2): 128-142.

Acharya, U., S. Patel, E. Koundakjian, K. Nagashima, X. Han and J. K. Acharya (2003). "Modulating sphingolipid biosynthetic pathway rescues photoreceptor degeneration." Science **299**(5613): 1740-1743.

Adachi-Yamada, T., T. Gotoh, I. Sugimura, M. Tateno, Y. Nishida, T. Onuki and H. Date (1999). "De novo synthesis of sphingolipids is required for cell survival by down-regulating c-Jun N-terminal kinase in *Drosophila* imaginal discs." Mol Cell Biol **19**(10): 7276-7286.

Ahmed, Y., S. Hayashi, A. Levine and E. Wieschaus (1998). "Regulation of armadillo by a *Drosophila* APC inhibits neuronal apoptosis during retinal development." Cell **93**(7): 1171-1182.

Ancellin, N., C. Colmont, J. Su, Q. Li, N. Mittereder, S. S. Chae, S. Stefansson, G. Liau and T. Hla (2002). "Extracellular export of sphingosine kinase-1 enzyme. Sphingosine 1-phosphate generation and the induction of angiogenic vascular maturation." J Biol Chem **277**(8): 6667-6675.

Andersen, R., Y. Li, M. Resseguie and J. E. Brenman (2005). "Calcium/calmodulin-dependent protein kinase II alters structural plasticity and cytoskeletal dynamics in *Drosophila*." J Neurosci **25**(39): 8878-8888.

Anderson, E., S. Maday, J. Sfakianos, M. Hull, B. Winckler, D. Sheff, H. Folsch and I. Mellman (2005). "Transcytosis of NgCAM in epithelial cells reflects differential signal recognition on the endocytic and secretory pathways." J Cell Biol **170**(4): 595-605.

Bartke, N. and Y. A. Hannun (2009). "Bioactive sphingolipids: metabolism and function." J Lipid Res **50 Suppl**: S91-96.

Bejaoui, K., C. Wu, M. D. Scheffler, G. Haan, P. Ashby, L. Wu, P. de Jong and R. H. Brown, Jr. (2001). "SPTLC1 is mutated in hereditary sensory neuropathy, type 1." Nat Genet **27**(3): 261-262.

Bellen, H. J., C. Tong and H. Tsuda (2010). "100 years of *Drosophila* research and its impact on vertebrate neuroscience: a history lesson for the future." Nat Rev Neurosci **11**(7): 514-522.

Bonilha, V. L., A. D. Marmorstein, L. Cohen-Gould and E. Rodriguez-Boulan (1997). "Apical sorting of influenza hemagglutinin by transcytosis in retinal pigment epithelium." J Cell Sci **110 ( Pt 15)**: 1717-1727.

Boyle, M., A. Nighorn and J. B. Thomas (2006). "Drosophila Eph receptor guides specific axon branches of mushroom body neurons." Development **133**(9): 1845-1854.

Bozidis, P., C. D. Williamson and A. M. Colberg-Poley (2007). "Isolation of endoplasmic reticulum, mitochondria, and mitochondria-associated membrane fractions from transfected cells and from human cytomegalovirus-infected primary fibroblasts." Curr Protoc Cell Biol **Chapter 3**: Unit 3 27.

Brand, A. H. and N. Perrimon (1993). "Targeted gene expression as a means of altering cell fates and generating dominant phenotypes." Development **118**(2): 401-415.

Brown, D. A. and E. London (2000). "Structure and function of sphingolipid- and cholesterol-rich membrane rafts." J Biol Chem **275**(23): 17221-17224.

Brown, D. A. and J. K. Rose (1992). "Sorting of GPI-anchored proteins to glycolipid-enriched membrane subdomains during transport to the apical cell surface." Cell **68**(3): 533-544.

Burack, M. A., M. A. Silverman and G. Banker (2000). "The role of selective transport in neuronal protein sorting." Neuron **26**(2): 465-472.

Carter, H. E., W. J. Haines and et al. (1947). "Biochemistry of the sphingolipides; preparation of sphingolipides from beef brain and spinal cord." J Biol Chem **169**(1): 77-82.

Chesler, A. T., D. J. Zou, C. E. Le Pichon, Z. A. Peterlin, G. A. Matthews, X. Pei, M. C. Miller and S. Firestein (2007). "A G protein/cAMP signal cascade is required for axonal convergence into olfactory glomeruli." Proc Natl Acad Sci U S A **104**(3): 1039-1044.

Clark, I. E., L. Y. Jan and Y. N. Jan (1997). "Reciprocal localization of Nod and kinesin fusion proteins indicates microtubule polarity in the Drosophila oocyte, epithelium, neuron and muscle." Development **124**(2): 461-470.

Da Silva, J. S., T. Hasegawa, T. Miyagi, C. G. Dotti and J. Abad-Rodriguez (2005). "Asymmetric membrane ganglioside sialidase activity specifies axonal fate." Nat Neurosci **8**(5): 606-615.

De Matteis, M. A. and A. Luini (2008). "Exiting the Golgi complex." Nat Rev Mol Cell Biol **9**(4): 273-284.

Dickson, R. C. (1998). "Sphingolipid functions in *Saccharomyces cerevisiae*: comparison to mammals." Annu Rev Biochem **67**: 27-48.

Dietzl, G., D. Chen, F. Schnorrer, K. C. Su, Y. Barinova, M. Fellner, B. Gasser, K. Kinsey, S. Opiel, S. Scheiblauer, A. Couto, V. Marra, K. Keleman and B. J. Dickson (2007). "A genome-wide transgenic RNAi library for conditional gene inactivation in Drosophila." Nature **448**(7150): 151-156.

Folsch, H. (2005). "The building blocks for basolateral vesicles in polarized epithelial cells." Trends Cell Biol **15**(4): 222-228.

Friant, S., R. Lombardi, T. Schmelzle, M. N. Hall and H. Riezman (2001). "Sphingoid base signaling via Pkh kinases is required for endocytosis in yeast." EMBO J **20**(23): 6783-6792.

Futerman, A. H. and Y. A. Hannun (2004). "The complex life of simple sphingolipids." EMBO Rep **5**(8): 777-782.

Garrido, J. J., F. Fernandes, A. Moussif, M. P. Fache, P. Giraud and B. Dargent (2003). "Dynamic compartmentalization of the voltage-gated sodium channels in axons." Biol Cell **95**(7): 437-445.

Gauthier, M. S., K. Couturier, J. G. Latour and J. M. Lavoie (2003). "Concurrent exercise prevents high-fat-diet-induced macrovesicular hepatic steatosis." J Appl Physiol **94**(6): 2127-2134.

Golic, K. G. and S. Lindquist (1989). "The FLP recombinase of yeast catalyzes site-specific recombination in the *Drosophila* genome." Cell **59**(3): 499-509.

Goode, S., M. Melnick, T. B. Chou and N. Perrimon (1996). "The neurogenic genes egghead and brainiac define a novel signaling pathway essential for epithelial morphogenesis during *Drosophila* oogenesis." Development **122**(12): 3863-3879.

Guerin, C. M. and S. G. Kramer (2009). "RacGAP50C directs perinuclear gamma-tubulin localization to organize the uniform microtubule array required for *Drosophila* myotube extension." Development **136**(9): 1411-1421.

Guirland, C., S. Suzuki, M. Kojima, B. Lu and J. Q. Zheng (2004). "Lipid rafts mediate chemotropic guidance of nerve growth cones." Neuron **42**(1): 51-62.

Gut, A., F. Kappeler, N. Hyka, M. S. Balda, H. P. Hauri and K. Matter (1998). "Carbohydrate-mediated Golgi to cell surface transport and apical targeting of membrane proteins." EMBO J **17**(7): 1919-1929.

Hallem, E. A. and J. R. Carlson (2004). "The odor coding system of *Drosophila*." Trends Genet **20**(9): 453-459.

Hanada, K. (2003). "Serine palmitoyltransferase, a key enzyme of sphingolipid metabolism." Biochim Biophys Acta **1632**(1-3): 16-30.

Hannun, Y. A. and L. M. Obeid (2008). "Principles of bioactive lipid signalling: lessons from sphingolipids." Nat Rev Mol Cell Biol **9**(2): 139-150.

Hedstrom, K. L., X. Xu, Y. Ogawa, R. Frischknecht, C. I. Seidenbecher, P. Shrager and M. N. Rasband (2007). "Neurofascin assembles a specialized extracellular matrix at the axon initial segment." J Cell Biol **178**(5): 875-886.

Heisenberg, M. (1980). "Mutants of brain structure and function: what is the significance of the mushroom bodies for behavior?" Basic Life Sci **16**: 373-390.

Heisenberg, M. (2003). "Mushroom body memoir: from maps to models." Nat Rev Neurosci **4**(4): 266-275.

Hensel, F., R. Hermann, C. Schubert, N. Abe, K. Schmidt, A. Franke, A. Shevchenko, M. Mann, H. K. Muller-Hermelink and H. P. Vollmers (1999). "Characterization of glycosylphosphatidylinositol-linked molecule CD55/decay-accelerating factor as the receptor

- for antibody SC-1-induced apoptosis." Cancer Res **59**(20): 5299-5306.
- Hirokawa, N., Y. Noda, Y. Tanaka and S. Niwa (2009). "Kinesin superfamily motor proteins and intracellular transport." Nat Rev Mol Cell Biol **10**(10): 682-696.
- Holthuis, J. C., T. Pomorski, R. J. Raggars, H. Sprong and G. Van Meer (2001). "The organizing potential of sphingolipids in intracellular membrane transport." Physiol Rev **81**(4): 1689-1723.
- Hornemann, T., A. Penno, S. Richard, G. Nicholson, F. S. van Dijk, A. Rotthier, V. Timmerman and A. von Eckardstein (2009). "A systematic comparison of all mutations in hereditary sensory neuropathy type I (HSAN I) reveals that the G387A mutation is not disease associated." Neurogenetics **10**(2): 135-143.
- Hummel, T., M. L. Vasconcelos, J. C. Clemens, Y. Fishilevich, L. B. Vosshall and S. L. Zipursky (2003). "Axonal targeting of olfactory receptor neurons in *Drosophila* is controlled by *Dscam*." Neuron **37**(2): 221-231.
- Hummel, T. and S. L. Zipursky (2004). "Afferent induction of olfactory glomeruli requires N-cadherin." Neuron **42**(1): 77-88.
- Hunziker, W. and I. Mellman (1991). "Relationships between sorting in the exocytic and endocytic pathways of MDCK cells." Semin Cell Biol **2**(6): 397-410.
- Ito, K., W. Awano, K. Suzuki, Y. Hiromi and D. Yamamoto (1997). "The *Drosophila* mushroom body is a quadruple structure of clonal units each of which contains a virtually identical set of neurones and glial cells." Development **124**(4): 761-771.
- Ito, K. and Y. Hotta (1992). "Proliferation pattern of postembryonic neuroblasts in the brain of *Drosophila melanogaster*." Dev Biol **149**(1): 134-148.
- Jefferis, G. S., E. C. Marin, R. J. Watts and L. Luo (2002). "Development of neuronal connectivity in *Drosophila* antennal lobes and mushroom bodies." Curr Opin Neurobiol **12**(1): 80-86.
- Jefferis, G. S., R. M. Vyas, D. Berdnik, A. Ramaekers, R. F. Stocker, N. K. Tanaka, K. Ito and L. Luo (2004). "Developmental origin of wiring specificity in the olfactory system of *Drosophila*." Development **131**(1): 117-130.
- Kim, C. W., H. M. Lee, T. H. Lee, C. Kang, H. K. Kleinman and Y. S. Gho (2002). "Extracellular membrane vesicles from tumor cells promote angiogenesis via sphingomyelin." Cancer Res **62**(21): 6312-6317.
- Kiselev, A., M. Socolich, J. Vinos, R. W. Hardy, C. S. Zuker and R. Ranganathan (2000). "A molecular pathway for light-dependent photoreceptor apoptosis in *Drosophila*." Neuron **28**(1): 139-152.
- Kitamoto, T. (2001). "Conditional modification of behavior in *Drosophila* by targeted expression of a temperature-sensitive shibire allele in defined neurons." J Neurobiol **47**(2): 81-92.

Kitatani, K., J. Idkowiak-Baldys and Y. A. Hannun (2007). "Mechanism of inhibition of sequestration of protein kinase C alpha/beta1 by ceramide. Roles of ceramide-activated protein phosphatases and phosphorylation/dephosphorylation of protein kinase C alpha/beta1 on threonine 638/641." J Biol Chem **282**(28): 20647-20656.

Kleene, R., H. Yang, M. Kutsche and M. Schachner (2001). "The neural recognition molecule L1 is a sialic acid-binding lectin for CD24, which induces promotion and inhibition of neurite outgrowth." J Biol Chem **276**(24): 21656-21663.

Koch, C. and G. Laurent (1999). "Complexity and the nervous system." Science **284**(5411): 96-98.

Kole, M. H., S. U. IIschner, B. M. Kampa, S. R. Williams, P. C. Ruben and G. J. Stuart (2008). "Action potential generation requires a high sodium channel density in the axon initial segment." Nat Neurosci **11**(2): 178-186.

Kordeli, E., S. Lambert and V. Bennett (1995). "AnkyrinG. A new ankyrin gene with neural-specific isoforms localized at the axonal initial segment and node of Ranvier." J Biol Chem **270**(5): 2352-2359.

Kurusu, M., T. Awasaki, L. M. Masuda-Nakagawa, H. Kawauchi, K. Ito and K. Furukubo-Tokunaga (2002). "Embryonic and larval development of the Drosophila mushroom bodies: concentric layer subdivisions and the role of fasciclin II." Development **129**(2): 409-419.

Kurusu, M., T. Nagao, U. Walldorf, S. Flister, W. J. Gehring and K. Furukubo-Tokunaga (2000). "Genetic control of development of the mushroom bodies, the associative learning centers in the Drosophila brain, by the eyeless, twin of eyeless, and Dachshund genes." Proc Natl Acad Sci U S A **97**(5): 2140-2144.

Lamaze, C., L. M. Fujimoto, H. L. Yin and S. L. Schmid (1997). "The actin cytoskeleton is required for receptor-mediated endocytosis in mammalian cells." J Biol Chem **272**(33): 20332-20335.

Lattemann, M., A. Zierau, C. Schulte, S. Seidl, B. Kuhlmann and T. Hummel (2007). "Semaphorin-1a controls receptor neuron-specific axonal convergence in the primary olfactory center of Drosophila." Neuron **53**(2): 169-184.

Lee, T., A. Lee and L. Luo (1999). "Development of the Drosophila mushroom bodies: sequential generation of three distinct types of neurons from a neuroblast." Development **126**(18): 4065-4076.

Lee, T. and L. Luo (1999). "Mosaic analysis with a repressible cell marker for studies of gene function in neuronal morphogenesis." Neuron **22**(3): 451-461.

Lisanti, M. P., I. W. Caras, M. A. Davitz and E. Rodriguez-Boulan (1989). "A glycopospholipid membrane anchor acts as an apical targeting signal in polarized epithelial cells." J Cell Biol **109**(5): 2145-2156.

Marek Cebecauer, D. M. O., Anna Markiewicz (2009). "Lipid order and molecular assemblies

in the plasma membrane of eukaryotic cell." Biochemical Society Transactions **37**(5): 1056-1060.

Martini, S. R., G. Roman, S. Meuser, G. Mardon and R. L. Davis (2000). "The retinal determination gene, *dachshund*, is required for mushroom body cell differentiation." Development **127**(12): 2663-2672.

McCartney, B. M., H. A. Dierick, C. Kirkpatrick, M. M. Moline, A. Baas, M. Peifer and A. Bejsovec (1999). "Drosophila APC2 is a cytoskeletally-associated protein that regulates wingless signaling in the embryonic epidermis." J Cell Biol **146**(6): 1303-1318.

Melzig, J., K. H. Rein, U. Schafer, H. Pfister, H. Jackle, M. Heisenberg and T. Raabe (1998). "A protein related to p21-activated kinase (PAK) that is involved in neurogenesis in the Drosophila adult central nervous system." Curr Biol **8**(22): 1223-1226.

Merrill, A. H., Jr. (2002). "De novo sphingolipid biosynthesis: a necessary, but dangerous, pathway." J Biol Chem **277**(29): 25843-25846.

Miranda, K. C., T. Khromykh, P. Christy, T. L. Le, C. J. Gottardi, A. S. Yap, J. L. Stow and R. D. Teasdale (2001). "A dileucine motif targets E-cadherin to the basolateral cell surface in Madin-Darby canine kidney and LLC-PK1 epithelial cells." J Biol Chem **276**(25): 22565-22572.

Mombaerts, P. (2006). "Axonal wiring in the mouse olfactory system." Annu Rev Cell Dev Biol **22**: 713-737.

Mostov, K. E. (2003). "Epithelial polarity and morphogenesis." Methods **30**(3): 189-190.

Mummary-Widmer, J. L., M. Yamazaki, T. Stoeger, M. Novatchkova, S. Bhalerao, D. Chen, G. Dietzl, B. J. Dickson and J. A. Knoblich (2009). "Genome-wide analysis of Notch signalling in Drosophila by transgenic RNAi." Nature **458**(7241): 987-992.

Nagiec, M. M., R. L. Lester and R. C. Dickson (1996). "Sphingolipid synthesis: identification and characterization of mammalian cDNAs encoding the Lcb2 subunit of serine palmitoyltransferase." Gene **177**(1-2): 237-241.

Nakada, C., K. Ritchie, Y. Oba, M. Nakamura, Y. Hotta, R. Iino, R. S. Kasai, K. Yamaguchi, T. Fujiwara and A. Kusumi (2003). "Accumulation of anchored proteins forms membrane diffusion barriers during neuronal polarization." Nat Cell Biol **5**(7): 626-632.

Nakata, T. and N. Hirokawa (2003). "Microtubules provide directional cues for polarized axonal transport through interaction with kinesin motor head." J Cell Biol **162**(6): 1045-1055.

Nathke, I. (2004). "APC at a glance." Journal of Cell Science **117**(21): 4873-4875.

Nathke, I. S. (2004). "The adenomatous polyposis coli protein: the Achilles heel of the gut epithelium." Annu Rev Cell Dev Biol **20**: 337-366.

Niethammer, P., M. Delling, V. Sytnyk, A. Dityatev, K. Fukami and M. Schachner (2002). "Cosignaling of NCAM via lipid rafts and the FGF receptor is required for neuritogenesis." J Cell Biol **157**(3): 521-532.



Obeid, L. M., C. M. Linardic, L. A. Karolak and Y. A. Hannun (1993). "Programmed cell death induced by ceramide." Science **259**(5102): 1769-1771.

Pan, Z., T. Kao, Z. Horvath, J. Lemos, J. Y. Sul, S. D. Cranstoun, V. Bennett, S. S. Scherer and E. C. Cooper (2006). "A common ankyrin-G-based mechanism retains KCNQ and NaV channels at electrically active domains of the axon." J Neurosci **26**(10): 2599-2613.

Poyatos, I., F. Ruberti, R. Martinez-Maza, C. Gimenez, C. G. Dotti and F. Zafra (2000). "Polarized distribution of glycine transporter isoforms in epithelial and neuronal cells." Mol Cell Neurosci **15**(1): 99-111.

Proszynski, T. J., R. W. Klemm, M. Gravert, P. P. Hsu, Y. Gloor, J. Wagner, K. Kozak, H. Grabner, K. Walzer, M. Bagnat, K. Simons and C. Walch-Solimena (2005). "A genome-wide visual screen reveals a role for sphingolipids and ergosterol in cell surface delivery in yeast." Proc Natl Acad Sci U S A **102**(50): 17981-17986.

Rao, R. P. and J. K. Acharya (2008). "Sphingolipids and membrane biology as determined from genetic models." Prostaglandins Other Lipid Mediat **85**(1-2): 1-16.

Reuter, J. E., T. M. Nardine, A. Penton, P. Billuart, E. K. Scott, T. Usui, T. Uemura and L. Luo (2003). "A mosaic genetic screen for genes necessary for Drosophila mushroom body neuronal morphogenesis." Development **130**(6): 1203-1213.

Riboni, L., P. Viani, R. Bassi, A. Prinetti and G. Tettamanti (1997). "The role of sphingolipids in the process of signal transduction." Prog Lipid Res **36**(2-3): 153-195.

Rigogliuso, S., C. Donati, D. Cassara, S. Taverna, M. Salamone, P. Bruni and M. L. Vittorelli (2010). "An active form of sphingosine kinase-1 is released in the extracellular medium as component of membrane vesicles shed by two human tumor cell lines." J Oncol **2010**: 509329.

Rodriguez-Boulan, E. and A. Musch (2005). "Protein sorting in the Golgi complex: shifting paradigms." Biochim Biophys Acta **1744**(3): 455-464.

Rolls, M. M., D. Satoh, P. J. Clyne, A. L. Henner, T. Uemura and C. Q. Doe (2007). "Polarity and intracellular compartmentalization of Drosophila neurons." Neural Dev **2**: 7.

Schmucker, D., J. C. Clemens, H. Shu, C. A. Worby, J. Xiao, M. Muda, J. E. Dixon and S. L. Zipursky (2000). "Drosophila Dscam is an axon guidance receptor exhibiting extraordinary molecular diversity." Cell **101**(6): 671-684.

Schuldiner, O., D. Berdnik, J. M. Levy, J. S. Wu, D. Luginbuhl, A. C. Gontang and L. Luo (2008). "piggyBac-based mosaic screen identifies a postmitotic function for cohesin in regulating developmental axon pruning." Dev Cell **14**(2): 227-238.

Scott, E. K., T. Lee and L. Luo (2001). "enok encodes a Drosophila putative histone acetyltransferase required for mushroom body neuroblast proliferation." Curr Biol **11**(2): 99-104.

Sharp, D. J., R. Kuriyama, R. Essner and P. W. Baas (1997). "Expression of a

minus-end-directed motor protein induces Sf9 cells to form axon-like processes with uniform microtubule polarity orientation." J Cell Sci **110 ( Pt 19)**: 2373-2380.

Shi, L., H. H. Yu, J. S. Yang and T. Lee (2007). "Specific Drosophila Dscam juxtamembrane variants control dendritic elaboration and axonal arborization." J Neurosci **27(25)**: 6723-6728.

Shipman-Appasamy, P. M., K. S. Cohen and M. B. Prystowsky (1991). "Nucleotide sequence of murine PCNA: interspecies comparison of the cDNA and the 5' flanking region of the gene." DNA Seq **2(3)**: 181-191.

Silverman, M. A., S. Kaech, M. Jareb, M. A. Burack, L. Vogt, P. Sonderegger and G. Banker (2001). "Sorting and directed transport of membrane proteins during development of hippocampal neurons in culture." Proc Natl Acad Sci U S A **98(13)**: 7051-7057.

Simons, K. and E. Ikonen (1997). "Functional rafts in cell membranes." Nature **387(6633)**: 569-572.

Song, A. H., D. Wang, G. Chen, Y. Li, J. Luo, S. Duan and M. M. Poo (2009). "A selective filter for cytoplasmic transport at the axon initial segment." Cell **136(6)**: 1148-1160.

Stancevic, B. and R. Kolesnick (2010). "Ceramide-rich platforms in transmembrane signaling." FEBS Lett **584(9)**: 1728-1740.

Steffes, G. (2007). "Genetische Kontrolle axonaler Konvergenz und synaptischer Spezifität olfaktorischer Rezeptorneurone in Drosophila melanogaster ( PhD. thesis )."

Stone, M. C., F. Roegiers and M. M. Rolls (2008). "Microtubules have opposite orientation in axons and dendrites of Drosophila neurons." Mol Biol Cell **19(10)**: 4122-4129.

Stuart, G., J. Schiller and B. Sakmann (1997). "Action potential initiation and propagation in rat neocortical pyramidal neurons." J Physiol **505 ( Pt 3)**: 617-632.

Tahirovic, S. and F. Bradke (2009). "Neuronal polarity." Cold Spring Harb Perspect Biol **1(3)**: a001644.

Thudichum, J. L. (1884). "A Treatise on the Chemical Constitution of the Brain. Bailliere,," Tindall and Cox, London.

Tsui-Pierchala, B. A., M. Encinas, J. Milbrandt and E. M. Johnson, Jr. (2002). "Lipid rafts in neuronal signaling and function." Trends Neurosci **25(8)**: 412-417.

van Blitterswijk, W. J., A. H. van der Luit, R. J. Veldman, M. Verheij and J. Borst (2003). "Ceramide: second messenger or modulator of membrane structure and dynamics?" Biochem J **369(Pt 2)**: 199-211.

Van Wart, A., J. S. Trimmer and G. Matthews (2007). "Polarized distribution of ion channels within microdomains of the axon initial segment." J Comp Neurol **500(2)**: 339-352.

Wandall, H. H., J. W. Pedersen, C. Park, S. B. Lavery, S. Pizette, S. M. Cohen, T. Schwientek and H. Clausen (2003). "Drosophila egghead encodes a beta 1,4-mannosyltransferase predicted to form the immediate precursor glycosphingolipid substrate for brainiac." J Biol Chem **278(3)**:

1411-1414.

Wang, G., K. Krishnamurthy, Y. W. Chiang, S. Dasgupta and E. Bieberich (2008). "Regulation of neural progenitor cell motility by ceramide and potential implications for mouse brain development." J Neurochem **106**(2): 718-733.

Wang, J., X. Ma, J. S. Yang, X. Zheng, C. T. Zugates, C. H. Lee and T. Lee (2004). "Transmembrane/juxtamembrane domain-dependent Dscam distribution and function during mushroom body neuronal morphogenesis." Neuron **43**(5): 663-672.

Wang, J., C. T. Zugates, I. H. Liang, C. H. Lee and T. Lee (2002). "Drosophila Dscam is required for divergent segregation of sister branches and suppresses ectopic bifurcation of axons." Neuron **33**(4): 559-571.

Watts, R. J., E. D. Hoopfer and L. Luo (2003). "Axon pruning during Drosophila metamorphosis: evidence for local degeneration and requirement of the ubiquitin-proteasome system." Neuron **38**(6): 871-885.

Weisz, O. A. and E. Rodriguez-Boulan (2009). "Apical trafficking in epithelial cells: signals, clusters and motors." J Cell Sci **122**(Pt 23): 4253-4266.

Williams, R. W. and K. Herrup (1988). "The control of neuron number." Annu Rev Neurosci **11**: 423-453.

Wilson, R. I. and Z. F. Mainen (2006). "Early events in olfactory processing." Annu Rev Neurosci **29**: 163-201.

Winckler, B., P. Forscher and I. Mellman (1999). "A diffusion barrier maintains distribution of membrane proteins in polarized neurons." Nature **397**(6721): 698-701.

Wojtowicz, W. M., J. J. Flanagan, S. S. Millard, S. L. Zipursky and J. C. Clemens (2004). "Alternative splicing of Drosophila Dscam generates axon guidance receptors that exhibit isoform-specific homophilic binding." Cell **118**(5): 619-633.

Xu, T. and G. M. Rubin (1993). "Analysis of genetic mosaics in developing and adult Drosophila tissues." Development **117**(4): 1223-1237.

Yang, J. S., J. M. Bai and T. Lee (2008). "Dynein-dynactin complex is essential for dendritic restriction of TM1-containing Drosophila Dscam." PLoS ONE **3**(10): e3504.

Yap, C. C., R. L. Nokes, D. Wisco, E. Anderson, H. Folsch and B. Winckler (2008). "Pathway selection to the axon depends on multiple targeting signals in NgCAM." J Cell Sci **121**(Pt 9): 1514-1525.

Yu, W., C. Cook, C. Sauter, R. Kuriyama, P. L. Kaplan and P. W. Baas (2000). "Depletion of a microtubule-associated motor protein induces the loss of dendritic identity." J Neurosci **20**(15): 5782-5791.

Zanolari, B., S. Friant, K. Funato, C. Sutterlin, B. J. Stevenson and H. Riezman (2000). "Sphingoid base synthesis requirement for endocytosis in *Saccharomyces cerevisiae*." EMBO J **19**(12): 2824-2833.

Zhan, X. L., J. C. Clemens, G. Neves, D. Hattori, J. J. Flanagan, T. Hummel, M. L. Vasconcelos, A. Chess and S. L. Zipursky (2004). "Analysis of Dscam diversity in regulating axon guidance in *Drosophila* mushroom bodies." Neuron **43**(5): 673-686.

Zheng, Y., J. Wildonger, B. Ye, Y. Zhang, A. Kita, S. H. Younger, S. Zimmerman, L. Y. Jan and Y. N. Jan (2008). "Dynein is required for polarized dendritic transport and uniform microtubule orientation in axons." Nat Cell Biol **10**(10): 1172-1180.

Zhu, S., S. Lin, C. F. Kao, T. Awasaki, A. S. Chiang and T. Lee (2006). "Gradients of the *Drosophila* Chinmo BTB-zinc finger protein govern neuronal temporal identity." Cell **127**(2): 409-422.

## 7 APPENDIX

### 7.1 List of Figures and tables

- Figure 1.1 Organization of the *Drosophila* olfactory system
- Figure 1.2 MB neurons development
- Figure 1.3 Scheme of sphingolipid metabolism
- Figure 1.4 A schematic representation of modulation of endocytosis by sphingolipids.
- Figure2.1 Schematic of the GAL4–UAS system with GAL80 and the MARCM genetic system.
- Figure2.2 Dissection method for adult brains
- Figure 3.1 Structural organization of the Serine palmitoyltransferase (SPT) enzyme and *spt-1* gene.
- Table 3.1 Summery of *spt-1* and *lace* alleles used in this study
- Figure 3.2 Mutations of *spt-1* and *lace* disrupt ORN axon targeting
- Figure 3.3 *spt-1* and *lace* have similar ORN phenotypes for Or47a
- Figure 3.4 *spt-1* and *lace* also have similar phenotypes for maxillary palp Or46a
- Figure 3.5 *lace* does not affect axons sorting of maxillary palp ORNs
- Figure 3.6 ORNs targeting unaffected in *spt* MARCM clone
- Figure 3.7 *spt* mutant axon fibers have abnormal terminal morphology.
- Figure 3.8 Genetic rescue of *lace* phenotype
- Figure 3.9 Rescue of *lace* mutant by feeding with sphingosine.
- Figure 3.10 *lace* mutations have weak phenotype at lower temperature
- Figure 3.11 Genetic dissection of *spt* defects in ORNs by elav Gal4 driven RNAi.
- Table 3.2 Genetic dissection of *spt* defects in ORNs.

- 
- Figure 3.12 Genetic dissection of *spt* defects in ORNs by *elav gal4* and *eyGal4* double driven RNAi
- Figure 3.13 DMR components are not changed in *lace* hypomorphic mutants
- Figure 3.14 Genetic interaction between *Spt* and *Dscam*
- Figure 3.15 Misexpression of *Dscam* in *spt* background
- Figure 3.16 MB neurons development
- Figure 3.17 *lace* mutation affect formation of bifurcated axons in MB
- Figure 3.18 Genetic dissection MB phenotype
- Figure 3.19 Genetic dissection MB phenotype gives a hint that membrane ceramide is the candidate product responded to the lost lobe defect.
- Figure 3.20 *Dscam* mutant has MB phenotypes
- Figure 3.21 *spt* mutant axons are normal in MARCM clones
- Figure 3.22 Overexpression of *Dscam*[TM1] and *Dscam*[TM2] isoforms in MB by *Gal4-OK107* and *Gal4-201Y*
- Figure 3.23 *Dscam* [TM1] mistargeting in *lace* background
- Figure 3.24 Overexpression of *Dscam*[TM1] in *lace* background enhance MB phenotype
- Figure 3.25 Knockdown of *Dscam*[TM1] in *lace* background suppress MB phenotype
- Figure 3.26 MB dendritic proteins mistargeting in *lace* mutant
- Figure 3.27 Protein sorting and transport machinery disruption give MB phenotype
- Figure 3.28 Colocalization of Rab4 and *Dscam* [TM1>::GFP in MB neurons
- Figure 4.1 The model of *spt* function in Mushroom body.
- Figure 4.2 Two models of *spt* and *dscam* genetic interaction
- Figure 4.3 Trafficking routes and sorting mechanisms
- Figure 4.4 The organization of axon initial segment

---

## 7.2 Abbreviations

AL	Antenna Lobe
APF	After Pupal Formation
CNS	Central Nervous System
Dscam	Down syndrome cell adhesion molecule
FLP	Flipase
FRT	FLP-Recombinase Target
HSN1	Hereditary Sensory Neuropathy Type I
MARCM	Mosaic Analysis with a Repressible Cell Marker
MB	Mushroom Body
N-Cad	Neuronal Cadherin
OR	Olfactory Receptor
ORN	Olfactory Receptor Neuron
PN	Project Neuron
PNS	Peripheral Nervous System
S1P	Sphingosine-1-Phosphate
SM	Sphingomyelin
SOG	Suboesophageal ganglion
SPT	Serine Palmitoyltransferase
UAS	Upstream Activating Sequence

## Lebenslauf

### JUNFENG ZHENG

<b>Geburtsdatum</b>	02.01.1975
<b>Geburtsort</b>	Tianjin, P.R. China
<b>Eltern:</b>	ShiChen Zheng YaQin Gao
<b>Schulbildung</b>	1982-1988 Shengli Primary School
<b>Studium:</b>	1988-1991 Benxi 26 <sup>th</sup> Medial School 1991-1994 Benxi High School 1994-1998 BSc, Liao Ning Normal University, China 2001-2004 MSc, Peking Union Medical College
<b>Promotionsstudiengang:</b>	2007-2010 Promotionsstudiengang an der WWU Münster, Institut für Neuro- und Verhaltensbiologie, Arbeitsgruppe PD Dr. Thomas Hummel
<b>Tätigkeiten:</b>	1/2006–10/2007 Beschäftigung als wissenschaftlicher Mitarbeiter am Institut für Biochemistry, Justus-Liebig-Universität Gießen 3/2007- Beschäftigung als wissenschaftlicher Mitarbeiter am Institut für Neuro- und Entwicklungsbiologie, WWU Münster



# Erklärung

Hiermit erkläre ich, dass ich die vorliegende Arbeit selbstständig verfasst und keine anderen als die angegebenen Hilfsmittel und Quellen benutzt habe. Alle Stellen der Arbeit, die dem Wortlaut oder dem Sinn nach anderen Werken entnommen sind, habe ich in jedem Fall unter Angabe der Quelle deutlich als Entlehnung kenntlich gemacht.

Münster, den.....

---

## ACKNOWLEDGEMENTS

I would like to thank to specially thank my supervisor PD Dr.Thomas Hummel for his constant support, excellent guidance and creative discussions during this project. Moreover, it is his encouragement and valuable suggestions that gave me the motivation to continue my scientific research.

I would like to thank Prof. Christian Klämbt for his invaluable comments on my project.

I would like to thank to Georg Steffes for his preciouy work on *spt* project and also for his excellent supervision during my earlier projects.

I would like to thank my colleagues: Abi, Anna, Ariane, Bernd, Britta, Christian, Christoph, Georg, Lorin, Maliana, Marc, Milan, Sven, who create such a nice atmosphere in the lab.

I would like to thank all the Allumi and present members of Klämbt, Bogdan and Aberle groups for help and suggestions.

I am indebted to my parents for their supporting and encouragement during my study. I am deepest grateful to my wife, who has been shared weal and woe with me over the years.